Copyright Warning & Restrictions

The copyright law of the United States (Title 17, United States Code) governs the making of photocopies or other reproductions of copyrighted material.

Under certain conditions specified in the law, libraries and archives are authorized to furnish a photocopy or other reproduction. One of these specified conditions is that the photocopy or reproduction is not to be "used for any purpose other than private study, scholarship, or research." If a, user makes a request for, or later uses, a photocopy or reproduction for purposes in excess of "fair use" that user may be liable for copyright infringement,

This institution reserves the right to refuse to accept a copying order if, in its judgment, fulfillment of the order would involve violation of copyright law.

Please Note: The author retains the copyright while the New Jersey Institute of Technology reserves the right to distribute this thesis or dissertation

Printing note: If you do not wish to print this page, then select "Pages from: first page # to: last page #" on the print dialog screen

ABSTRACT

REDUCTION IN SALT DEPOSITION ON CARBON NANOTUBE IMMOIBLIZED MEMBRANE DURING DESALINATION VIA MEMBRANE DISTILLATION

by

Madihah Saud Humoud

As water scarcity increases globally under the stresses of increasing demand, aquifer depletion, and climate change, the market for efficient desalination technologies has grown rapidly to fill the void. One such developing technology, membrane distillation (MD), has found much interest in the scientific community. MD has also been powered by solar energy and waste heat resources because it can be operated at relatively low temperatures. Recent studies indicate that MD could potentially achieve the efficiencies of state-of-the-art mature thermal desalination technologies, although additional engineering and scientific challenges must first be overcome.

MD can be used to treat high salinity water where the salt concentration is high. The aim of this research is to better understand and provide solutions for one of the major challenges being faced by high concertation applications of MD, more specifically membrane fouling. Through experiments, this thesis compares different heating systems in MD, namely conventional and microwave heating, and their effect on fouling. It also looks at carbon nanotube immobilized membrane, and studies the effect of carbon nanotubes on fouling. In this research MD is carried out using highly concentrated aqueous calcium carbonate, calcium sulfate and barium sulfate solutions, and it is observed that the decline in flux over time is significantly less in microwave induced membrane distillation (MIMD). As compared to conventional heating, the salt deposition on the membrane is 50-79 % less during microwave heating.

The second and third part of this research shows the effects of adding different antiscalant materials to the feed side of the experiment to investigate the fouling behavior under fixed operating parameters such as feed concentration, temperature, and feed flowrate. The results show a strong influence of using antiscalant materials on the highly concentrated salt solutions and on produced water from hydraulic fracturing as well. It is observed that using carbon nanotube based membranes and antiscalants, the fouling behavior could be reduced and water vapor flux in MD can be enhanced. Results also show that the presence of CNTs facilitates the removal of deposited salts by washing and the CNIM regains 97% of its initial water flux, whereas the unmodified polypropylene only regains 85% of the original value.

REDUCTION IN SALT DEPOSITION ON CARBON NANOTUBE IMMOIBLIZED MEMBRANE DURING DESALINATION VIA MEMBRANE DISTILLATION

by

Madihah Saud Humoud

A Dissertation
Submitted to the Faculty of
New Jersey Institute of Technology
in Partial Fulfillment of the Requirements for the Degree of
Doctor of Philosophy in Chemistry

Department of Chemistry and Environmental Science

December 2019

APPROVAL PAGE

REDUCTION IN SALT DEPOSITION ON CARBON NANOTUBE IMMOBILIZED MEMBRANE DURING DESALINATION VIA MEMBRANE DISTILLATION

Madihah Saud Humoud

Dr. Somenath Mitra, Dissertation Advisor — Date
Distinguished Professor of Chemistry and Environmental Science, NJIT

Dr. Tamara Gund, Committee Member — Date
Professor of Chemistry and Environmental Science, NJIT

Dr. Kim I. Yong, Committee Member — Date
Assistant Professor of Chemistry and Environmental Science, NJIT

Dr. Pradyot Patnaik, Committee Member — Date
Adjunct Professor of Chemistry and Environmental Science, NJIT

Dr. N.M. Ravindra, Committee Member — Date
Professor of Physics, NJIT

BIOGRAPHICAL SKETCH

Author: Madihah Saud Humoud

Degree: Doctor of Philosophy

Date: December 2019

Undergraduate and Graduate Education:

- Doctor of Philosophy in Chemistry,
  New Jersey Institute of Technology, Newark, NJ, 2019

- Master of Science in Pharmaceutical Chemistry,
  Fairleigh Dickinson University, Florham Park, NJ, 2012

- Bachelor of Science in Chemistry,
  Dammam University, Dammam, Saudi Arabia, 2007

Major: Chemistry

Presentations and Publications:

M.S. Humoud, W. Intrchom, S. Roy, S. Mitra, Reduction of Scaling in Microwave Induced Membrane Distillation on a Carbon Nanotube Immobilized membrane, Environmental Science: Water Research & Technology, 5 (2019) 1012-1021.

M.S. Humoud, S. Roy, S. Mitra, Scaling Reduction in Carbon Nanotube Immobilized Membrane during Membrane Distillation: MDPI-Water, Received: 19 November 2019; Accepted: 6 December 2019; Published: 8 December 2019.

M.S. Humoud, S. Roy, S. Mitra, Treatment of Produced Water using Carbon Nanotube Immobilized Membrane via Direct Contact Membrane Distillation (In preparation).

S. Roy, M.S. Humoud, W. Intrchom, S. Mitra, Microwave-Induced Desalination via Direct Contact Membrane Distillation, ACS Sustainable Chemistry & Engineering, 6 (2017) 626-632.

W. Intrchom, S. Roy, M. Humoud, S. Mitra, Immobilization of Graphene Oxide on the Permeate Side of a Membrane Distillation Membrane to Enhance Flux, Membranes, 8 (2018) 63.

M.S. Humoud, S. Roy, S. Mitra, Using Antiscalant in Membrane Fouling via Membrane Distillation. Paper presented at the National American Chemical Society Conference 254th ACS national meeting, August 2017, Washington DC.

M.S. Humoud, S. Roy, Smruti Ragunath, S. Mitra, Functionalized Carbon Nanotube Enhanced Membrane Distillation. Paper presented at NJWEA (New Jersey Water Environment Association) 103rd annual Conference, May 2018, Atlantic City, NJ.

M.S. Humoud, S. Roy, S. Mitra, The Effect of Using f-CNIM Membranes to Enhance the Performance of MD. Paper presented at Rutgers University, New Brunswick, NJ. Sponsored by the Northern and Central New Jersey Chapter of the Air & Waste Management Association. February 27th.2019.

M.S. Humoud, S. Roy, S. Mitra, Functionalized Carbon Nanotube Enhanced Membrane Distillation. Paper presented at the National American Chemical Society Conference 256th ACS national meeting, April 2019, Orlando, FL.

W. Intrchom, S. Roy, S, M.S. Humoud, Mitra, Immobilization of Graphene Oxide on the Permeate Side of a Membrane Distillation Membrane to Enhance Flux. Paper presented at the National American Chemical Society Conference 256th ACS national meeting, April 2019, Orlando, FL.

M.S. Humoud, S. Roy, S. Mitra, The performance of using Carbon Nanotube Immobilized Membrane and Antiscalant for Produced Water Treatment via DCMD. Paper presented at NJWEA (New Jersey Water Environment Association) 104th annual Conference, May 2019, Atlantic City, NJ

First of all, I dedicated this PhD to Almighty Allah, thank you for guidance, strength, power of mind, protection and for giving us a healthy life. Then, I dedicated this to my beloved mother Fatimah Al kardoos who thought me how to be strong and never give up in life without her support I wouldn't make it through my PhD. Also, to my lovely sister Zainab Hamoud who lived with me through out until this point, who provide me advises, emotional support and encouragements to achieve my dream and to all my family who supported me during my PhD journey: Kholoud, Khaled, Fathya, Nada, and Hussain. Finally, to all my friends for their encouragement and support.

ACKNOWLEDGEMENT

Obtaining a PhD degree was a long journey that finally culminated. It was not easy to achieve but with Grace of Allah Almighty the long journey is about to end. I would like to especially thank my advisor professor Somenath Mitra, who has been more than an advisor to me. His passionate interest, unwavering dedication to research, and understanding has motivated me to overcome all challenges that arose during my PhD journey.

I would like to acknowledge my dissertation committee members, Dr. Tamara Gund, Dr. N.M. Ravindra, Dr. Young I. Kim, and Dr. Pradyot Patnaik. I want to thank them for finding time out from their busy schedules to review my dissertation and provide considerate advice, important feedback, constructive, and critical comments.

I would like to acknowledge all of the financial support that made this dissertation possible, provided by King Abdullah Scholarship Program, Ministry of Higher education, Kingdom of Saudi Arabia for their financial support and the National Science Foundation (Chemical, Bioengineering, Environmental, and Transport Systems Division, Grant no. CBET-1603314).

Also, I'd like to thank Dr. Xueyan Zhang, Dr. Larisa Krishtopa, and Dr. Jeong Shim for their training, help and advice on Raman, AFM, FTIR, ICP-MS and SEM measurement and operation.

Moreover, I'd like to thank my group members, Dr. Sager Roy, Dr. Zhiqian Wang, Oindrila Gupta, Worawit Intrchom, Indrani Gupta, Mitun Chandra Bhoumick, Sumona Paul, Samar Azizighannad, Emine Karaman, and Mohammad Saiful Islam. I really appreciate their valuable help and support during the period of my research. Furthermore, words fail me to express my appreciation to my dearest friends: Abdullah Gabrazli,

Mayadah Yusuf, Isra Aljamed, Aysha Almutiri, and Wejdan Ibrahim for their generous care and encouragement, which made my stay in USA not lonely but enjoyable. Those lovely persons gave me lots of happiness and energy whenever I am up or down. Lastly but the most importantly, I would not succeed in this endeavor without my parent's long-lasting support, understanding, encouragement, and patience, which accompany me through all the hardship during the research adventure.

TABLE OF CONTENTS

Chapter	Page
1 INTRODUCTION……..…….	1
1.1 Background…….……..…….....	2
1.2 Objective of Thesis …….…….....	3
1.3 Dissertation Outline …….....…….…….....	4
2 LITERATURE REVIEW ……..……..…..	6
2.1 Membrane Distillation for Desalination Application ……...	6
2.1.1 Potentials of MD for Desalination Applications …….....	9
2.1.2 Temperature and Concentration Polarization Effects ……..……....	10
2.1.3 Sources of Heat in MD …….....	15
2.1.4 Membrane Pore Wettability in MD ……...……	18
2.1.5 Membrane Fouling and Scaling in MD ……..……....	19
2.2 MD for Seawater Desalination Applications ……...	21
2.2.1 Membrane Fouling and Scaling in Seawater MD Desalination ……...	21
2.2.2 Energy Consumption of Seawater MD Desalination …….……..	23
2.2.3 MD for Produced Water Treatment …….....	26
2.3 Membranes …….....	28
2.3.1 Nanostructured Membranes …….....	28
2.3.2 Carbon Nanotube Membranes …….....	32

TABLE OF CONTENTS
(Continued)

Chapter	Page
2.3.3 Applications of Nano Structured Membranes…….....	36
3 REDUCTION OF INORGANIC FOULING IN MICROWAVE INDUCED MEMBRANE DISTILATION IN CARBON NANOTUBE IMMOBLIZED MEMBRANE …….…...…	43
3.1 Introduction …….....	43
3.2 Experimental ……...……	45
3.2.1 Chemicals, Materials and Membrane Module …….....	45
3.2.2 Experimental Setup ……..…….**.....**	46
3.2.3 Membrane Performances ……..…….**.....**	47
3.3 Results and Discussion ……..**.....**	48
3.3.1 Effect of Temperature and Feed Flowrate ……..…….**.....**	48
3.3.2 Membrane Fouling in MD and MIMD ……..…….**.....**	51
3.3.3 Deposition of Salts on MD and MIMD Membranes …...…….**.....**	54
3.4 Proposed Mechanism ……..……..	58
3.5 Conclusion …….....	63
4 FOULING REDUCTION IN CARBON NANOTUBE IMMOBLIZED MEMBRANE DURING MEMBRANE DISTILATION ……...	64
4.1 Introduction ……**.....**	64

TABLE OF CONTENTS
(Continued)

Chapter	Page
4.2 Experimental …….....	66
4.2.1 Materials and Chemicals ……...…..	66
4.2.2 Experimental Procedure.……....….	67
4.2.3 DCMD Performance …….….....	68
4.3 Results and Discussion ……...	69
4.3.1 Characterization of the Membranes ……...…..	69
4.3.2 Effect of Temperature and Feed Flowrate on the Water vapor flux	72
4.3.3 Membrane Fouling …….....	74
4.3.4 Deposition of Salts on the Membranes ……	79
4.3.5 Membrane Regeneration and Stability …….....	82
4.4 Conclusion ……..……	85
5 INHANCED PREFORMANCE OF CARBON NANOTUBE IMMOBLIZED MEMEMBRANE FOR TREATMENT OF HIGH SALINITY PRODUCED WATER VIA DCMD …….....……..……..……..….	86
5.1 INTRODUCTION ……..……..….	86
5.2 Materials and Methods ……..	89
5.2.1 Chemicals and Materials ……...……...	89
5.2.2 Water Sample Composition ……...……...	89
5.2.3 Water Sample and Pretreatment Methods ……...….....	90
5.2.4 CNIM Fabrication ……...……...…..…	92

TABLE OF CONTENTS
(Continued)

Chapter	Page
5.2.5 Experimental Procedure ……..…….…..…..	94
5.2.6 DCMD Performance using CNIM and PTFE Membrane ……....…....	95
5.3 Results and Discussion ……....….	96
5.3.1 Membrane Characterization ……...…..….….....	96
5.3.2 Effect of Temperature and Feed Flow Rate on Water Vapor Flux	98
5.3.3 Fouling Behavior of Produced Water …….....	100
5.3.4 Deposition of Foulants on the Membrane Surface ……	102
5.3.5 Membrane Regeneration ……...……	104
5.3.6 Mass Transfer Coefficient ……...……...…....	105
5.4 Membrane Stability …….....	106
5.5 Proposed Mechanism …….....	107
5.6 Conclusion ……...…..	108
6 SUMMARY ……..……....	109
REFERENCES …….	111

LIST OF TABLES

Table		Page
3.1	Deposition of Salts on the Membrane Surface after 7 hrs. of operation at 70^{o}C	55
4.1	Normalized Flux Decline (FDn) for various salt solutions ……..…..……...	78
4.2	Deposition of salts on the membrane surface after 6 hrs. of operation at 70^{o}C ..	79
4.3	Membrane Regeneration data...……..……..……	83
4.4	Amount of salt deposition on the membrane surface after washing…….....	85
5.1	Analysis of produced water before filtration (A) in Figure1……...	90
5.2	Analysis of produced water after filtration (b) and with HEDP (c) …...……....	92
5.3	Normalized Flux Decline (FDn) for produced water solution....…….……...	101
5.4	Deposition of foulants on the membrane surface after 7 hr of operation at 70^{o}C.	102
5.5	Membrane Regeneration Data …..……..…….	104
5.6a	Effect of varying feed flow rate on Mass Transfer Coefficient at 70 ^{o}C.….....	106
5.6b	Mass Transfer Coefficient of various membranes as a function of temperature..	106

LIST OF FIGURES

Figure		Page
2.1	Four main MD configurations ……..……	7
2.2	Types of MD Modules that have been studied in the literature …….……..	8
2.3	Temperature and Concentration Polarization Effects in DCMD……..…….....	12
2.4	SEM of Thin-film Composite (Polyamide Surface Layer Supported by Polypropylene) and Microporous Polypropylene. ……..……..……...…	30
2.5	(a) Photograph of Carbon-Nanotube Immobilized Membrane (CNIM); (b) photograph of pure polypropylene; (c) SEM image of unmodified polypropylene membrane; and, (d) CNIM. ……..……	34
2.6	Aligned Carbon-Nanotube (CNT) Membrane Fabrication Steps ……..…...…	36
2.7	Mechanism of Pervaporation in Carbon-Nanotube Immobilized Membrane	38
2.8	Carbon-nanotube (CNT)-assisted extraction and enrichment. triangles represent the analyte molecules and the circles Represent the solvent Molecules ……...	40
2.9	(a) Membrane Distillation (MD) as an on-line preconcentration technique; (b) membrane device; (c) MD performance on unmodified membrane and Carbon-Nanotube Immobilized Membrane (CNIM) ……..……...	42
3.1	Schematic of Microwave Induced Membrane Distillation System…….....	47
3.2	Effect of Increasing (a) Feed Temperature and (b) Flow Rate on water vapor flux for CaSO4 solution during MD and MIMD...……..……..…….	50
3.3	Water vapor Flux in PP-CNIM Membranes for (a) $CaSO_4$ at a concentration of 2.95g/l; (b) $CaCO_3$ at a Concentration of 3.5g/l ; and (c) $BaSO_4$ at a Concentration of 2.5g/l. All Analysis was done at a Temperature of 70 °C and Feed Flow Rate of 200 mL/min ...……..……	53

LIST OF FIGURES
(Continued)

Chapter		Page
3.4	a) Original PP Membrane; b) CNIM; c) $CaSO_4$ scale with conventional heating; d) $CaSO_4$ scale with MIMD; e) $CaCO_3$ scale with conventional heating; f) $CaCO_3$ scale in MIMD; g) $BaSO_4$ scale with conventional heating; and h) BaSO4 scale with MIMD conventional heating; and h) $BaSO_4$ scale with MIMD...…….……	57
3.5	FTIR Spectra of a) CaSO4-water solution (2.95g/l); b) CaCO3-water solution (3.5g/l); c) BaSO4-water solution (2.5g/l) under room temperature (RT) Microwave (MIMD) and conventional heating (MD)....……..……..	60
3.6	The Influence of Microwave Irradiation on particle size distribution of a) CaSO4; b) CaCO3; and c) BaSO4…..……	62
4.1	Screening effect of CNTs in preventing the salt deposition on the membrane surface……	66
4.2	Schematic representation of the experimental setup …….….....	67
4.3	Surface SEM image of (a) PP Membrane and (b) CNIM; c) The TGA curves of plain and modified membranes …….	70
4.4	Contact angle measurements on unmodified PP and CNIM membrane (a) contact angle: 115 (pure water plain PP); (b) contact angle: 125 (pure water PP CNIM); (c) contact angle: 112 (salt water plain PP); (d) contact angle: 117 (salt water CNIM) …….....	71
4.5	a. Effect of Temperature on permeate flux of pure water and CaSO4 solution at 200 mL/min Feed and distillate Flow Rate ……..…….	73
4.5	b. Effect of Flow Rate on permeate flux of CaSO4 solution at 70 °C and 200 mL/min distillate Flow Rate …….	75
4.6	Water vapor flux in PP Membrane and CNIM at 70^{o}C and 200 mL/min Feed Flow Rate for (a) pure water (run time 1 hr); (b) CaSO4 solution (2.95g/L) (c) CaCO3 solution (3.5g/L); and (d) BaSO4 Solution (2.5g/L) (b-d run time 10 hr)……...…	76

LIST OF FIGURES
(Continued)

	Chapter	Page
4.7	(a) SEM image of CaSO4 deposition on (i) PP; (ii) PP-AS; (iii) CNIM and (iv) CNIM-AS after running the experiment given in Figure 4.6b.....	80
4.7	(b) SEM image of CaCO3 deposition on (i) PP; (ii) PP-AS; (iii) CNIM and (iv) CNIM-AS after running the experiment given in Figure 4.6c.	81
4.7	(c) SEM image of BaSO4 deposition on (i) PP; (ii) PP-AS; (iii) CNIM and (iv) CNIM-AS after running the experiment	82
4.8	SEM image of the fouled membrane after washing (a) PP; (b) PP-AS; (c) CNIM and (d) CNIM-AS	84
5.1	A) Produced water sample before filtration; B) Produced water sample after filtration; and C) Produced water sample with HEDP.....	90
5.2	Schematic representation of the experimental Setup	95
5.3	a) SEM image of PTFE membrane; b) CNIM; and c) The TGA curves of PTFE membrane and CNIM	97
5.4	a) Effect of temperature on permeate flux of produced water solution at 200mL/min flowrate; b) Effect of flowrate on permeate flux of produced water solution at 70^{o}C Temperature and 200 mL/min Flow Rate.	99
5.5	Water vapor flux in PTFE and CNIM membranes for produced water solution with and without using HEDP	101
5.6	SEM image of foulants deposition on (a) PTFE; (b) PTFE-HEDP; (c) CNIM and (d) CNIM-HEDP	103
5.7	Proposed Mechanism	107

CHAPTER 1
INTRODUCTION

1.1 Background

As population grows, a number of people experiencing water shortage is expected to multiply fourfold between 2000 and 2025 [1, 2]. Desalination is progressively being touted as a solution to the water crisis in the last decades. Desalination processes, including thermal distillation and membrane-based separation, can extract fresh water from various saline water sources such as seawater and produced water from oil and gas industries. While the natural fresh water availability has been gradually depleted due to water pollution, saline water sources are virtually limitless. In addition, recent technological advancements in the desalination field have significantly reduced the cost, and at the same time improved the quality of desalted water to satisfy stringent regulations. Desalination processes can be environmentally friendly when they are driven by renewable energy [3, 4].

Large-scale thermal distillation and membrane-based desalination processes have been well used for fresh water provision to large and centralized communities [5]. However, sufficient fresh water provision in small and remote coastal areas remains a considerable challenge. Thermal distillation desalination processes, including multi-stage flash (MSF) and multi-effect distillation (MED) are energy intensive. Thus, they are only economically applicable in areas (i.e; the Middle East) where energy costs are affordable [6]. The desalination technology, reverse osmosis (RO) has expanded rapidly in the last two decades; its market share now dominates, and its costs have now approached near that of conventional water sources [7]. Other desalination technologies have grown as well,

including the thermal technologies of membrane distillation (MD), humidification dehumidification (HDH), multi-effect distillation (MED), as well as other technologies such as ion exchange resins and mechanical vapor compression [2, 8]. The thermal technologies have advantages over RO, including superior fouling resistance, reduced pretreatment needs, and lower energy use if paired with waste heat or renewable heat sources, and higher purity product water [9]. Membrane based desalination processes, most notably reverse osmosis (RO), consume less energy than the thermal distillation. Nevertheless, RO desalination requires extensive feed water pretreatment owning to its susceptibility to fouling [6, 10]. Furthermore, RO desalination relies on electricity to run high pressure pumps to achieve the salt-water separation. RO systems are made of expensive materials such as duplex stainless steel to withstand the high pressure and corrosion [11]. Thus, RO is only economically viable for large-scale desalination applications.

Membrane distillation (MD), a thermally driven membrane separation process, embodies notable attributes that are particularly promising for strategic desalination applications. These applications include small-scale seawater desalination for fresh water provision in remote coastal areas and desalination of hypersaline solutions (e.g; brine from the RO desalination process or liquid desiccant solution used in air conditioners). In MD, a hydrophobic microporous membrane is used as a barrier against dissolved salts and non-volatile substances, but acts as a facilitator for water vapor transfer [9, 12]. A water vapor pressure gradient is induced by a temperature difference between two sides of the MD membrane which acts as the driving force for the water vapor transfer, and the MD process is negligibly affected by the feed osmotic pressure. Thus, the desalination process using

MD can produce ultrapure water from highly saline solution feeds at a mild feed water temperature without the need for high hydraulic pressure. MD can employ low-grade heat sources such as waste heat or solar thermal energy to meet its primary energy demands [13, 14]. In addition, the absence of high hydraulic pressure allows the MD system manufacture from inexpensive and noncorrosive materials, hence reducing both process investment and operational costs [9, 12]. Given these advantages, MD desalination has been studied extensively in recent decades. To date, the application of MD for saline water desalination is still restricted to laboratory or pilot-scale demonstrations. The full realization of MD for seawater and oil/gas produced water desalination has been hindered by the limited understanding of the thermal energy consumption and the susceptibility to pore wetting due to membrane fouling/scaling of the process [15, 16].

MD processes can be practiced in four basic configurations, including direct contact membrane distillation (DCMD), air gap membrane distillation (AGMD), vacuum membrane distillation (VMD), and sweeping gas membrane distillation (SGMD). Amongst these configurations, DCMD and AGMD have simple arrangements with fewer process equipment and hence offering more cost-effective desalination means as compared to VMD and SGMD. As a result, DCMD and AGMD are considered more suitable for strategic and small-scale desalination applications than VMD and SGMD.

1.2 Objectives and Scope of the Dissertation

The overall goal of this research is to optimize the MD process with respects to membrane Fouling/scaling which is one of the biggest challenge in the upcoming desalination technology, membrane distillation. This work aims to improve understanding of the fouling

in MD and introduced new solutions and techniques to reduce fouling and enhance the overall yield in MD process. Specific objectives to achieve this goal are to:

- Reduction of Inorganic Fouling in Microwave Induced Membrane Distillation on Carbon Nanotube Immobilized Membrane.
- Fouling Reduction in Carbon Nanotube Immobilized Membrane during Membrane Distillation using antiscalant materials.
- Treatment of Produced Water using Carbon Nanotube Immobilized Membrane via Direct Contact Membrane Distillation.

The dissertation focusses on determining suitable operating conditions for example, feed temperature, feed concentration and feed flowrate to minimize membrane scaling and evaluating membrane cleaning efficiency during the MD process for treating highly concentrated feed solution. Carbon nanotube immobilization on the unmodified membrane surface was used as the feed side in all experiments. Surface morphology was observed to differ for membranes fabricated with CNTs and its different functionalization which in turn altered the interaction with water vapor.

1.3 Dissertation Outline

This dissertation has three major chapters in addition to the Introduction, Literature Review, and the Conclusions sections. The first project focused on using microwave irradiation in MD process for highly concentrated salt solutions to study the inorganic fouling/scaling on the membrane surfaces in desalination application, and will be covered in Chapter 3. In Chapter 3, the membrane fouling/ scaling will be investigated during a DCMD process with three types of inorganic salts solutions such as $CaSO_4$, $CaCO_3$, and $BaSO_4$ in high concentrations. The second project is Chapter 4 that will show the effect of using antiscalant materials on the feed side solution to reduce inorganic fouling on the

membrane surface and enhanced the MD performance via DCMD by using carbon nanotube immobilized membrane. The washability and regenerability was also studied during the MD operation to report the effect of carbon nanotube on the membrane life time. The third project is Chapter 5 which include the treatment of produced water using carbon nanotube immobilized Membrane via direct contact membrane distillation (DCMD). This chapter reported the effect of using antiscalant on produced water solution to reduce fouling on the membrane surface. The fouling characteristics of produced water was investigated in this research to show the effect of using this technique to improve the antifouling behavior during the MD process. The last part is conclusion and recommendations for future work which is Chapter 6.

CHAPTER2

LITERATURE REVIEW

2.1 Membrane Distillation for Desalination Applications

Membrane distillation (MD) is a thermally driven separation process. In MD desalination, a microporous hydrophobic membrane and a temperature difference across the membrane are used to help the salt-water separation. The membrane acts as a barrier against liquid water and hence all dissolved salts and non-volatile substances, while allowing for the permeation of water in vapor phase through its pores [9, 12]. A hot brine solution is kept in direct contact with the membrane on the feed side while a cool fluid is maintained on the permeate side [17, 18]. The temperature difference between two sides of the membrane induces a water vapor pressure gradient, thus facilitating the transfer of water vapor through the membrane pores.

Membrane distillation is classified into four basic configurations depending on the methods applied on the permeate side to collect the distillate as it shown in Figure 2.1 [9, 12]. These configurations include direct contact membrane distillation (DCMD), air gap membrane distillation (AGMD), vacuum membrane distillation (VMD), and sweeping gas membrane distillation (SGMD). Amongst these configurations, DCMD and AGMD are the most suitable for desalination applications. DCMD has the simplest arrangement as compared with other MD configurations. The hot saline feed and the cold distillate streams are in direct contact with the membrane, and the vapor condensation occurs inside the DCMD membrane module. The direct contact arrangement also facilitates the heat and mass transfer between the process streams and the membrane surfaces, thus rendering

DCMD high water flux [13, 19, 20]. However, the simple arrangement also leads to a significant heat loss due to conduction via the membrane from the hot feed to the cold distillate stream, therefore limiting thermal efficiency of the DCMD process. In AGMD, an air gap is introduced between the membrane and the distillate stream to alleviate the heat conduction for improved thermal efficiency [21, 22]. The air gap also increases the resistance to the transfer of water vapor, hence reducing water flux of AGMD when comparing to DCMD [23]. The substitution of the air gap by a gas flow in SGMD or vacuum in VMD helps reduce the mass transfer resistance and at the same time mitigate the heat conduction. As a result, SGMD and VMD can attain high water flux together with improved thermal efficiency [24, 25]. Nevertheless, SGMD and VMD require external condensers for distillate collection and additional equipment [9, 12]. Therefore, the SGMD and VMD processes are more complex and costly than DCMD and AGMD [9, 12].

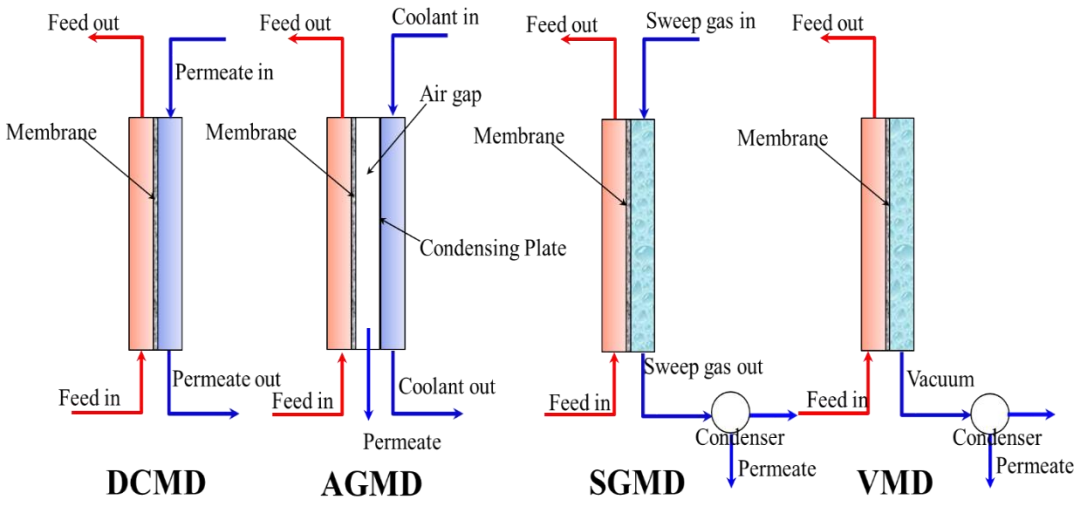

Figure 2.1 Four main MD configurations.

In addition to different heat transfer designs for the MD module, the construction technique may also vary. Four types of MD modules have been used in the literature, as seen in Figure 2.2.

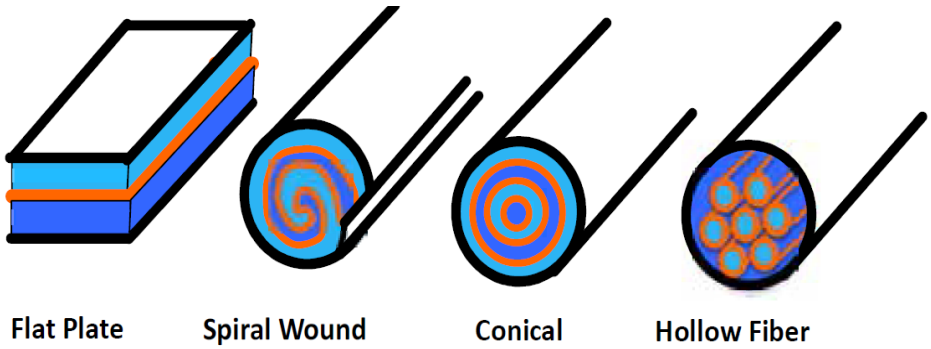

Figure 2.2 Types of MD Modules that have been studied in the literature.
Source:[26]

Flat plate systems are usually composed of sheets sandwiched together. Because they are so simple to construct, they are used very frequently in bench-scale systems, as well as in industry. Spiral wound functions very much like flat plate in terms of gap sizes, heat transfer, and modeling, and have the added benefit of reducing the amount of metal condenser surface and are more compact. Because of these benefits, other membrane technologies such as reverse osmosis very frequently use spiral wound membranes. However, because MD is a relatively immature technology, this potentially more cost-effective to mass produce design is rarely seen. MD systems can also be conical, with a series of tubes alternating between feed and condensate. In practice, these systems are still largely theoretical. All three of these types are similar enough in gap dimensions and flow regime that they can usually be modeled as flat plate systems, neglecting the curvature. The final type, hollow fiber membranes, is fundamentally different and must be modeled separately. These systems use small capillary tubes to transport permeate or feed, which

are contained in a larger chamber. Because these tubes are very small (e.g; 1 mm) [27], these flows are laminar, while the larger flat plate systems tend to use turbulent flow to minimize temperature and concentration polarization. Additionally, because the flow channels are fully-filled cylinders, the curvature cannot be neglected, and they must be modeled in polar coordinates. These systems are usually DCMD, although VMD [27], and AGMD systems have been developed as well [28].

2.1.1 Potentials of MD for Desalination Applications

MD has some prominent features that make it a promising candidate for desalination applications, particularly for hyper saline solutions. As a thermally driven process, water flux in MD is negligibly affected by the feed osmotic pressure as compared with other pressure driven membrane desalination processes such as reverse osmosis (RO) and nano-filtration (NF). As a result, the MD process can concentrate saline waters up to the saturation limits of salts in the feed waters. Given this capability, MD has been employed for treatment of concentrated brine from RO processes of seawater and gas drilling water [29-32], and hyper saline draw solutions from forward osmosis (FO) processes [33, 34]. Moreover, because the MD process does not involve high hydraulic pressure to achieve salt-water separation as in RO and NF, MD systems can be made from inexpensive non-corrosive materials for example plastics and aluminum alloys to reduce the process investment and operational costs. MD also inherits typical attributes of membrane processes, including modulation, compactness, and process efficiency; therefore, it requires significantly less physical and energy footprints as compared to conventional thermal distillation such as MSF and MED. Finally, the primary energy input to the MD process is heat at mild temperatures which are ranging from 40 to 80 ^{o}C. Low-grade heat

such as waste heat or solar thermal energy can be sourced to meet the energy demand of the MD process, leading to noticeable process energy cost savings. As a result, MD can be an ideal replacement for RO or MSF and MED in the desalination applications which require a low-cost and maintenance-free process or involve highly saline feed waters. These applications can be small-scale seawater desalination for fresh water provision in remote coastal areas, and treatments of brine following other desalination processes or hyper saline liquid desiccant solution used in air conditioning systems.

2.1.2 Temperature and Concentration Polarization Effects

Temperature and concentration polarization effects are intrinsic problems of the MD process [9, 12]. MD is a non-isothermal separation process in which heat and mass transfer simultaneously occur and are interconnected [9, 12]. The MD process involves three main steps: (1) the vaporization of the feed water at liquid-vapor interface in the feed channel, (2) the movement of water vapor through the membrane pores, and (3) the condensation of water vapor into distillate in the permeate channel. With the transfer of water, heat is taken away at the liquid-vapor interfaces on the feed and permeate sides of the membrane. As a result, the temperatures and salt concentrations at the liquid-vapor interfaces are different from those in the bulk feed and permeate, and boundary layers are established on both sides of the membrane as shown in Figure 2.3. These phenomena are termed temperature and concentration polarization effects. Temperature polarization effect renders the temperature difference between two sides of the membrane smaller than that between the feed and the distillate (or coolant) streams, thus reducing the process water flux. On the other hand, concentration polarization effect increases the salt concentrations at the membrane surface as compared with the bulk feed concentrations. For MD desalination of seawater or other

saline feed waters with similar feed salinity, the influence of concentration polarization effect on water flux is negligible as compared to that of temperature polarization effect [9, 35, 36]. For the MD process of hyper saline feeds, concentration polarization effect can greatly reduce water flux and increase the process propensity for membrane scaling. The negative effects of temperature and concentration polarization on MD water flux are more severe for the process operated at high temperature and low feed velocity [35]. Under extreme conditions, negative flux can occur as a result of polarization effects [12]. Thus, temperature and concentration polarization effects are deemed a drawback of MD, and are desired to be minimized [36-39]. Various methods such as using spacers, applying turbulent flow, transverse vibration, and aeration, and employing microwave irradiation have been approached to mitigate the effects of temperature and concentration polarization on MD performance [39, 40].

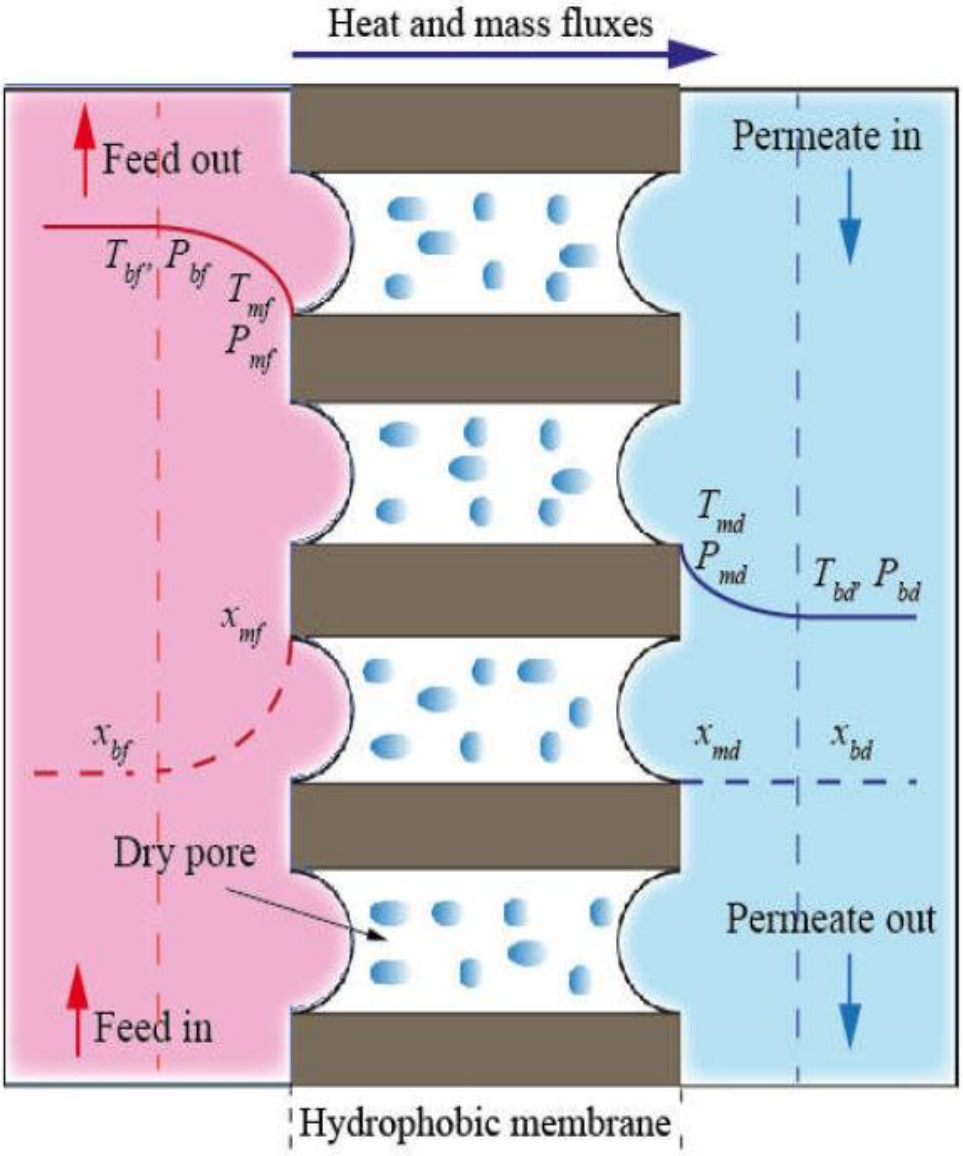

Figure 2.3 Temperature and concentration polarization effects in DCMD.
Source:[41]

The magnitude of the temperature polarization effect can be evaluated using the temperature polarization coefficient (∅). For the DCMD process, ∅ can be calculated using Eq. (2.1). The value of ∅ depends on the process fluid dynamic, and can vary from 0.4 to

0.7 [37]; however, a temperature polarization coefficient as high as 0.93 has been reported in the literature [35].

$$\emptyset = \frac{T_{mf} - T_{md}}{T_{pf} - T_{pd}} \tag{2.1}$$

Similarly, the concentration polarization coefficient ($\emptyset$) is used to assess the concentration polarization effect, and it is calculated as:

$$\emptyset = \frac{X_{mf} - X_{md}}{X_{pf} - X_{pd}} \tag{2.2}$$

The MD process can achieve a nearly complete salt rejection. Thus, salt concentration in the distillate can be ignored, and $\emptyset$ can be simplified as:

$$\emptyset = \frac{X_{mf}}{X_{bf}} \tag{2.3}$$

The mass transfer of water flux through the MD membrane is proportional to the water vapor pressure difference between two sides of the membrane, and is given as:

$$J = C_m \times (P_{mf} - P_{md}) \tag{2.4}$$

Where *Cm* is the membrane mass transfer coefficient, P_{mf} and P_{md} are the water vapour pressures at the liquid-vapour interfaces on two sides of the membrane. The water vapour pressure (*P*) of a saline solution at temperature *T* is calculated as:

$$P = exp\left(23.1964 - \frac{3816.44}{T - 46.13}\right) \times \chi_w \times \chi_w \tag{2.5}$$

Where χ_w and a_w are the molar fraction and activity of water, respectively. For aqueous saline solution, the water activity can be estimated using the molar fraction of salt (χ_s) as follow [42]

$$a_w = 1 - 0.5\chi_s - 10\chi_s^2 \tag{2.6}$$

The membrane mass transfer coefficient, *Cm*, can be calculated using empirical correlations. The selection of empirical correlations for *Cm* calculation is determined by mass transfer mechanisms inside the membrane pores. Possible mass transfer mechanisms within MD membrane pores are viscous flow, surface diffusion, Knudsen diffusion, and molecular diffusion [9, 43, 44]. However, surface diffusion is often neglected in general MD applications [12]. Thus, depending on the structural properties of membrane, the properties of transported vapor, and operating parameters, the dominant MD mass transfer mechanism can be viscous flow, Knudsen diffusion, molecular diffusion, or a transition between them [45, 46]. The calculation of water flux using the Eq. (2.4) involves the temperature and salt concentration at the membrane surfaces, hence it is impractical. Due to polarization effects, the temperature and salt concentration of the process solutions at

the membrane surfaces differ from those in the bulk solutions, and it is unviable to measure them. Alternatively, water flux of the MD process can be calculated using properties of the bulk process streams as follow:

$$J = K_m \times (P_{bf} - P_{pd}) \quad (2.7)$$

Where K_m is the process mass transfer coefficient, P_{bf} and P_{bd} are respectively the water vapour pressure of the feed and distillate streams. K_m depends on the membrane properties and operating conditions, and its value can be experimentally determined. It is noteworthy that temperature and concentration polarization might be included in the experimental determination of K_m.

2.1.3 Sources of Heat in MD

Energy-efficient desalination and water treatment technologies play a critical role in augmenting freshwater resources without placing an excessive strain on limited energy supplies. By desalinating high-salinity waters using low-grade or waste heat, membrane distillation (MD) has the potential to increase sustainable water production, a key facet of the water-energy nexus. However, despite advances in membrane technology and the development of novel process configurations, the viability of MD as an energy-efficient desalination process remains uncertain. Because of the challenges being faced by MD it is important to explore more opportunities for in MD membranes and system design because the energy efficiency of MD is limited by the thermal separation of water and dissolved solutes. However, in DCMD configuration, high fluxes could be achieved, however, heat losses are considerable and lead to low thermal efficiency process relative to the other MD configurations. Heat transfer through the membrane takes place via two ways; (1) latent

heat of vaporization carries out by the permeate flux and (2) conduction heat transfer through the membrane matrix [47]. Conduction heat transfer represents the heat loss during the separation process and it should be minimized to enhance the membrane thermal performance. Previous studies showed that about 20–50% of heat transferred through the membrane was by conduction due to higher heat transfer coefficient of the permeate side of DCMD configuration [48].

The solar energy is one of the most important energy sources in which MD systems can only depend on. Thermal energy from a solar collector such as flat plate solar collector [49] or evacuated tube solar collector [50], which work at low temperatures, is of interest in MD process. Also, photovoltaic (PV) cells can be used to convert solar radiation into electricity to provide the circulating pumps with the required power and consequently the MD system can be described as a stand-alone system with low energy consumption [51]. Another source of heating energy in MD is microwave irradiation. It is generally believed that microwave irradiation produces two effects: thermal effect and non-thermal effect (special effect) [52]. The special effect is an interesting and often confusing phenomenon in many researches, such as microwave-assisted synthesis or preparation of organic compounds [53-58], microwave-enhanced molecules diffusion in polymeric materials [59, 60], and microwave-assisted extraction or removal [61-65]. It is considered by many scholars that the light quantum (the quantum of electromagnetic radiation) of microwave has some special effects on reducing the Gibbs free energy of activation of reactions. The effects may be shown in two respects: (1) microwave energy is absorbed and stored in the internal molecule; (2) the arrangement of molecules is changed [52]. Moreover, in a liquid reaction system, the polar molecules irradiated by microwave change directions quickly to

form a “micro-agitation” effect, which can also be considered as a microwave special effect. For ionic solutions placed in a microwave field, the ions will migrate toward corresponding electric field direction and change migration direction continuously with the alternation of the electric field. Based on this principle, it has been confirmed that the rate of ion exchange can be enhanced by using microwave as heat source for ion exchange reactions [66]. This mode of ion migration and changing direction has a special effect on crystallization process.

There are only a few reports on the use of microwaves in membrane processes. They have been employed in gas separation where they successfully enhanced gas transfer in membrane pores [60]and in vacuum-based membrane distillation.[67, 68] These processes have been carried out in microwave ovens where the membrane is also exposed to the microwave, and can be problematic if the latter absorbs microwave. The placing of the membrane module in a microwave cavity is not always feasible, and this is particularly true in processes such as direct contact membrane distillation (DCMD) where the microwave would also heat the water in the permeate side and reduce the vapor pressure gradient. In addition, putting the whole membrane modules in microwave heaters can be challenging during scale up.

2.1.4 Membrane Pore wettability in MD

One vital requirement for the MD process to sustain its separation efficiency is the non-wettability of the membrane pores. To achieve a complete salt rejection, only water vapor is allowed to transfer through the membrane pores, and the pores must be in dry condition. Under certain conditions, liquid water can penetrate the membrane pores and render them wet. The resistance of the MD process to membrane pore wetting is evaluated using the membrane liquid entry pressure (*LEP*). The calculation of *LEP* is as follow:

$$LEP = -2B \times \tau_l \times \cos\theta / r_{max} \quad (2.8)$$

Where *B* is the geometric factor representing the pore structure, τ_l is the liquid surface tension, θ is the liquid-solid contact angle, and r_{max} is the maximum membrane pore radius. According to Lawson and Lloyd [42], the membrane pores become wetted when the pressure difference between liquid phase and vapor phase at the pore entrance exceeds *LEP*.

Factors that can lead to membrane pore wetting during the MD process are the deposition of contaminants in the feed water on the membrane surface and the resultant degradation of the membrane. As implied in the Eq. (2.8), a higher *LEP* value can be achieved when using a more hydrophobic membrane (i.e. $\Theta > 90^o$) with the feed solution having a high surface tension (τ_l). Most membranes used in MD have water-membrane contact angle in the range from 120^o to 130^o [69], and fabricated surface-modified membranes with water-membrane contact angle as high as 160^o and 178^o have been proposed for the MD process for desalination applications [23, 70]. Contaminants depositing on the membrane surface can alter its hydrophobicity, thus reducing *LEP* and increasing the risk of membrane pore wetting. Moreover, organic contaminants such as

surfactants and detergents can greatly reduce the surface tension of the feed water [71], leading to further reduction in *LEP*.

2.1.5 Membrane Fouling and Scaling in MD

Membrane fouling is a major hindrance to the commercialization of MD for water treatment and desalination [15, 72]. Fouling reduces permeability, shortens the lifetime of membranes, and increases energy consumption. Consequently, membrane fouling raises the operational costs of the MD process. The investment cost of the MD process is also increased because of additional pre-treatment facilities and chemicals required to prevent and control fouling [72, 73].

Membrane fouling in MD is defined as the accumulation of undesirable deposits onto the membrane surface or into the membrane pores leading to a decline of membrane efficiency [74, 75]. The formation of unwanted materials adds extra resistance to the total mass transfer resistance of the MD process. The undesirable deposits might be particulates, gels formed by organic substances, precipitated crystals of sparingly soluble salts, and biofilm formed by microorganisms. Membrane fouling is categorized into four types, namely colloidal fouling, organic fouling, scaling, and biofouling according to the nature of particles that induce fouling. Amongst these types, organic fouling and scaling are the most prevalent during the MD desalination process [74, 75].

Organic fouling is a result of adsorption of dissolved organic substances such as oil, macromolecules, protein, humic acids onto membrane surface. The accumulation of these organic matters on the membrane surface leads to a decline in membrane permeability. It is worth mentioning that despite their low concentration in the feed water, organic foulants often cause severe declines in MD water flux because they can form

complexation with calcium scales in the feed water [76, 77]. Moreover, hydrophobic membranes are more prone to organic fouling due to hydrophobic adsorption of organic materials to the membrane surface [76, 78].

Scaling (or inorganic fouling) in the MD process is caused by the precipitation of sparingly soluble salts at their super-saturation state. The most likely scalants faced in MD desalination are calcium sulphate ($CaSO_4$), calcium carbonate ($CaCO_3$), and silicate [15, 79-81]. These scalants have limited and temperature-inverse solubility (except silicate) in the MD operating temperature range [82]. During the MD process, when water is extracted from the feed solution, the concentrations of the sparingly soluble salts in the feed channel increase and might reach super-saturation, posing a high risk of scaling. The scale formation on the membrane can constrain the MD desalination process from achieving high water recovery ratios [79, 80].

MD operating parameters exert great effects on the scale formation rate and the scale morphology. Gryta [83] reported that increasing feed temperature resulted in a higher rate of the carbonate scale formation, and low feed flow velocity led to a more compact deposit layer on the membrane. A similar trend was observed in the study of Wang et al. [84] . Nghiem and Cath [15] observed more severe scale formation of $CaSO_4$ than that of $CaCO_3$ and silicate, and they also found that increased feed temperature and $CaSO_4$ concentration led to a decrease in the induction time and an increase in the $CaSO_4$ crystal size. He et al. [80] declared that the co-precipitation of $CaCO_3$ and $CaSO_4$ formed more adherent and tenacious deposit layers on the membrane than those consisted of single salts.

The scale formation on the membrane in MD is also influenced by the temperature and concentration polarization. Due to the polarization effect, concentrations of the

sparingly soluble salts in boundary layers adjacent to the membrane are higher than those in the bulk feed solution, hence increasing the scale formation tendency [82, 84, 85]. In contrast, the temperature polarization effect reduces the temperature of the feed solution next to the membrane, and might increase the solubility of sparingly soluble calcium salts; therefore, it lowers potential for the scale formation. However, the influence of the temperature polarization effect on the scale formation is trivial in comparison with that of the concentration polarization effect [80, 82]. It is noteworthy that unlike sparingly soluble calcium salts, silica has solubility proportional to temperature, thus temperature polarization tends to raise the deposition of silica on the membrane surface [81].

2.2 MD for Seawater Desalination Applications

2.2.1 Membrane Fouling and Scaling in Seawater MD Desalination

There is a consensus that MD is much less susceptible to membrane fouling than pressure-driven filtration processes such as RO for seawater desalination applications. Unlike in RO, in MD water permeates through the membrane in vapor phase, while liquid water and foulants are retained on the membrane surface. The MD process does not involve high hydraulic pressure on the membrane surface to drive the water transport through the membrane as RO does. Membrane fouling in MD is caused by the adsorption of foulants onto the membrane surface. As a result, the seawater MD desalination process requires noticeably less feed water pre-treatment as compared to RO.

The MD process demonstrates enormous potential for seawater desalination with high water recovery ratios. As a thermally driven separation process, water flux in MD is negligibly affected by the feed osmotic pressure. Therefore, the MD process can achieve water recovery ratios appreciably higher than those of the seawater RO process. In the

context of high water recovery, inorganic membrane fouling (membrane scaling) caused by the precipitation of sparingly soluble salts such as salts of calcium, magnesium, Barium, and silicate that counts as considerable challenge to the sustainable seawater MD process.

There has been abundance of studies on membrane scaling and mitigation techniques in MD as summarized in the two recent review papers [75, 86]. These studies have elucidated the detrimental effects of membrane scaling on the process performance (e.g. water flux and distillate quality), and examined various techniques to alleviate and control membrane scaling during the MD process. Notable examples include the studies by Nghiem and Cath [79] ,Hickenbottom et al. [87] , He et al. [80], Martinetti et al. [32], Mericq et al. [31], Adam et al. [88], Chen et al. [89], Ge et al. [30], Hou et al. [90], Peng et al. [91], and Zhang et al. [29]. However, most of these scaling studies used lab-scale DCMD systems with either synthetic saline feed solutions or brine from the seawater RO desalination process. None of the previous studies has explored membrane scaling and mitigation techniques during seawater desalination using the pilot or large-scale AGMD process. It is worth reiterating that AGMD together with DCMD are the most used MD configurations for seawater desalination applications. Membrane scaling in the DCMD process might differ from that during the AGMD process given the much lower operating flux of AGMD as compared to DCMD. In addition, the characteristics and hence the scaling propensity of synthetic saline solutions and seawater RO brine are different from those of actual seawater. Last but not least, some membrane scaling mitigation techniques proposed in the previous studies (e.g. resetting the scale induction period by regular membrane flushing with fresh water [15], flow and temperature reversal [87], and ultrasonication [90, 92], microwave irradiation [93, 94],antiscalant materials [95] are

effective for DCMD, but might not be practicable for AGMD. As a result, membrane scaling during the AGMD process of actual seawater, particularly under operating conditions practiced for pilot or large-scale processes, is still a research gap that needs addressed.

2.2.2 Energy Consumption of Seawater MD Desalination

Together with membrane scaling, intensive energy consumption has been considered a hindrance to the realization of MD for seawater desalination applications. As a phase-change separation process, MD consumes huge amount of thermal energy (i.e. heating and cooling) to facilitate the phase conversion of water from liquid to vapor and vice versa. The transfer of the latent heat that is associated with the transfer of water coincides with the heat conduction through the membrane during the MD process. The heat conduction through the membrane, which is the heat loss, can account for up to 50% of the total heat input of the MD process [12]. As a result, most MD processes reported in the literature demonstrate poor energy efficiency with specific energy consumption of several orders of magnitude higher than that of RO [14, 96, 97].

It is noteworthy that specific thermal energy consumption (*STEC*) of the MD processes reported in the literature is widely dispersed as recently highlighted by Khayet [47]. The *STEC* of the MD process can differ in 3 orders of magnitude, ranging from as low as 1 up to 9,000 kWh/m3 [47]. The wide dispersion in *STEC* values is attributed to the variation in the configuration, membrane module geometry, and operating conditions of the MD process [47].

As a notable example, Carlsson [98] reported a very low *STEC* of 1.25 kWh/m3, but failed to provide any analytical details and operating parameters of the MD process

used in his study. Koschikowski et al. [99] reported a *STEC* value of 117 kWh/m3 for a MD system with an 8 m^2 spiral-wound AGMD membrane module at 75 ^oC evaporator inlet temperature and 350 L/h water flow rate. A larger AGMD system (i.e. with membrane area of 40 m^2) exhibited a higher *STEC* value ranging from 200 to 300 kWh/m^3 [100]. Much higher *STEC* values were reported for the MD processes using DCMD configuration. Of a particular note, Criscuoli et al. [101] demonstrated a DCMD process with really high *STEC* values ranging from 3500 to 4580 kWh/m^3.

Thermal efficiency of the MD process can be significantly enhanced, and thus the process *STEC* can be reduced by recovering the latent heat associated with the water vapour transfer.

In AGMD, the recovery of the latent heat can be achieved inside the membrane module. The feed water can be fed to the coolant channel to act as a coolant fluid, and in tandem to be preheated by the latent heat of water vapor condensation. Then, the preheated feed water can be additionally heated by an external heat source to reach a desired temperature prior to entering the feed channel of the AGMD membrane module (Figure 2.1). Thus, *STEC* of the AGMD process can be noticeably reduced. Operating conditions, including feed inlet temperature, feed salinity, and particularly water circulation rate, are expected to exert strong influences on the *STEC* of the AGMD process. It is noteworthy that no previous studies have systematically elucidated the influences of operating conditions on thermal and electrical energy consumption of the AGMD process with actual seawater. Optimization of the seawater AGMD desalination process at pilot or large-scale level remains a gap in the MD literature.

Unlike in AGMD, in DCMD the heat recovery can be achieved using an external heat exchanger [102]. The latent heat accumulated in the distillate stream is recovered to preheat the feed stream in the heat exchanger. When the heat exchanger is coupled with the DCMD membrane module, the relative flow rate between the feed and the distillate stream and the surface areas of the heat exchanger and the membrane module strongly determine the process *STEC* [102]. The DCMD process obtains minimum *STEC* at a critical relative flow rate and with infinite heat exchanger and membrane module surfaces [102]. In practice, however, it is unfeasible to have heat exchanger and membrane module with infinite surfaces.

Thermal efficiency of the DCMD process can also be improved by brine recycling. In the DCMD process, particularly for the small-scale system with short membrane channels, the warm brine leaving the membrane module contains a considerable amount of sensible heat. When the brine is recycled in the process, the brine sensible heat can be utilized, hence reducing the total heat demand and *STEC* of the process. Brine recycling also helps enhance the utilization of the available membrane surface area to increase the water recovery ratio of the DCMD process. Indeed, Saffarini et al. [103] have suggested brine recycling for MD thermal efficiency improvement. A major challenge to brine recycling in seawater DCMD desalination is to manage the negative influence of membrane scaling and increased feed salinity on the water flux and salt rejection of the process. It is noteworthy that brine recycling for optimization of the seawater DCMD process has not yet been experimentally evaluated.

2.2.3 MD for Produced Water Treatment

Shale oil and gas is an unconventional energy resource that is found in relatively impermeable rock and requires hydraulic fracturing to recover the hydrocarbons [104]. The shale oil and gas industry has significantly improved the energy security of the United States, and has disrupted the oil and gas markets by driving down prices worldwide [105]. However, shale oil and gas production consumes substantial amounts of freshwater and produces vast quantities of wastewater [106-108]. For example, shale oil and gas production in the U.S. has led to a total water usage of 940 billion liters from 2005 to 2014, and has produced 775 billion liters of hazardous wastewater [106]. There are growing concerns associated with the handling and disposal of shale oil and gas wastewater. The majority of this wastewater is currently injected underground into deep and isolated formations, but this technology may induce seismic events and is constrained by geological and legal restrictions [104, 109, 110]. Also, the discharge of shale oil and gas wastewater into publicly owned treatment works (POTWs) pollutes the water environment due to its high salinity and toxicity [104, 111, 112]. Furthermore, many of the western shale plays in the U.S. coincide with areas suffering high to severe water stress [108]. Therefore, effective treatment and reuse of shale oil and gas wastewater as an additional source for beneficial purposes will address the dual challenges of water scarcity and pollution associated with the shale oil and gas industry, thereby promoting sustainability at the water-energy nexus. Shale oil and gas wastewater, including flow back and produced water, contains high concentrations of total dissolved solids (TDS) and complex organic and inorganic components [112-114]. Hence, the treatment of such complicated wastewater is an extremely challenging task. Although reverse osmosis (RO) is the most energy efficient

desalination technology [5], the TDS of shale oil and gas wastewater (up to 360,000 mg/L) typically approaches or exceeds the salinity limit of RO (~70,000 mg/L TDS) [115], rendering RO an inappropriate technology for shale oil and gas wastewater treatment. Membrane distillation (MD) is a hybrid thermal, membrane-based desalination technology, which utilizes a partial vapor pressure difference to drive the transport of water vapor across a hydrophobic, microporous membrane [12, 116]. Like other thermal desalination processes, MD is able to desalinate hypersaline feed water beyond the salinity limit of RO [117]. The capability of MD to utilize low-grade heat (e.g., geothermal energy), which is commonly contained in shale oil and gas wastewater [115], reduces primary energy consumption and operational costs of the treatment system [117]. Further, the modular configuration of a MD system renders it adaptable to the fluctuation in both quantity and quality of shale oil and gas wastewater [117]. Thus, MD is a promising technology that is potentially suitable to the desalination of shale oil and gas wastewater [118]. Since MD is typically used in the desalination of concentrated feed water with high salinities, MD membranes are facing high concentrations of foulants and scalants. As a result, membrane fouling and scaling significantly constrain the efficiency of MD [74, 119]. Also, pore wetting, which is caused by low surface tension foulants, results in significant salt passage and may eliminate the desalination function of the MD process [120, 121]. Accordingly, various modification approaches have been applied to MD membranes to hinder fouling and wetting, primarily by optimizing the wetting properties of membrane surface [121-129]. For example, super hydrophobic or omniphobic membranes with high wetting resistance have been fabricated by introducing both a re-entrant structure and low surface tension materials [121-124, 128, 129]. Recently, a thin in-air hydrophilic layer has been

coated on MD membrane surface to reduce organic fouling [125, 126, 130]. The underwater oleophobic property of the hydrophilic layer deters the attachment of hydrophobic foulants (e.g., oil droplets) to the membrane surface and prevents pore blocking [125, 126]. To date, novel MD membranes developed by means of the above approaches have been dominantly tested with synthetic feed solutions containing individual foulants. However, the performance of these MD membranes in desalinating real industrial wastewater with complex and variable chemical compositions has not been systematically understood.

2.3 Membranes

2.3.1 Nanostructured Membranes

As already mentioned, the two important membrane characteristics are their flux and selectivity. These are controlled by chemical and physical characteristics, morphology as well the presence of and absence of pores. A broad classification for membranes is that between the porous and nonporous. This essentially refers to the presence or absence of pores in the membrane. The former has openings through which select molecules pass. Movement through these membranes can also be by size exclusion and is used in applications such as nanofiltration and dialysis. Separation can also be accomplished by hydrophobicity, for example a hydrophobic porous membrane does not allow water to permeate. During extraction, two liquid phases meet at the pores, and during pervaporation the analyte vaporize at these sites. Non-porous membranes are solid (pore-free) structures and the molecules must move through them via diffusion, and therefore the partitioning of the analyte is critical.

The membrane may also have diverse structures. For instance, homogenous (isotropic) membranes are uniform throughout while asymmetric (anisotropic) and composite thin-films are not. Isotropic membranes include micro porous, nonporous dense and electrically charged membranes. Separation in micro porous membranes (pore size between 10^1-10^4nm) is a function of particle and pore size distribution, and are used for processes such as microfiltration. In nonporous dense membranes, transport is via diffusion and separation is influenced by partition coefficient as well as diffusivity of components in the membrane. These types of membranes are commonly used for extraction, reverse osmosis and pervaporation. Anisotropic membranes refer to those in which the material, the porosity and pore size vary throughout the structure and include thin-film composites and Loeb-Sourirajan membranes [131]. The composite membrane usually consists of different polymers where the surface layer determines selectivity, while the porous layer serves as a support.

Homogenous solid membranes such as silicone tend to provide lower fluxes but higher selectivity. On the other hand, the porous membranes provide higher flux but lower selectivity. Composite membranes are a compromise. The porous part provides for a high flux, while the solid layer on top provides selectivity. For example, a one-micron silicone layer on top of a polypropylene composite provides high VOCs flux while preventing large amounts of water from permeating through. For thin-film composites, the thin surface layer represents a small percentage of the overall membrane but is responsible for much of the membrane's selectivity. Scanning electron microscope (SEM) images of porous and composite membranes are shown Figure 2.4.

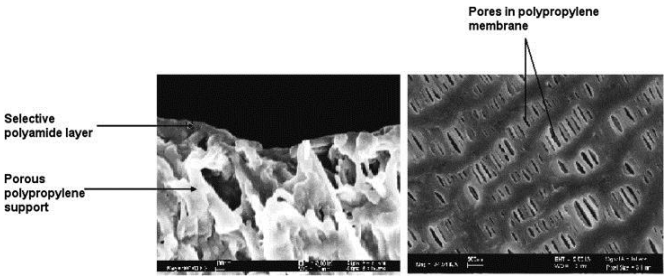

Figure 2.4 SEM of thin-film composite (polyamide surface layer supported by polypropylene) and microporous polypropylene.
Source:[132]

An assessment of permeability and selectivity has shown asymptotic limitations on the separation capability of pure polymeric membranes. Efforts at improving these have looked at the development of novel materials as well as the modification of their structure and morphology. Recent interest has been focused on developing strategies for incorporation of nanomaterials such as carbon nanotubes, zeolites, carbon black, gold in membrane matrix or surface for the generation of nanostructured membranes with higher flux and selectivity.

The rate of mass transport through the membrane, Q, is controlled by the diffusion of solute can be estimated under steady-state conditions by use of the following equation:

$$Q = BAD(\Delta P)C_w/b \qquad (2.9)$$

Where, *A* is the surface area of the membrane, *D* is the diffusion coefficient in the membrane material, ΔP is the vapor pressure (or concentration) gradient, *b* is the thickness of the membrane, *B* is a geometric factor defined by the porosity of the membrane and C_w is the inlet concentration. The presence of nanomaterials can affect several of these parameters; *B* and *D* are altered by the presence of the nanoparticles, while the partition coefficient is affected by the physical/chemical properties of the nanomaterials while their high surface area can facilitate greater flux. Therefore, an important consideration

associated with the incorporation of nanomaterials in the membranes are their chemical properties, size distribution, agglomeration, interaction with the membrane matrix, effect on porosity, surface area and morphology. Additionally, such nanomaterials can be effective sorbents. Together these can enhance the selective partitioning as well as the permeation of the solute of interest.

A common approach to the fabrication of nanostructured membrane involves adding the filler material to a polymer solution followed by film casting or spinning and is referred to as the mixed matrix membrane (MMM). Good polymer-filler adhesion and uniform dispersion allows the formation of uniform membranes of submicron thickness. Such membranes possess some unique properties that benefit from the polymer as well as the nanofillers. Due to their small sizes, the nanoparticles can be implemented within micron or submicron thick films to serve as high flux barriers. For example, in fabrication of a polymeric layer tightly packed with nanomaterials like zeolite or CNTs form a dense mixed matrix region. Incorporation of nanocarbons within polymeric membranes have been studied to increase permeate flux in extraction and pervaporation processes [133, 134]. Dense arrays of aligned MWNTs can potentially be used for solute transport though the tube pores [134]. These exceptionally high transport rates as demonstrated by the CNTs was attributed to the specific pore size of the nanotubes, molecular smoothness of the surface and hydrophobicity and has been proposed as means for desalination [135] via membrane distillation. Additionally, ability to tailor surface properties by chemical and biochemical functionalization of a specific nanomaterials is an attractive route for membrane development. Similarly, they can be incorporated in porous structures where they alter the shape, size selective nature and allow molecular sieving [136].

2.3.2 Carbon Nanotube Membranes

Since their discovery in 1991, CNTs have received much attention. Carbon nanotubes (CNTs), which are essentially graphene sheets rolled into tubes as single-walled (SWNT) or multiple-walled (MWNT) structures, can be interesting materials for membrane systems. There has been much interest in these materials because of their excellent thermal, electrical and structural properties. In addition, their favorable adsorption properties have fostered their use as sorbent materials in many analytical and extraction processes [137, 138]. They are found to be excellent sorbents for volatile and semivolatle organics [139] as well as small molecules such as methane [140], water vapors [141] and other gases [142]. Consequently, they have found applications in chromatography as well as air and water sampling. They have also been used as effective media in SPE [143] and SPME [144]. In membranes, they can increase the selective partitioning and permeation of the solutes of interest.

In typical CNT membrane-based liquid extraction, when the two phases contact at the pores, the interactions can take place via rapid solute exchange on the CNTs, thus increasing the effective rate of mass transfer and flux. The high aspect ratio of the CNTs dramatically increases the active surface area as well which contribute to flux enhancement. Fabrication of CNT membranes are discussed in the following section.

2.3.2.1 Carbon Nanotube Immobilized Membranes (CNIM). Mitra et al. [145] immobilized Carbon Nanotubes within the pores of membranes leading to the development of unique membrane structure referred to as the CNIM. This was achieved by immobilizing CNT using dispersion in a polymer solution. The dispersion was injected into the lumen of a conventional hollow fiber under pressure. This served as the immobilization step, and the

polymer served as the glue that held the CNTs in place. Such membranes were robust, thermally stable and possessed high selectivity. The goal here was to immobilize CNTs without covering its active surface with the polymer, or having a thick polymeric layer over it. This is advantageous as well as challenging. However, accomplishing this is highly desirable so that their surface is free to interact directly with the solute. The membrane produced from this method has been used for liquid-liquid extractions, membrane distillation and pervaporation [145-149]. Typical membrane produced by this process is shown in Figure 2.5 (a –b). Additionally, Figure 2.5 (c – d) shows the typical SEM image of CNIM membrane in comparison to the unmodified polypropylene membrane.

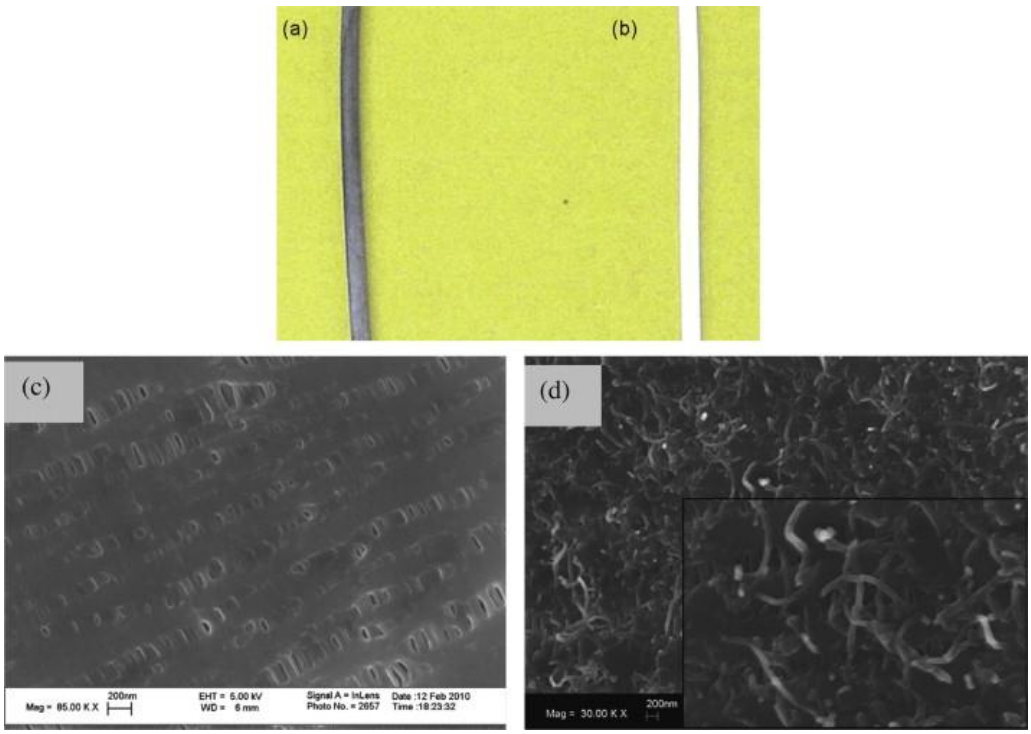

Figure 2.5 (a) Photograph of carbon-nanotube immobilized membrane (CNIM); (b) photograph of pure polypropylene; (c) SEM image of unmodified polypropylene membrane; and, (d) CNIM. *Source:[145]*

2.3.2.2 Carbon Nanotube Nanocomposite Membrane. Initial attempts at incorporating CNTs in membranes involved the formation of CNT-nanocomposite by solution casting. Peng and coworkers[150] fabricated membranes with chitosan functionalized MWNTs. Surface decoration/wrapping of carbon nanotubes with chitosan biopolymer led to dissolution and dispersion in PVA solution. The mixture was subsequently mechanically stirred, ultrasonically agitated and cast onto a glass plate. The pristine nanocomposite was dried to form 80 μm thick membrane. The membrane was used in pervaporation of benzene/cyclohexane (50/50, w/w) mixture.

2.3.2.3 Aligned Carbon Nanotube Membranes (ACNTs). Although great deal of practical and fundamental studies has been reported on CNT- Mixed Matrix Membrane (MMM), related researches in this area did not receive much attention until Hinds et. al. [134] reported aligned carbon nanotubes (ACNTs) membrane using CVD on quartz substrate across a polystyrene film**.** The quartz substrate (2cm x 2cm) with aligned multiwalled CNTs was coated drop wise with 50% (by weight) of polystyrene (PS). Excess polymer was removed by spin coating at 3000 rpm for 1 minute. Following that, neat toluene was poured dropwise onto the sample and allowed to set for 1 minute to further dissolve excess polymer covering the tops of CNTs and spin coated for 1 minute at 3000 rpm. Finally, the sample was dried in a vacuum oven at 70^{o}C for 4-5 days under 25-inch Hg pressure to fabricate the aligned CNT/PS composite film which was removed from quartz substrate by HF solution (1:2 by volume). Additionally, plasma oxidation was performed to remove excess polymer as well as open CNT tips. The resulting free standing composite films as formed, with the CNT alignment intact from top to bottom were accessible to the outer molecule both sides of the formed membrane. Figure 2.6 illustrates the fabrication of cross sectional schematic of aligned CNT (ACNTs) membrane fabrication steps.

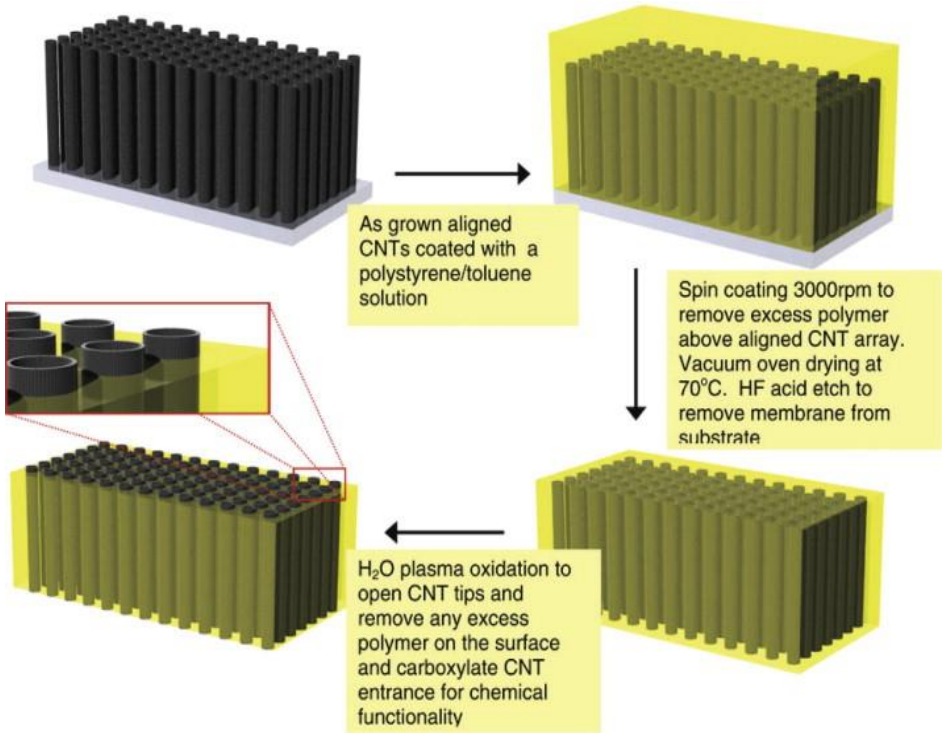

Figure 2.6 Aligned carbon-nanotube (CNT) membrane fabrication steps.
Source:[151]

2.3.3 Application of Nano Structured Membranes

The nanostructured membranes are relatively new developments and even newer when it comes to analytical chemistry. Some applications that show a great deal of promise are presented here. In the analytical field, the largest application has been with the incorporation of CNTs. This is an attractive because the CNTs are excellent sorbents that can enhance partition coefficients, increase the selectivity and result in enhanced enrichment and extraction efficiency. Functionalization of CNTs can also be used to alter selectivity because it alters solute solvent interactions.

2.3.3.1 Carbon Nanotube Membranes in Pervaporation. The outstanding sorbent characteristic of CNTs has led to the exploration in pervaporation. Pervaporation performance of the resulting MWNTs incorporated polyvinyl alcohol PVA-MMM) was carried out by Choi et al. [152] where an increase in flux and a decrease in the selectivity was reported with the increase in MWNTs content. These were attributed to two key factors: the crystallinity of membrane and the molecular transport through the nanotubes. Higher amount of MWNTs created strong interaction with PVA and therefore prevented the packing of molecules to form crystal, resulting in a decrease in the crystallinity of the PVA matrix. Peng et al. [153] studied the pervaporation properties of CNT-PVA membranes for the separation of benzene/cyclohexane mixtures. The CNTs were dispersed with cyclodextrin by grinding during the formation of MMM in order to reduce the aggregation and improve the compatibility of CNTs in the polymer matrix. The resulting MMMs exhibited the highest benzene permeation flux of 61.0 gm^{-2} h^{-2} with separation factors of 41.2 for the mixture with weight percent of 1:1. Upon the comparison of pervaporation properties with the PVA and cyclodextrin dispersed PVA membranes, the MMMs prepared through the incorporation of CNTs demonstrated enhanced mechanical strength properties and pervaporation properties. Mondal and Hu [154] have reported the adverse effects of the presence of high MWNT content in pervaporation process. Functionalized MWNTs were incorporated into segmented polyurethane (SPU) to study the water vapor transport properties. In such MMM system, MWNTs were found to influence both crystalline and amorphous regions of SPU matrix by imparting stiffness to the polymer matrix, particularly when added in excess.

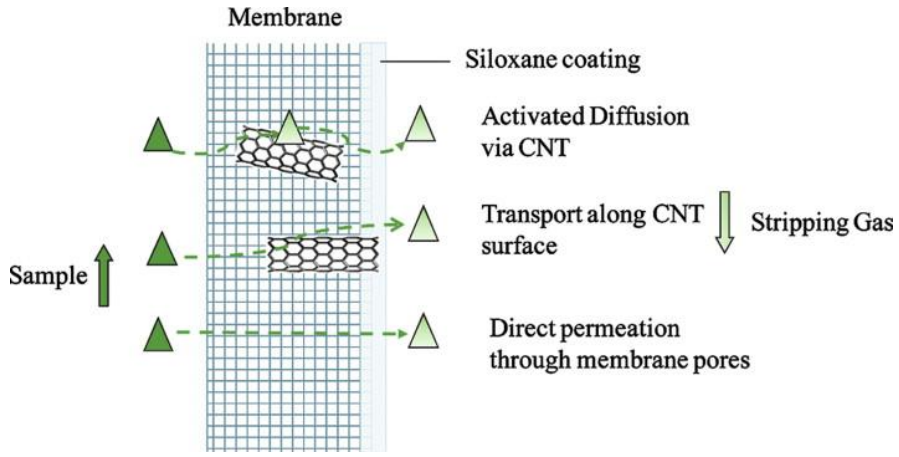

Figure 2.7 Mechanism of pervaporation in carbon-nanotube immobilized membrane (CNIM). *Source: [147]*

Sae - Khow and Mitra [147] reported the development of novel CNIM using a composite membrane for the pervaporative removal of organics from an aqueous matrix. The CNIM demonstrated several advantages including enhancement in organic removal and mass transfer by 108 and 95% respectively and also enhanced recovery at low concentrations, lower temperatures, and higher flow rates. The nanotubes provided additional pathways for enhanced solute transport, affecting both the partitioning and diffusion through the membrane as shown in detailed mechanism depicted as Figure 2.7.

2.3.3.2 Carbon Nanotube Membranes in Membrane Extractions. The sorbent characteristics of the CNT membrane have been exploited in membrane extraction as well. Eshaghi et al. [155] demonstrated a three-phase supported liquid membrane consisting of an aqueous (donor phase), organic solvent/nano sorbent (membrane) and aqueous (acceptor phase) system operated in direct immersion sampling mode. The MWNTs

dispersed in the organic solvent were held in the pores of a porous membrane supported by capillary forces and sonication. Their proposed method allowed the very effective and enriched recuperation of an acidic analyte into one single extract. The method showed good linearity in the range of 0.0001-50 micro g/L, reproducibility and detection limits in the pico gram/L with enrichment as high as 2100.

Hylton et al. [156] used CNIM to carry out three-phase supported liquid micro extraction (μ-SLME) as well as liquid-liquid extraction (μ-LLME). The immobilization was carried out such that the CNT surface was accessible to adsorption/desorption. Several organic compounds including haloacetic acids and non-polar organics were studied using a hollow fibre CNIM. The incorporation of MWNTs improved the extraction efficiency by as much as 144%. Sae Khow et al. [145] reported the effect of both polar and non-polar compounds as analyte and reported that the enrichment factor enhancement by 30-113% using CNIM. O.Sae Khow and Mitra[146] also demonstrated the simultaneous extraction and concentration on CNIM, where the CNTs enhanced both these phenomenon (Figure 2.8) leading to superior performance in terms of higher enrichment factors and extraction efficiency. The CNTs immobilized in the pores of a polypropylene hollow fiber, led to nearly 250% enrichment enhancement over the unmodified parent membranes. The detections limits for polycyclic aromatic compounds were between 0.042 and 0.25 μg/L. This flow through system was designed for on-line extraction in automated analysis.

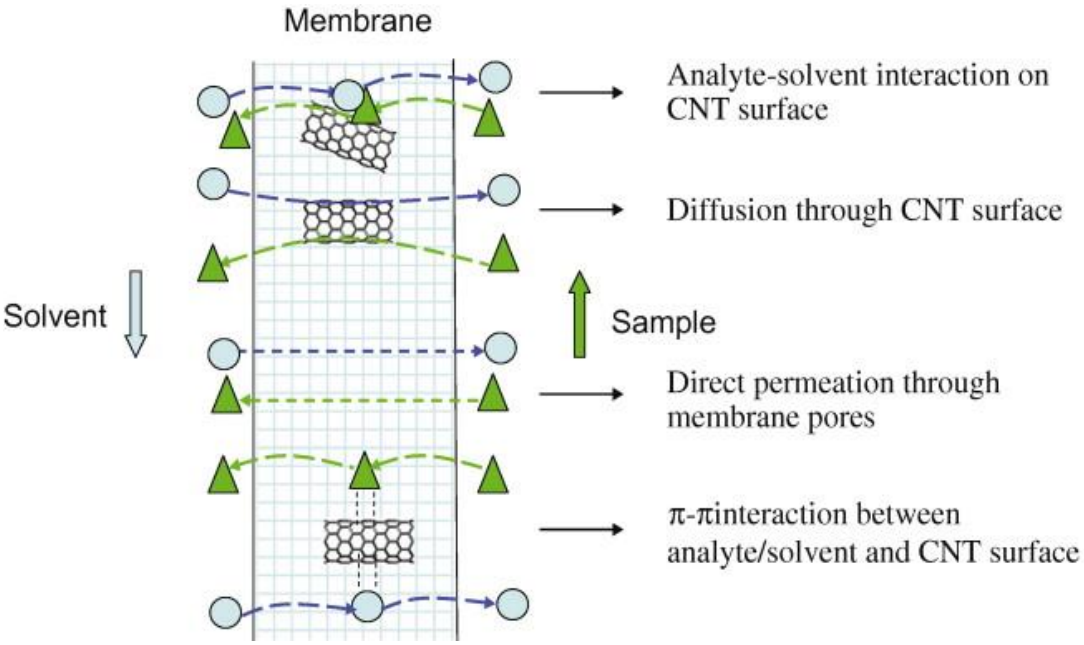

Figure 2.8 Carbon-nanotube (CNT)-assisted extraction and enrichment. Triangles represent the analyte molecules and the circles represent the solvent molecules. *Source: [146]*.

More recently, Bhadra et al. [157] demonstrated for the first time that Carbon Nanotubes could be immobilized on the surface of solid polymeric membranes, which can also lead to enhanced extraction of polar and non-polar organics. A polar membrane was used on which nonpolar CNTs were immobilized. This CNIM combination showed dramatic enhancement of enrichment factor by 92% and solvent retention by as much as 29%.

2.3.3.3 Carbon Nanotube Membranes in Membrane Distillation. A novel analytical method that also used carbon nanotube based membranes is membrane distillation (MD). Mitra et. al. [148, 149] recently reported this real-time, online concentration technique, where the aqueous matrix is removed from the sample to enhance analyte enrichment. Therefore, MD is a universal method that can be used for a wide range of compounds, and

is unlike conventional membrane extractions that rely on the permeation of the analyte into an extractant phase. An alternate to thermal distillation, here a heated aqueous solution (or polar solvent such as ethanol) is passed through the lumen of a hydrophobic hollow fiber, which prevents the transport of the liquid phase across the membrane. However, the solution is partially converted to vapor (60-90^{o}C) and MD relies on the net flux of this vapor from the warm to the cool side of the membrane. The driving force for the vapor transport is determined by the vapor pressure difference across the membrane, which depends upon the temperature difference.

MD provides a complimentary approach to conventional membrane extraction which relies on the selective permeation of the analyte, and is often a challenge because selective membranes for diverse analytes are not always available. MD with CNIM (Figure 2.9 (a)) has shown great promise because the CNTs were instrumental in increasing water vapor as well as solvent flux. The mechanism of MD with CNTs is shown in Figure 2.9(b) for removing polar solvents for concentrating pharmaceutical compounds. Comparison between MD performance with and without CNTs is shown in Figure 2.9(c). Enrichment using CNIM [149] doubled compared to membranes without CNTs, while the methanol flux and mass transfer coefficients increased by 61% and 519%, respectively. Additionally, the carbon nanotube enhanced MD process showed excellent precision (RSD of 3–5%), and the detection limits for pharmaceutical compounds were in the range of 0.001 to 0.009 mg L^{-1}. Overall, it was postulated that the CNTs served as sorbent sites thereby providing additional pathways for enhanced solvent vapor transport, thus enhancing preconcentration.

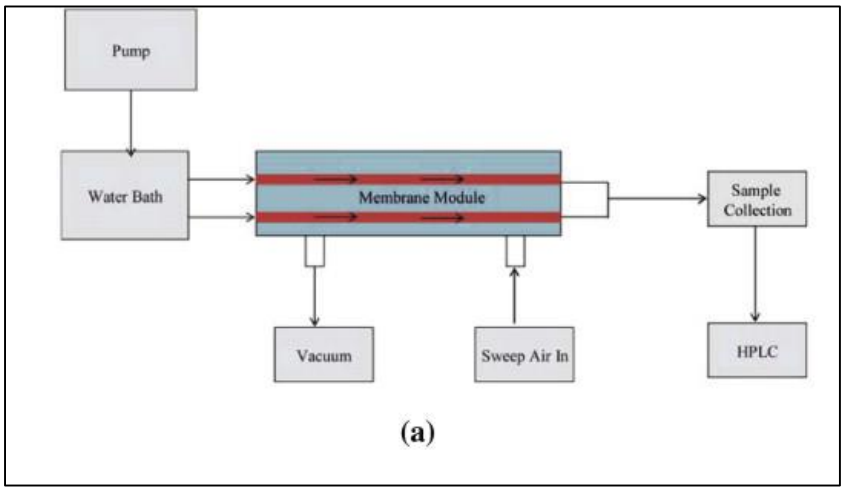

(a)

(b)

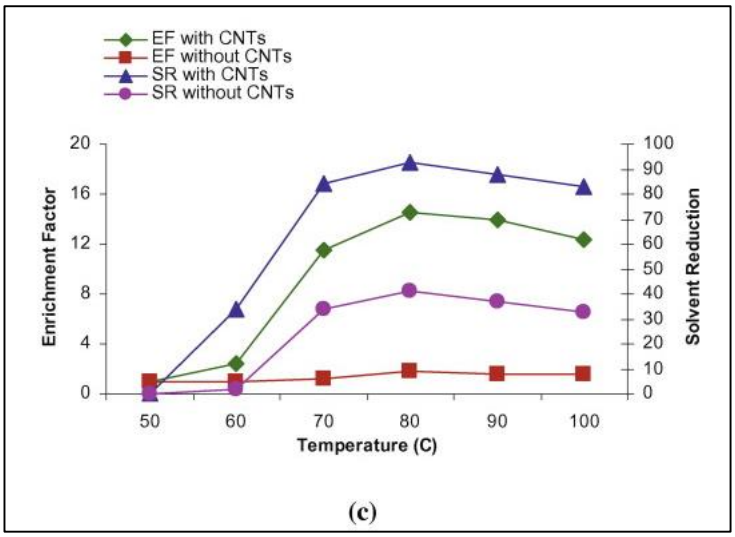

(c)

Figure 2.9 (a) Membrane distillation (MD) as an on-line preconcentration technique; (b) membrane device; (c) MD performance on unmodified membrane and carbon-nanotube immobilized membrane (CNIM).
Source: [149].

CHAPTER3

REDUCTION OF SCALING IN MICROWAVE INDUCED MEMBRANE DISTILATION ON CARBON NANOTUBE IMMOBLIZED MEMBRANE

3.1 Introduction

With water scarcity looming all over the horizon, the generation of potable water from sea/brackish water as well as the saline waste management are becoming important desalination technologies. Desalting is also important for zero to minimal liquid discharge (ZLD) systems that eliminate liquid waste from production facilities by recovering all salts and reusing the purified water [117, 158, 159]. Typical ZLD units use thermal distillation techniques because Reverse osmosis (RO) has limited applicability at high salinity encountered in ZLD [160, 161].

Compared to conventional thermal distillation, the relatively low temperature operation (50–90°C) and the lower CAPEX (capital expenditure) make membrane distillation (MD) an attractive alternative [9, 17, 18, 21]. In MD, the driving force is a temperature induced vapor pressure gradient generated by having a hot feed and a cold permeate [162]. The low operating temperature in MD makes desalination possible using low grade heat sources such as low pressure steam and solar energy [163-167]. Compared to reverse osmosis (RO) a major advantage of MD is that while the former uses dense hydrophilic membranes, MD uses microporous hydrophobic membranes that are less prone to fouling, and MD can be used to treat water with higher salinity [16, 74, 168, 169]

To make MD commercially viable, it is important to address some of its limitations such as low water vapor flux, fouling at high salt concentrations and high energy

consumption [74, 170-176]. Since MD can be used for treating high salt concentration waters, some major commercial opportunities for MD are the treatment of RO reject, power plant blow downs and water from [74, 122, 177-179]. One of the anticipated problems with increased salt concentrations is fouling where flux decreases due to the deposition of suspended or dissolved substances on the membrane [16, 74]. Membrane processes are susceptible to scaling at higher salt concentrations when the ionic product of sparingly soluble salts in the concentrated feed exceeds its equilibrium solubility product [180]. Some common scalants are calcium salts such as calcium carbonate ($CaCO_3$), Calcium sulfate ($CaSO_4$) and barium sulfate ($BaSO_4$) [16, 74, 168]. Several approaches such as the use of ultrasound, pH control of feed side, and incorporated gas bubbling into direct contact membrane distillation (DCMD) has been used to reduce fouling in MD [90, 181, 182].

Recently, we have reported microwave induced membrane distillation (MIMD) where the feed water is heated by microwave instead of conventional thermal heaters [94]. The mechanism of microwave heating is quite different from conventional heating [52, 94]. In general, saline water generates dipoles when placed in a microwave field which then develops orientation polarization, and the lag between the dipole orientation and the electric field leads to heating of the water [183-186]. In addition, non-thermal effects such as local super heating and generation of nanobubbles are associated with microwave heating [67, 187-189]. Together these lead to lower temperature polarization, higher vapor pressure gradient and flux [68]. The microwave process is also known to reduce the activation energy of physical and chemical processes, break down hydrogen bonded structures and reduce the average particle size salts in an aqueous environments [67, 68, 190-192]. The energy consumption in MIMD has also been reported to be significantly

lower than that by regular heating [94, 193, 194]. Based on the results so far, MIMD appears to be a promising technique.

Particle size of the dissolved solute is one of the key factors that influences membrane fouling. In general, it has been observed that the particles with smaller size tend to lower the fouling tendency [94]. Since important parameters such as hydrogen bonding and surface tension are affected by microwave radiations, the latter also affects the colloidal behavior of salts [94, 195-197]. Both crystal growth and decomposition which refers to the breakdown of salt crystals are effected by microwave radiations [198]. Since the mechanism of salt crystals formation in microwave is known to be quite different [199, 200], therefore, it is expected that the fouling behavior in MIMD will vary from conventional heating. The objective of this research is to explore the effect of microwave heating on fouling in a MD process, especially in the presence of common foulants such as calcium and barium salts.

3.2 Experimental

3.2.1 Chemicals, Materials and Membrane module

$CaSO_4$ (99% pure, anhydrous), $CaCO_3$ (98+%, pure heavy powder), and $BaSO_4$ (99%, precipitated) were obtained from Fisher Scientific (Hanover Park, IL) and deionized water (Barnstead 5023, Dubuque, Iowa) were used in all experiments.

The carboxylated carbon nanotubes (CNT-COOH) were incorporated on the polypropylene (PP) membrane (A carbon nanotube immobilized membrane (CNIM) was used in this study. The base membrane was a polypropylene (PP) membrane (0.45 μm pore size, STERLITECH company, WA, US) to fabricate the carbon nanotube immobilized

membrane (CNIM). The details for CNT-COOH synthesis and CNIM fabrication have been reported before [175, 201].

3.2.2 Experimental Setup

The MIMD setup for this experiment is shown in Figure 3.1 and it has been described in our previous work [94]. A polytetrafluoroethylene (PTFE) module with an effective membrane area of 11.94 cm^2 has been used for DCMD experiments. The experimental setup includes the membrane module, pumps (Cole Parmer, Vernon Hills, IL) for feed and permeate flow, temperature controlled water bath (GP-200), a circulating chiller (MGW Lauda RM6) and a microwave (Oster, OGZF1301). A temperature controlled water bath was used to heat the feed water for conventional MD and an 1100-watt domestic microwave for MIMD. The experiments were carried out at different feed flow rates and temperatures with constant permeate flow rate of 200 mL/min at 15^oC. K-type temperature probes (Cole Parmer) were used to monitor the temperatures of the system. The permeate water quality was monitored using a conductivity meter (Jenway, 4310). Under similar conditions, each of the experiment was conducted for three times. The relative standard deviation was found less than 1%.

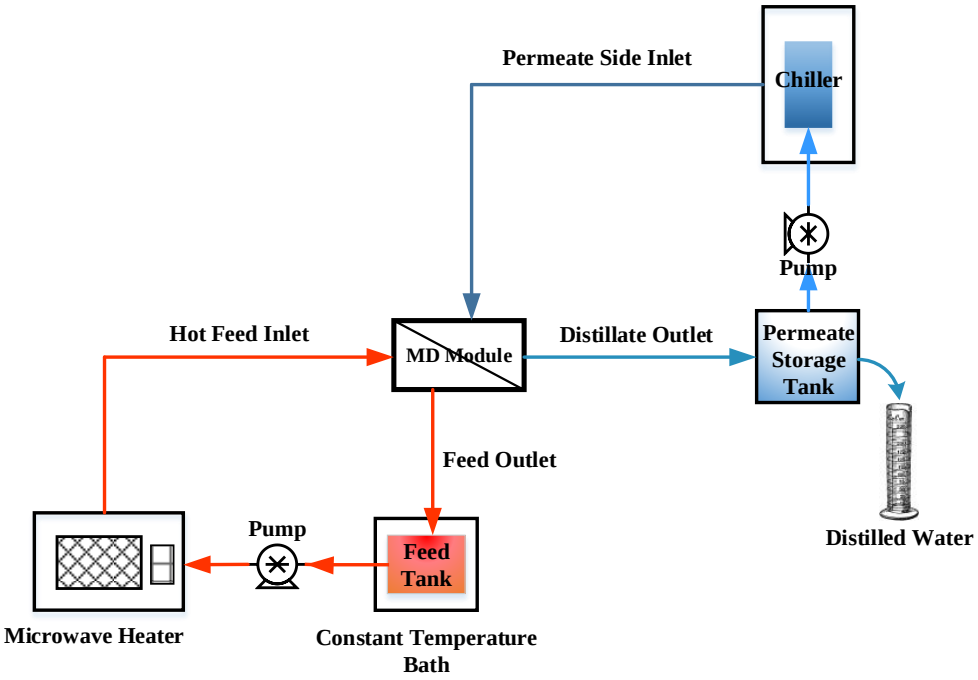

Figure 3.1 Schematic of microwave induced membrane distillation system.

3.2.3 Membrane Performances

The performance of MIMD, especially its fouling characteristics with CNIM was investigated using $CaSO_4$, $CaCO_3$, and $BaSO_4$ solutions at the concentrations of 2950, 3500 and 2500 ppm respectively. Comparisons were made with conventional MD. The water vapor permeate flux was used to determine the performance of MIMD and MD with varying feed temperatures and flow rates. The water vapor flux, J_w, is expressed as:

$$J_w = \frac{W_p}{t \cdot A} \tag{3.1}$$

Where, *Wp* is the total mass of permeate, t is the operation time and A is the effective membrane surface area. To compare fouling in conventional MD and MIMD, the flux was measured over a period of time and the normalized flux decline, FD_n, was measured as:

$$\mathrm{FD}_n\ (\%) = \left(1 - \frac{J_f}{J_o}\right) x\ 100 \tag{3.2}$$

Where, J_f and J_0 are the final permeate flux and initial flux, respectively.

The deposition of salt crystals was characterized by scanning electron microscopy (SEM) (JEOL; model JSM-7900F, JEOL USA inc., USA) and quantified using gravimetric measurements (Perkin Elmer, TGA 8000). Dynamic light scattering (Zetasizer Nano-ZS90, Malvern Instrument Ltd, UK) was used to determine the sizes of salt particles in simulated conventional and microwave heating. The water and salt-water interactions with microwave heating were characterized using Fourier transform infrared spectroscopy (FTIR) (IRAffinity-1, Shimadzu).

3.3 Results and Discussion

3.3.1 Effect of Temperature and Feed Flowrate

Figure 3.2 (a) shows the effect of temperature on water vapor flux in MD and MIMD. Highly concentrated $CaSO_4$ solution was used as the feed. The permeate fluxes of both MD and MIMD with CNIM increased with increase in temperatures as the water vapor pressure increased with temperature. It was observed that MIMD provided higher permeate flux at all temperatures when compared with the conventional MD. The highest enhancement was found at the feed temperature of 50°C with permeate flux of 38.6 kg/m^2.h, which was 90 % higher than conventional MD.

The effect of varying feed flow rate at 70^{o}C is shown in Figure 3.2 (b). The permeate flow rate was kept constant at 200 ml/min. Increase in feed flow rates increased the water vapor fluxes of both MIMD and MD. The increased feed flow rate not only

increases the amount of water vapor into the MD module, but created a turbulence and decreased the boundary layer effect at the bulk feed solution-membrane interface. As a result, the temperature polarization decreased and the permeate flux was enhanced. In general, these results are in line with our previous study with NaCl [94]**.** The enhancements in MIMD were attributed to the microwave effects such as localized super heating, nanobubbles formation, breakdown of hydrogen-bonded H_2O and salt-water cluster destruction. However, it is noted that the enhancements reported here for $CaSO_4$ were higher than those reported for NaCl [94].

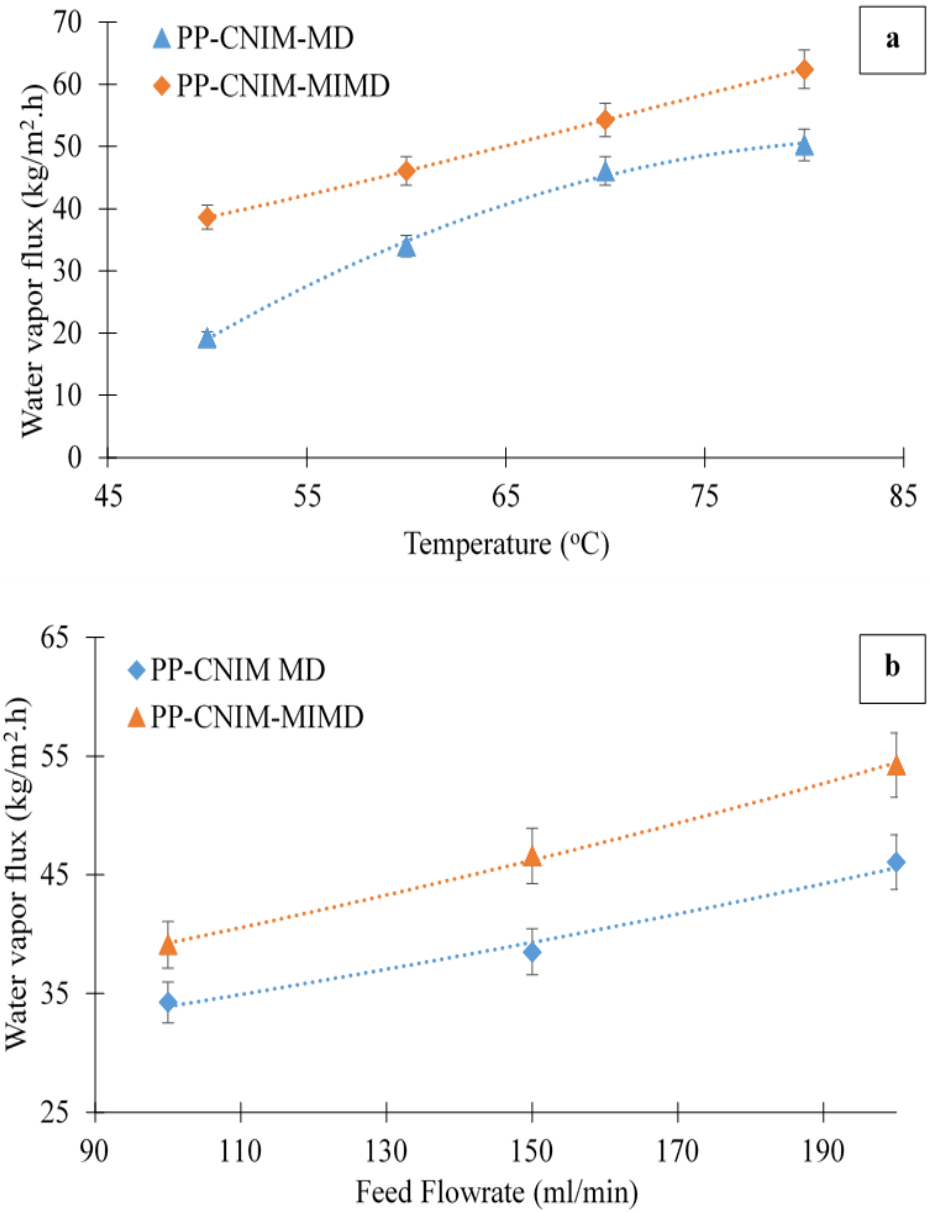

Figure 3.2 Effect of increasing (a) feed temperature and (b) flow rate on water vapor flux for $CaSO_4$ solution during MD and MIMD.

3.3.2 Membrane Fouling in MD and MIMD

As already mentioned, the membrane fouling in MIMD was studied using highly concentrated salt solutions such $CaSO_4$, $CaCO_3$, and $BaSO_4$, and compared to the conventional MD. These concentrations were clearly higher than what is normally encountered and were used only to test the level of fouling. Fouling was investigated by the reduction of flux over the period of operation time. All experiments were carried out at a feed temperature of 70^oC and feed flow rate of 200 ml/min. Figure 3.3 a, 3.3 b, and 3.3c show the water vapor flux as a function of time for $CaSO_4$, $CaCO_3$, and $BaSO_4$, respectively. The reduction in water vapor flux with time showed that fouling was quite serious with the salt solutions tested for both MIMD and MD.

Figure 3.3 a shows that the water vapor flux was 46.1 kg/m^2.h at the first hour for conventional MD with $CaSO_4$ solution, while it was 54.3 kg/m^2.h for MIMD. The flux for MD dropped to 12.6 kg/m^2.h after 12 h of continuous operation. The flux reduction pattern was somewhat different for MIMD, where the flux reduced rapidly within the first four hours and then gradually decreased to 23.5 kg/m^2.h after 12 h, which was 86.5 % higher than that of MD. The initial and final permeate fluxes were used to calculate the normalized flux decline. The results show that the normalized flux decline of MD and MIMD with $CaSO_4$ were 72.7% and 56.7%, respectively.

Figure 3.3 b illustrates the water vapor flux of MIMD and MD with $CaCO_3$. The flux for MD was 50.1 kg/m^2.h, while it was 55.3 kg/m^2.h for MIMD at the first hour. The flux decline was much slower for $CaCO_3$ than $CaSO_4$. The flux of MD modestly dipped and ended up at 32.4 kg/m^2.h after 20 hrs. For MIMD, the water vapor flux had the same trend as $CaSO_4$ with the significant reduction in the first five hours, followed by the gradual

decrement and the flux was 40.2 kg/m^2.h after the operation of 20 h, which was 24.1% higher than that of MD. The normalized flux decline of MD was 35.6%, while the value of MIMD was 27.3%.

Figure 3.3 c shows the fluxes of MD and MIMD for $BaSO_4$ with 16 h of continuous operation. The initial flux was 50.1 kg/m^2.h for MD and gradually decreased to 33.5 kg/m^2.h after 16-h operation. At the same time the flux of MIMD was 54.4 kg/m^2.h at the first hour and gradually reduced to 38.5 kg/m^2.h after 16 h, which is 14.9% higher than that of MD. The normalized flux decline of MD and MIMD with $BaSO_4$ were 33.4% and 29.2%, respectively.

The normalized flux decline of the three salts calculated at the operation time of 12 h showed that $CaSO_4$ was the strongest foulant and this was in agreement with results published previously [94]. The results also shown that $BaSO_4$ was the stronger foulant compared to $CaCO_3$. It was also evident that the microwave heating provided not only higher water vapor flux than MD, but also the fouling was less compared to conventional heating.

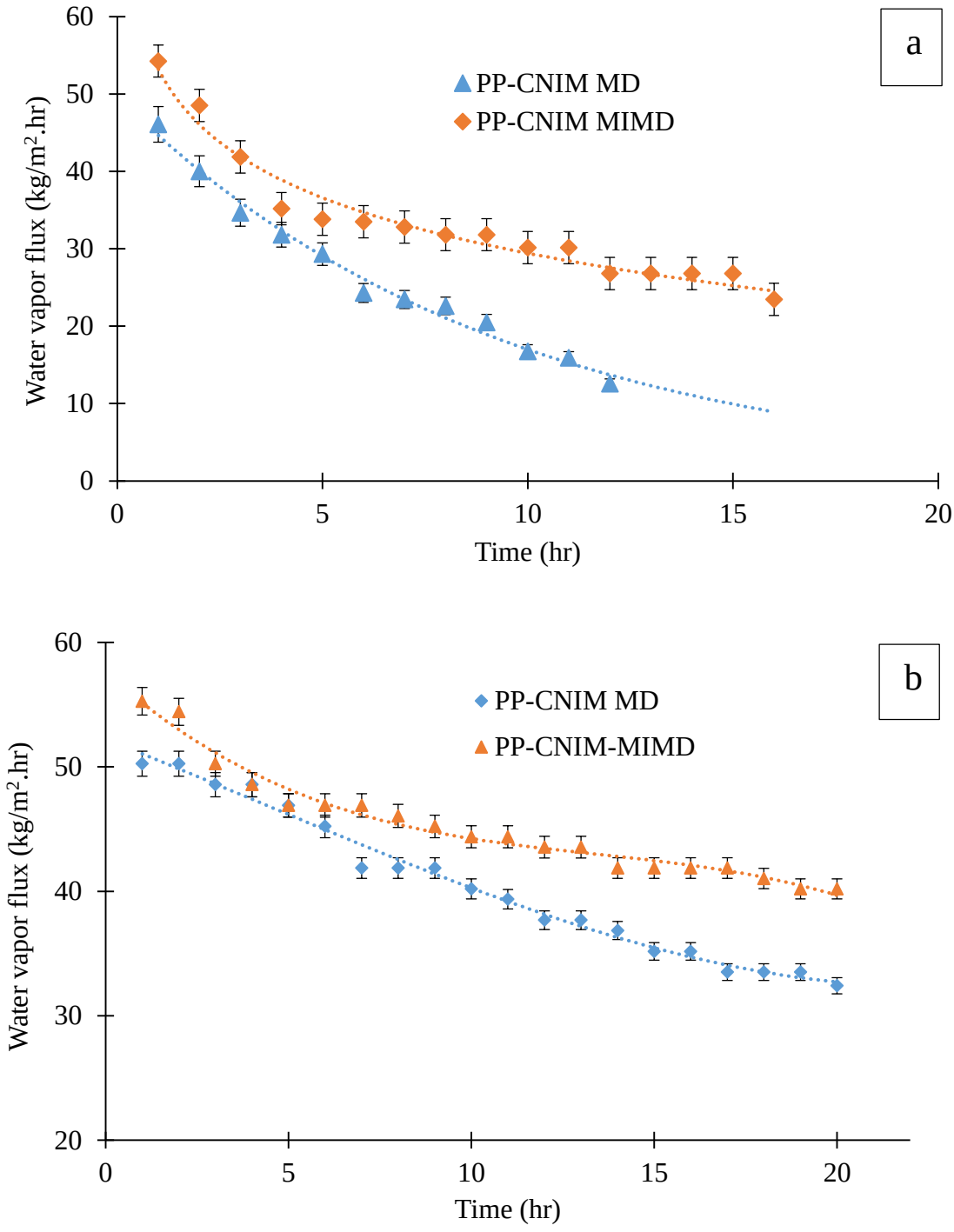

Figure 3.3 Water vapor flux in PP-CNIM membranes for (a) $CaSO_4$ at a concentration of 2.95g/l; (b) CaCO3 at a concentration of 3.5g/l ; and (c) $BaSO_4$ at a concentration of 2.5g/l. All analysis was done at a temperature of 70 °C and feed flow rate of 200 mL/min. (continued).

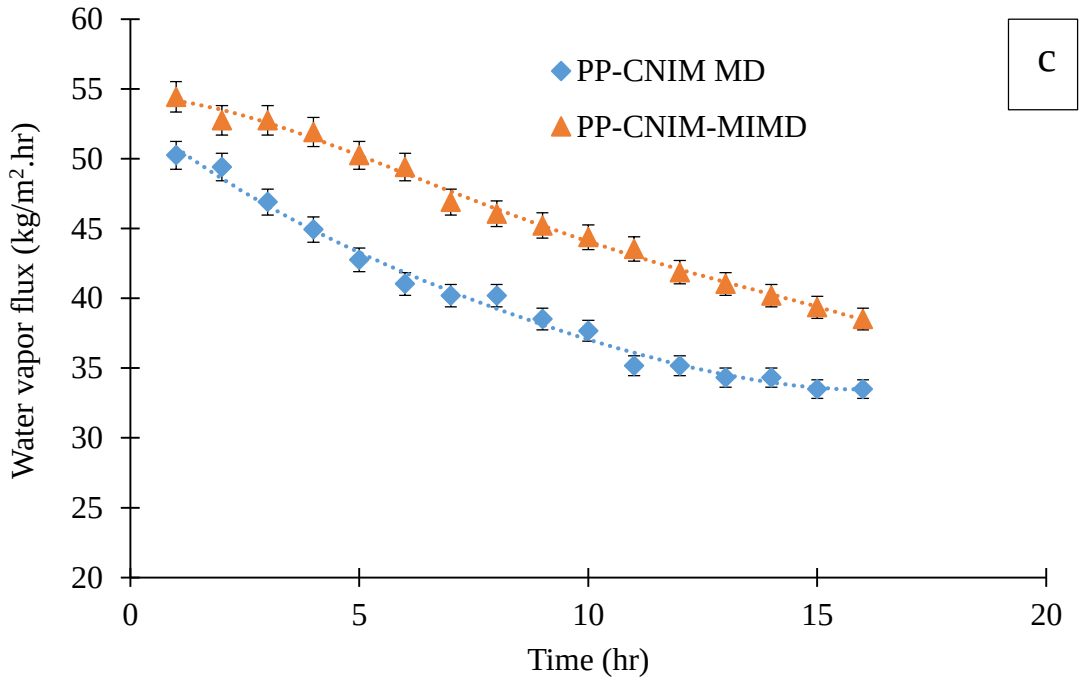

Figure 3.3 (continued) Water vapor flux in PP-CNIM membranes for (a) $CaSO_4$ at a concentration of 2.95g/l; (b) CaCO3 at a concentration of 3.5g/l ; and (c) $BaSO_4$ at a concentration of 2.5g/l. All analysis was done at a temperature of 70 °C and feed flow rate of 200 mL/min.

3.3.3 Deposition of Salts on MD and MIMD Membranes

The difference in the deposition of salt on CNIM by conventional MD and MIMD was quantified by weighing the amount of salt on the membrane before and after the experiment. The weight measurements were made after drying the membrane in an oven overnight at 70°C. Table 3.1 shows that the total amount salt deposited on the membrane surface after 7 h of continuous operation at 70°C under during MD and MIMD. The amount of salt deposited was significantly less, 50 to 79% for MIMD.

Table 3.1 Deposition of Salts on the Membrane Surface after 7 hrs of Operation at 70^{o}C

Salt	Amount of salt deposited on the membrane surface (mg)		% weight decrease
	Conventional heating	Microwave heating	
$CaSO_4$	20.8	9.4	54.8
$CaCO_3$	7.1	1.5	78.9
$BaSO_4$	3.6	1.8	50.0

Membrane fouling was further investigated by characterizing the deposition of the respective salt crystals on the CNIM. Figure 3.4a and 3.4b show SEM images of the original polypropylene membrane and the CNIM used in these experiments. Figure 3.4c and 3.4d show the deposition of calcium sulfate crystal scales on CNIM after the experiments with conventional heating and microwave heating respectively. It is evident that the formation of calcium sulfate crystal on the membranes was significantly different in MD and MIMD. With conventional heating, calcium sulfate salt seemed to form homogeneous crystals that adhere to the membrane surface (Figure 3.4c), while such crystal formation was not observed in MIMD. Here the calcium sulfate crystals were small and non-uniform, and the particles appeared to be sparsely dispersed certain areas on the membrane (Figure 3.4d). As a result, there was more active membrane surface available during MIMD that resulted in higher water vapor flux. Similar pattern of crystal formation was also observed in case of $CaCO_3$.With conventional MD, the rod like crystal of calcium carbonate densely packed the membrane surface (Figure 3.4e), whereas in MIMD, the crystals were smaller in size and flaky in nature with interstitial pores in-between them (Figure 3.4f).

The deposition of barium sulfate on the membrane was also studied as illustrated in Figure 4g and 4h. The crystals of barium sulfate salt with conventional heating appeared

to be quite uniform and agglomerated (Figure 3.4g). While, with microwave heating, the particles were smaller and loosely deposited on the membrane surface (Figure 3.4h), so these resulted in higher flux enhancement for MIMD, compared to MD.

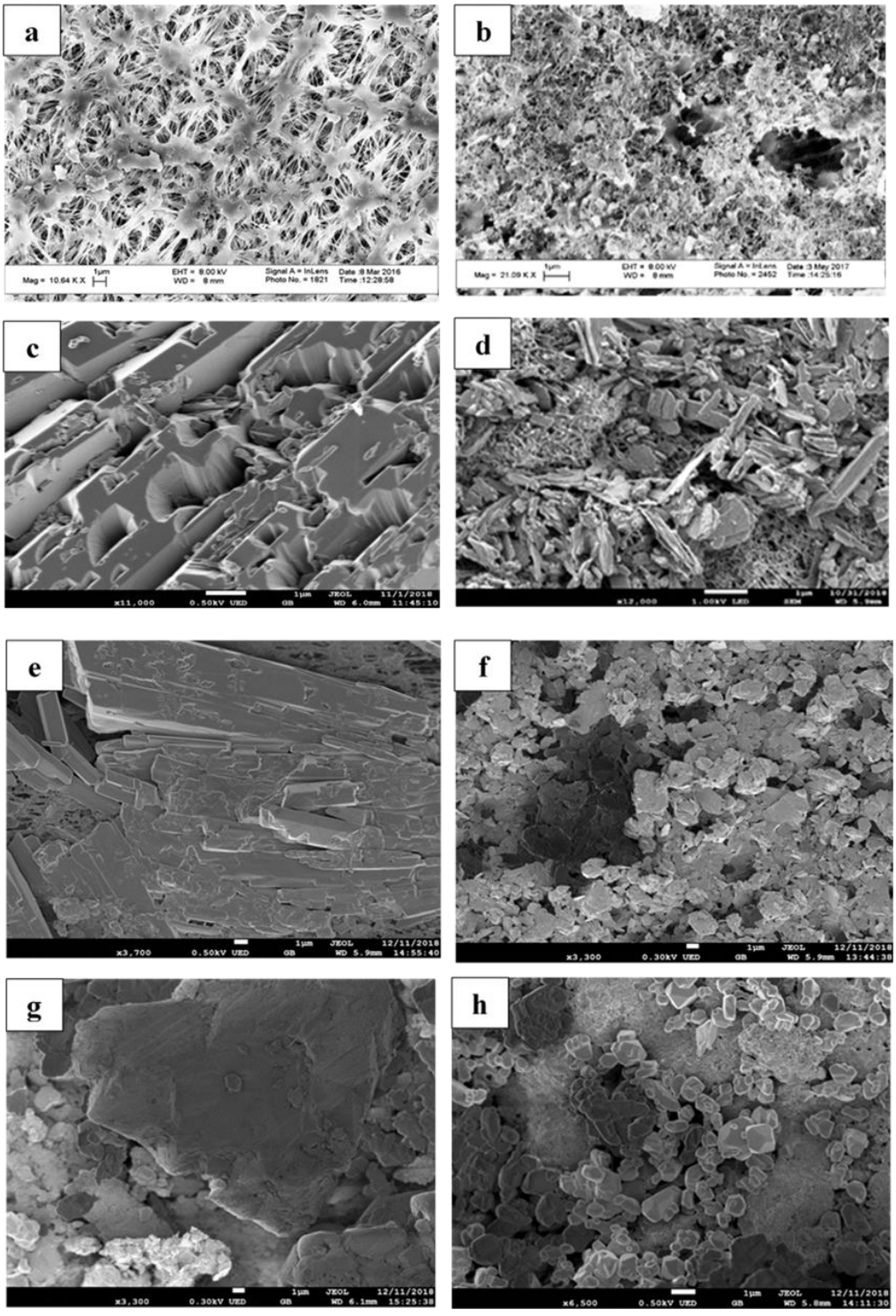

Figure 3.4. a) original PP membrane; b) CNIM; c) $CaSO_4$ scale with conventional heating; d) CaSO4 scale with MIMD; e) $CaCO_3$ scale with conventional heating; f) CaCO3 scale in MIMD; g) $BaSO_4$ scale with conventional heating; and h) BaSO4 scale with MIMD conventional heating; and h) BaSO4 scale with MIMD.

3.4 Proposed Mechanism

Applying microwave heating of the brine during MD can affect the solution in different ways. The microwave heating breaks down the hydrogen bonded structure in the aqueous phase and disintegrate the salt particles present in the solution [94]. FTIR [94]and Raman [197] measurements have shown that the O-H band changes significantly in microwave treated water.

From nucleation theory [199], nucleation rate per volume is described by :

$$\mathrm{I} = \frac{\mathrm{D}}{R_d^2}\, n^{-\Delta G^*/KT} \tag{3.2}$$

Where D is the diffusivity of nuclei, R_d is the space between the nuclei, ΔG^* is the activation energy, K is the Boltzmann constant, and T is the temperature. D, R_d, as well as the activation energy can later dramatically under microwave radiations. Another important consideration is the change in surface tension which is a measure of surface energy under microwave radiations. The reduction of surface tension is related to the nucleus radius salt granule by the equation below.

$$R^* = \frac{-2\gamma}{\Delta G_V} \tag{3.3}$$

Where R* is the critical nucleus radius, γ is the surface energy per area of nucleus or equal to σ (surface tension). Therefore, microwave radiation is expected to reduce surface tension, the nuclei radius and finally the size of the salt crystal. In addition, the nano-bubbles generated under microwave irradiation can also alter colloidal behavior of crystallizing salts, a phenomenon that has not been studied so far.

The influence of microwave heating on fouling reduction was investigated by using FTIR spectroscopy and studying the alterations of the particle size via dynamic light scattering. The FTIR spectra of $CaSO_4$, $CaCO_3$ and $BaSO_4$ solution at room temperature (RT), conventional heating and microwave heating are presented in Figure 3.5a, 3.5b and 3.5c, respectively. As can be seen from the figures that the IR absorption of water molecules differed under conventional and microwave heating due to the variation in water-water and salt-water interactions [94]. The peak at 2127 cm^{-1} resulted from the combination of bending and liberations. The bending frequency at 1644 cm^{-1} was attributed to the hydrogen bonding, which was much weaker for microwave treated water for $CaSO_4$ solution. The peak at ~3490 cm^{-1} arose due to the stretching of water molecules. The nature of the spectrum was observed to be different under changing heating conditions as the arrangement of hydrogen bonded water clusters changed differently, which led to the variation of the peaks. The nature of FTIR spectra for $BaSO_4$ solution at 1644 cm^{-1} and ~3490 cm^{-1} were found to be slightly different than other Ca^{+2} salt solutions due to the difference in the ionic interactions of the corresponding salt solutions.

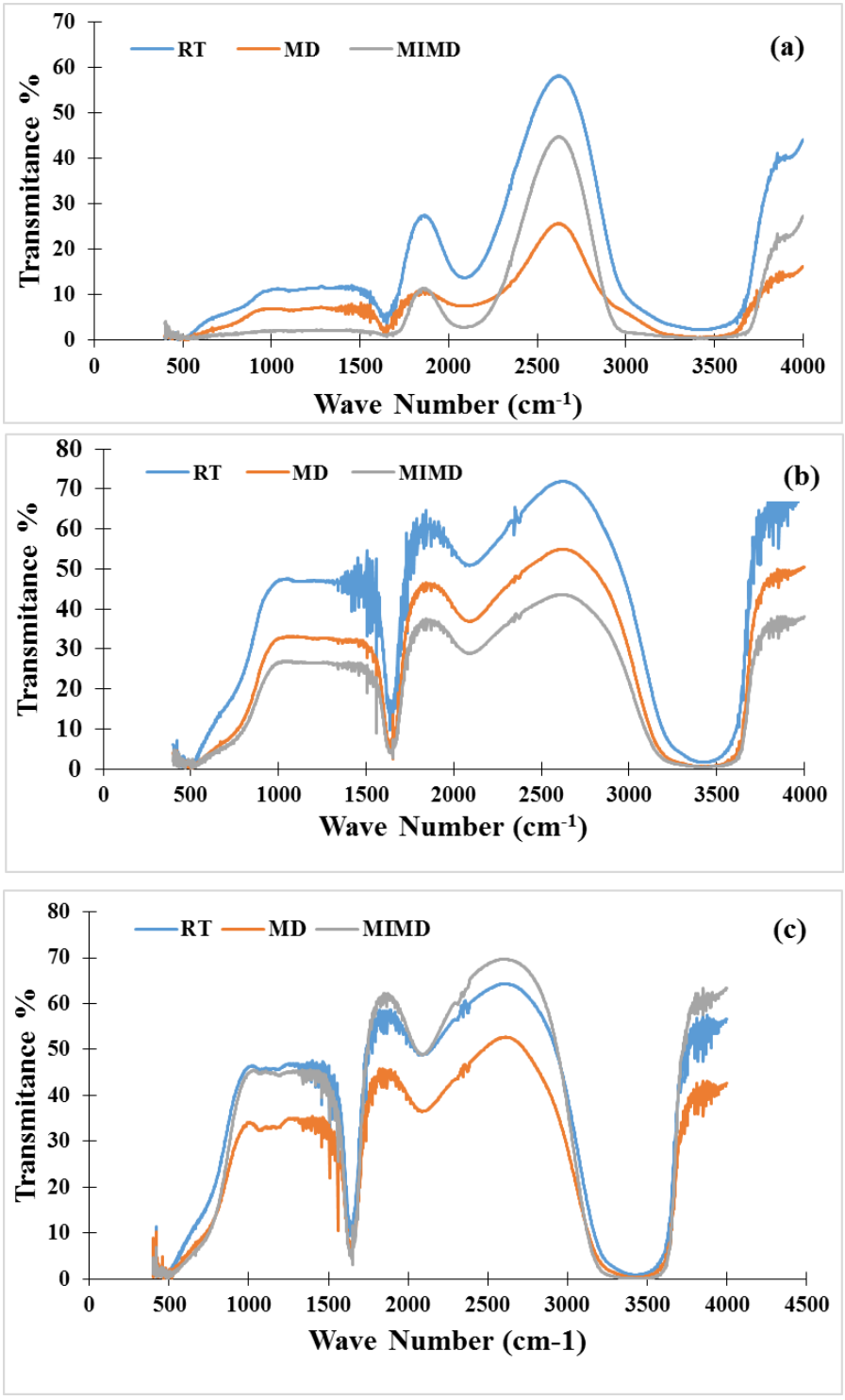

Figure 3.5 FTIR spectra of a) $CaSO_4$-water solution (2.95g/l); b) $CaCO_3$-water solution (3.5g/l); c) $BaSO_4$-water solution (2.5g/l) under room temperature (RT) microwave (MIMD) and conventional heating (MD

Dynamic Light Scattering (DLS) was used to measure changes of the particle size of salt molecules after microwave irradiation compare to conventional heating. Figure 3.6a shows the influence of microwave irradiation on particle size distribution of $CaSO_4$. The average $CaSO_4$ particle size was 1173 nm at room temperature and dropped to 994 nm at 70°C of regular heating, while it was 354 nm. When heated by the microwave heating at the same temperature. This showed that the microwave heating significantly lowered the average particle size of the $CaSO_4$ clusters. Figure 3.6b shows the influence of microwave heating on the particle size of $CaCO_3$ which was 1175 nm at room temperature, and it dropped to 371 nm at 70°C of regular heating and to 226 nm during microwave heating. Similar influences were seen for $BaSO_4$ as shown in Figure 3.6c, where the particle size dropped from 827 nm during regular heating to 362 nm during microwave heating. In general, the particle size of all the salts above was significantly reduced by regular heating and microwave heating compared to what was observed at room temperature. This is in line with the previous report on crystallization in microwave activated water where microwave radiation led to a reduction in crystal lattice volume and crystal size compared to samples without microwave treatment [94].

It is noted that the size reductions for $CaSO_4$, $CaCO_3$, and $BaSO_4$ were different. It appears that $BaSO_4$ was followed by $CaCO_3$, and $CaSO_4$. Among the other factors, the dissimilarities could be attributed to the difference in their dielectric constants. $BaSO_4$ had the highest dielectric constant, so it could absorb more energy and show more microwave effects while $CaCO_3$ had a higher electric constant than $CaSO_4$, which made the rate of size reduction of $CaCO_3$ higher than of $CaSO_4$.

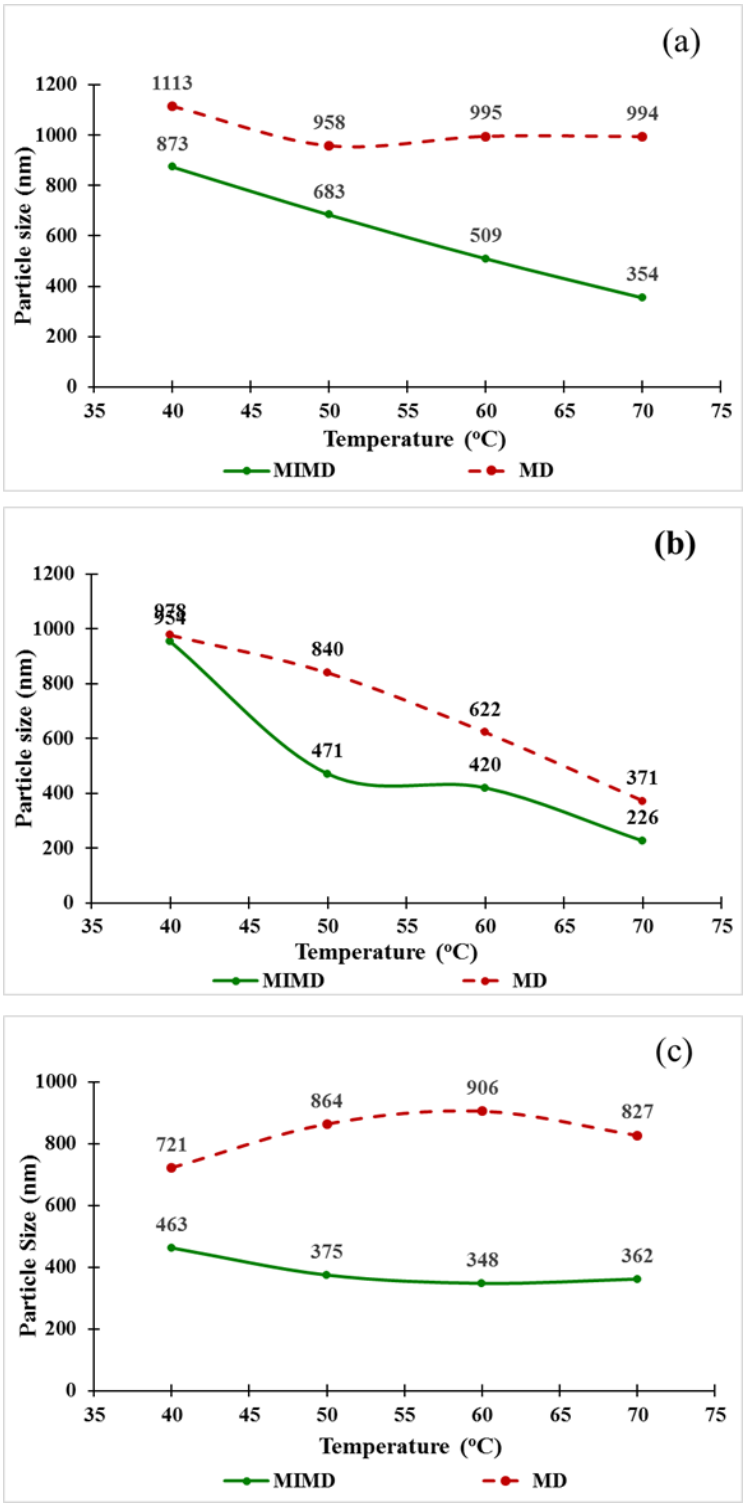

Figure 3.6 The influence of microwave irradiation on particle size distribution of a) $CaSO_4$; b) $CaCO_3$; and c) $BaSO_4$.

3.5 Conclusion

Microwave irradiation was used as a means to heat the highly concentrated $CaCO_3$, $CaSO_4$ and $BaSO_4$ solutions in the DCMD mode. Besides the enhancement of water vapor flux, the MIMD exhibited significantly less fouling and the normalized flux decline was lower than conventional MD. The salt deposition on the membrane surface was observed to be between 50-79% less during MIMD and the morphology of the deposits from MIMD was quite different from those of conventional MD. It appears that non-thermal effect, such as, localized super heating, the breakdown of hydrogen bonding, alternation of surface tension, the increase in ionic mobility altered colloidal behavior and particle formation in MIMD. Apart from the less energy requirement and higher flux in MIMD, the lower flux decline at very high salt concentrations could lead to dramatic improvements to the MD technology in the future.

CHAPTER 4

SCALING REDUCTION IN CARBON NANOTUBE IMMOBLIZED MEMBRANE DURING MEMBRANE DISTILLATION

4.1 Introduction

Reverse osmosis (RO), multi-stage flash and multi-effect distillation are the most common desalination techniques that have shown much promise. However, they have limitations such as fouling of RO membranes in presence of scaling ions, and the high energy and capital cost in thermal methods [119, 202]. As a result, alternative desalination technologies, including solar evaporation and membrane distillation (MD) are being explored [203-205]. The MD process paired with solar energy or low grade heat source can be an attractive alternate to the conventional membrane based desalination [51, 206]. MD is also evolving to be an effective desalination technique for treating the high salinity water that RO is unable to handle due to high osmotic pressure and extensive pretreatment requirements [207-209].

A major obstacle in membrane based desalination techniques is fouling [210-213] from the deposition of suspended or dissolved substances on the active membrane surface and/or within its pores [16, 214, 215]. Several types, such as inorganic fouling or scaling, particulate and colloidal fouling, organic fouling and biofouling are common [216-218]. Fouling has also been an important issue in RO, nano-filtration, and ultra-filtration [219-221] . Due to the use of porous hydrophobic membranes, fouling tends to be significantly less in MD than RO, but still is an important consideration for high salinity water desalting. Several approaches for fouling reduction such as the introduction of nano-bubble and ultra

sound have been reported [90, 222, 223]. Of particular interest has been the deposition of inorganic salts such as calcium carbonate ($CaCO_3$), calcium sulfate ($CaSO_4$) and barium sulfate ($BaSO_4$), which are found in hard waters as well as industrial waste from power plants, hydraulic fracturing and waste waters form industries such as textiles and pulp and paper [224]. The formation of a fouling layer comprising of salt crystals formed on/within the pores of MD membranes are known to cause progressive wettability of the membrane [225]. The addition of several antiscalants have been reported for the reduction of fouling [226] in RO and thermal distillation processes. The use of antiscalants in thermally driven MD process could potentially help to lower the scaling without any adverse effect [88, 95, 227].

We have described the development of carbon nanotube immobilized membrane (CNIM), where the carbon nanotubes (CNTs) increased the partitioning of the water vapor while rejecting the liquid phase leading to dramatic increase in MD flux [173, 228, 229]. Besides this, it is expected that the presence of CNTs may reduce the scale formation on membrane surfaces where the CNTs serve as a screen. This may resist the membrane pore blocking by salt deposition, and it is conceivable that the salt crystals deposited on the screen-like CNTs can be removed or washed off rather easily (as shown in Figure 4.1). In this way, the CNT-screen maintains the pore opening for the permeation of water vapor, while repelling the liquid water and salt clusters for longer period of time. The objective of this project was to study the fouling behavior of the CNIM for various highly concentrated feed mixtures and to evaluate the performance of CNIM with addition of antiscalant.

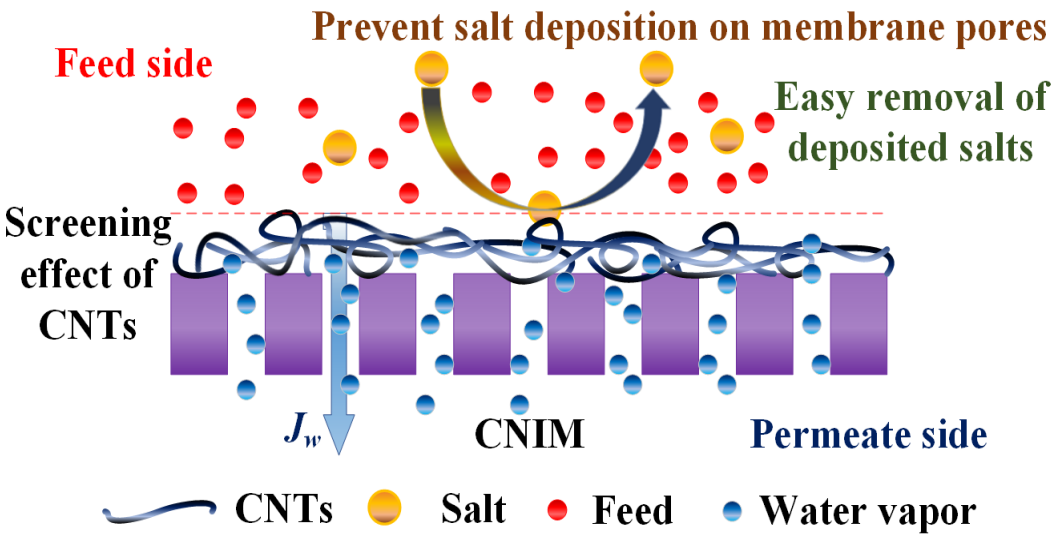

Figure 4.1 Screening effect of CNTs in preventing the salt deposition on the membrane surface.

4.2 Experimental

4.2.1 Materials and Chemicals

Flat polypropylene (PP) membrane (0.45 Micron pore size, from STERLITECH Inc., WA, USA) was used in this study. Calcium sulfate ($CaSO_4$), calcium carbonate ($CaCO_3$), barium sulfate ($BaSO_4$) salts and the antiscalant (AS) polyacrylic acid (PAA) (63 wt% solution in water, mol. Wt. ~2000) were purchased from Thermo Fisher Scientific Chemicals Inc. (Fair Lawn, NJ). Deionized water (Barnstead 5023, Dubuque, Iowa) was used to prepare the feed solutions and as cold distillate.

Multi-walled CNT was purchased from Cheap Tubes, Inc. (Brattleboro, VT, USA). The MWCNTs were functionalized with carboxylic acid groups in a Microwave Accelerated Reaction System (Model: CEM Mars, CEM Corporation, Matthews, NC,

USA) in our laboratory. The PP membrane was used as the base membrane to fabricate the carbon nanotube immobilized membrane (CNIM). The CNTs are immobilized on the membrane surface using small amount of polyvinylidene fluoride (PVDF) as binder. Excess PVDF has been removed from the surface by washing with acetone after fabrication. The functionalization process and CNIM fabrication methods have been reported before [171, 201, 230]. Our previous studies have already proven the ability to retain the CNT coating on the surface for longer period of time [175, 176].

4.2.2 Experimental Procedure

Figure 4.2 demonstrates the DCMD experiment set up in the laboratory. The details have been described before[93]. The hot aqueous feed solutions were circulated on one side of the membrane in the DCMD cell. The initial salt concentration in the feed were 2.95g/L for $CaSO_4$ solution, and 3.5g/L for $CaCO_3$ and 2.5 g/L for $BaSO_4$ salt solution. 50 mg of antiscalant was added in 1L of feed solution for the experiment. The data was reported after repeating each experiment at least three times to conform its reproducibility.

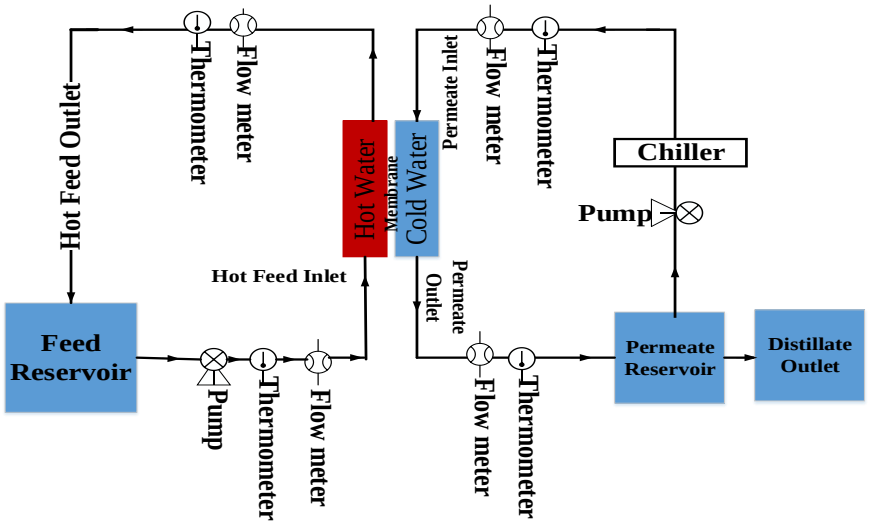

Figure 4.2 Schematic representation of the experimental setup.

Scanning electron microscopy (SEM) (JEOL, Model JSM-7900F, JEOL USA Inc.; USA) was used to characterized the surface morphology of the PP membrane and the CNIM before and after the experiment. Thermogravimetric analysis (TGA, Perkin–Elmer Pyris 7 TGA system at a heating rate of 10 °C/min in air) was used to investigate the thermal stability of the membranes.

4.2.3 DCMD Performance

The MD performances of CNIM membrane with and without the antiscalant was studied as a function of time, temperature, and feed flow rate. The water vapor flux, Jw, is measured as:

$$Jw = Wp/t.A \tag{4.1}$$

Where Wp is the mass of permeated water in time t through surface area A. The flux can also be denoted as:

$$Jw = k\,(P_f - P_p) \tag{4.2}$$

The overall mass transfer coefficient (k) was computed as:

$$k = Jw\,/\,(P_f - P_p) \tag{4.3}$$

Where P_f and P_p are the feed and permeate side water vapor pressure, respectively.

To compare fouling between the PP membrane and CNIM, the flux was measured over time and the normalized flux decline, FD_n, was determined as:

$$FDn(\%) = \left(1 - \frac{J_f}{J_0}\right) \times 100 \quad (4.4)$$

Where, J_o and J_f are the initial and final permeate flux over a period of time t, respectively.

4.3 Results and Discussion

4.3.1 Characterization of the Membranes

Figures 4.3a and b shows the surface SEM images of the original PP membrane and CNIM. Figure 4.3a illustrates the pores present on PP membrane surface, and the incorporation of the carboxylated CNTs led to a modification in morphology as can be seen from Figure 4.3b. AFM images from our previous studies have shown that the incorporation of CNTs on membrane surface also increases the surface roughness [175]. The gas permeation test of the membranes demonstrated no significant change in the effective surface porosity over the effective pore length of the membranes, as only small quantity of CNTs was immobilized on the membrane surface [201, 230].

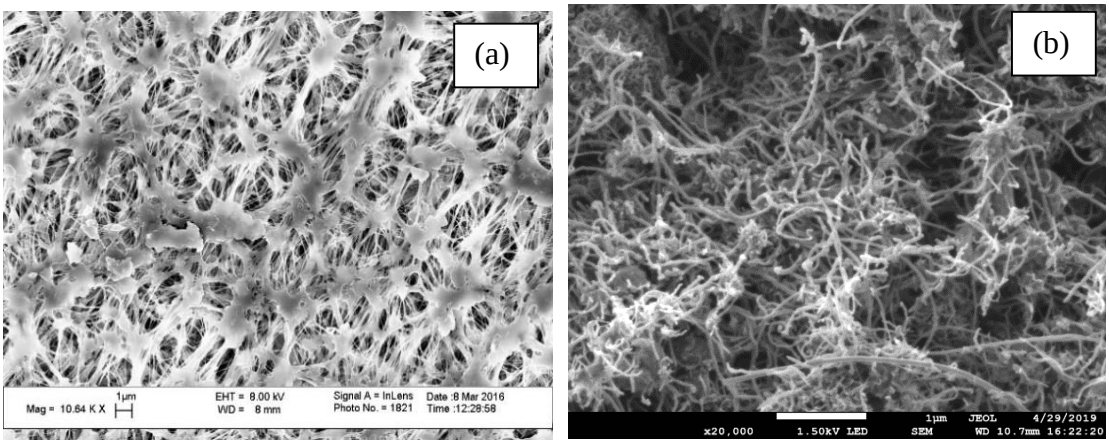

Figure 4.3 Surface SEM image of (a) PP membrane and (b) CNIM.

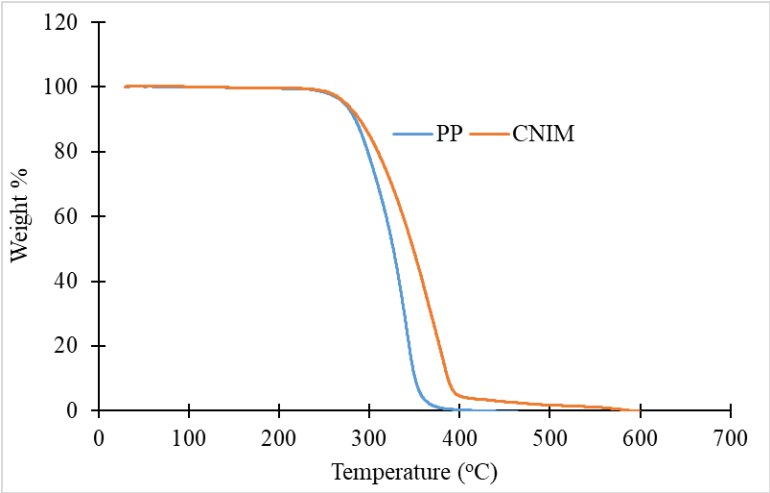

Figure 4.3 c) The TGA curves of plain and modified membranes.

The thermal stability of the PP membrane and CNIM was studied using TGA. The TGA curves of the two membranes are shown in Figure 4.3c. It can be seen from the TGA curves that both membranes are quite stable within the operating temperature ranges. The initial weight loss of the membrane was started at ~270°C and completely decomposed at ~380°C. The TGA curve for CNIM slightly shifted upward, which exhibited the enhanced thermal stability of the CNIM due to the presence of CNTs [231].

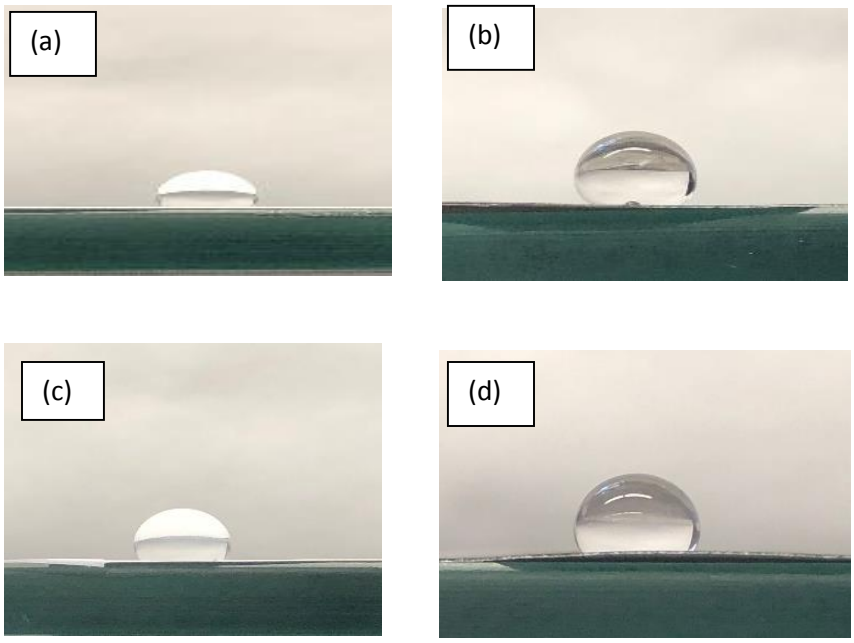

Figure 4.4 Contact angle measurements on unmodified PP and CNIM membrane (a) Contact angle: 115 (pure water plain PP); (b) Contact angle: 125 (pure water PP CNIM); (c) Contact angle: 112 (salt water plain PP); (d) Contact angle: 117 (salt water CNIM).

The contact angles of the unmodified PP and CNIM for pure water and salt solution are shown as above in Figure 4.4. Droplet size of 4mm was used to measure contact angles. The presence of CNTs dramatically altered the contact angle. With 100% water in the feed, the contact angle for CNIM was higher (125^{o}) than the unmodified PP membrane (115^{o}). In presence of salt, the contact angle reduces slightly. The liquid entry pressure (LEP) was measured using a method described before [201]. The LEP of the pure water solution was found to be 30 and 27 psig, which changed to 26 and 24 psig with the CaSO4, (2.95g/l) salt solution for unmodified PP and CNIM, respectively.

4.3.2 Effect of Temperature and Feed flowrate on the water vapor Flux

The influence of feed solution temperature on water permeation rate for PP membrane and CNIM with pure water and aqueous $CaSO_4$ solution (2.95g/L) at feed and distillate flow rate 200 mL min^{-1} is shown in Figure 4.5a. The legend key PP-AS or CNIM-AS in the graph denotes the membrane performance using AS in the feed solution. In all cases the initial permeate flux followed a direct relationship with temperature as the vapor pressure gradient increased with temperature. Among the two membranes, CNIM exhibited higher flux at any particular temperature, which was in line with our previously reported results [201]. It is important to note that the addition of PAA (antiscalant) did not show any negative effect on water permeation. Similar water vapor flux was observed for both membranes with antiscalant when pure water was used as feed. The mass transfer coefficient (k) was observed to be enhanced for CNIM (5.67×10^{-4} and 5.01×10^{-4} $kg/m^2.s.kPa$, for CNIM and PP membrane, respectively) compared to the PP membrane. However, the addition of antiscalant in pure water feed did not show any significant change in the mass transfer coefficient for both membranes. At high such concentrations, the $CaSO_4$ was expected to quickly foul the membrane and the temperature dependence graph did not show an exponential increment pattern like pure water as feed, as the fouling rate increased at higher temperatures [74, 119]. A slight increase in initial flux was due to the antifouling effect of antiscalant at short period of time (1 hr). At a temperature of 60°C, the water vapor flux with antiscalant increased from 25.1 to 31.8 $kg/m^2.hr$ and 32.7 to 37.7 $kg/m^2.hr$ for PP and CNIM, respectively.

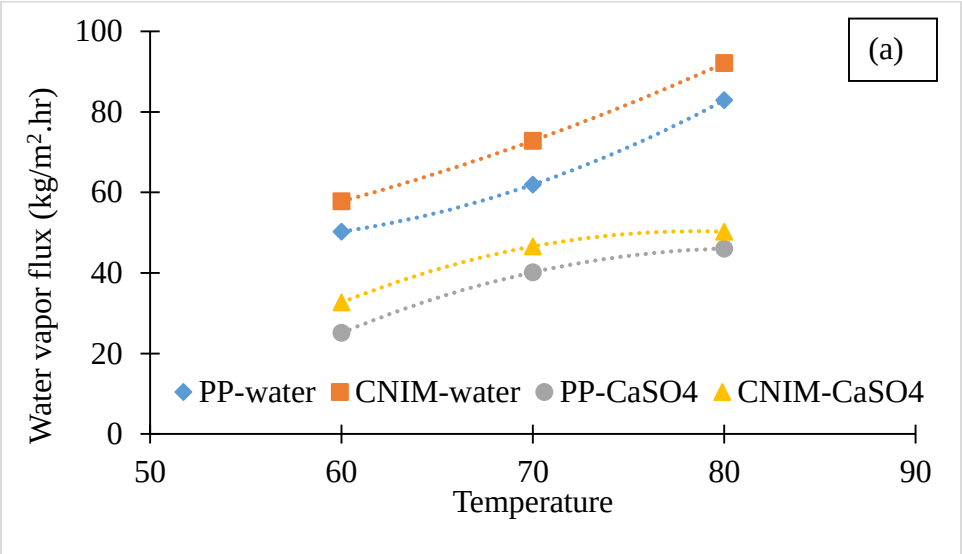

Figure 4.5 (a) Effect of temperature on permeate flux of pure water and $CaSO_4$ solution at 200 mL/min feed and distillate flow rate (run time 1hr).

Figure 4.5b illustrates the performance of the PP and CNIM as a function of feed flow rate at 100, 150 and 200 mL/min, while the permeate side flow rate was maintained constant at 200 mL/min at a feed temperature of 70°C. Results indicate that the water vapor flux was enhanced by feed flow rate for all membranes. The increase in feed flow rate reduced the boundary layer resistance by intensifying the turbulence at feed solution-membrane, and generated more water vapor per unit time [232] .The use of antiscalants in feed solution with CNIM did not show any significant effect with respect to flow rate.

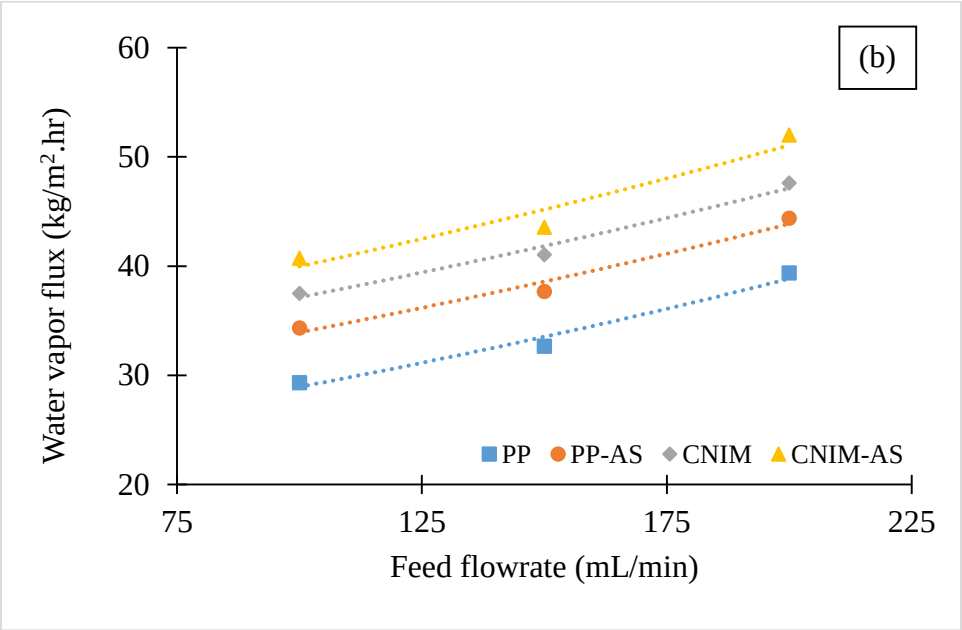

Figure 4.5 (b) Effect of flow rate on permeate flux of $CaSO_4$ solution at 70 °C and 200 mL/min distillate flow rate (run time 1hr).

4.3.3 Membrane Fouling

The fouling of PP membrane and CNIM was studied with highly saline feed solutions, namely $CaSO_4$ (2.95g/L), $CaCO_3$ (3.5g/L), and $BaSO_4$ (2.5g/L). The high concentrations were deliberately selected so that the membranes would foul quickly. The membrane fouling was evaluated by the reduction of permeated water flux with time during the operation. Figure 4.6a, 4.6b, 4.6c and 4.6d, show the deviation of water vapor flux as a function of time for all salts at 70^{o}C feed temperature, feed and permeate flow rate of 200 mL/min.

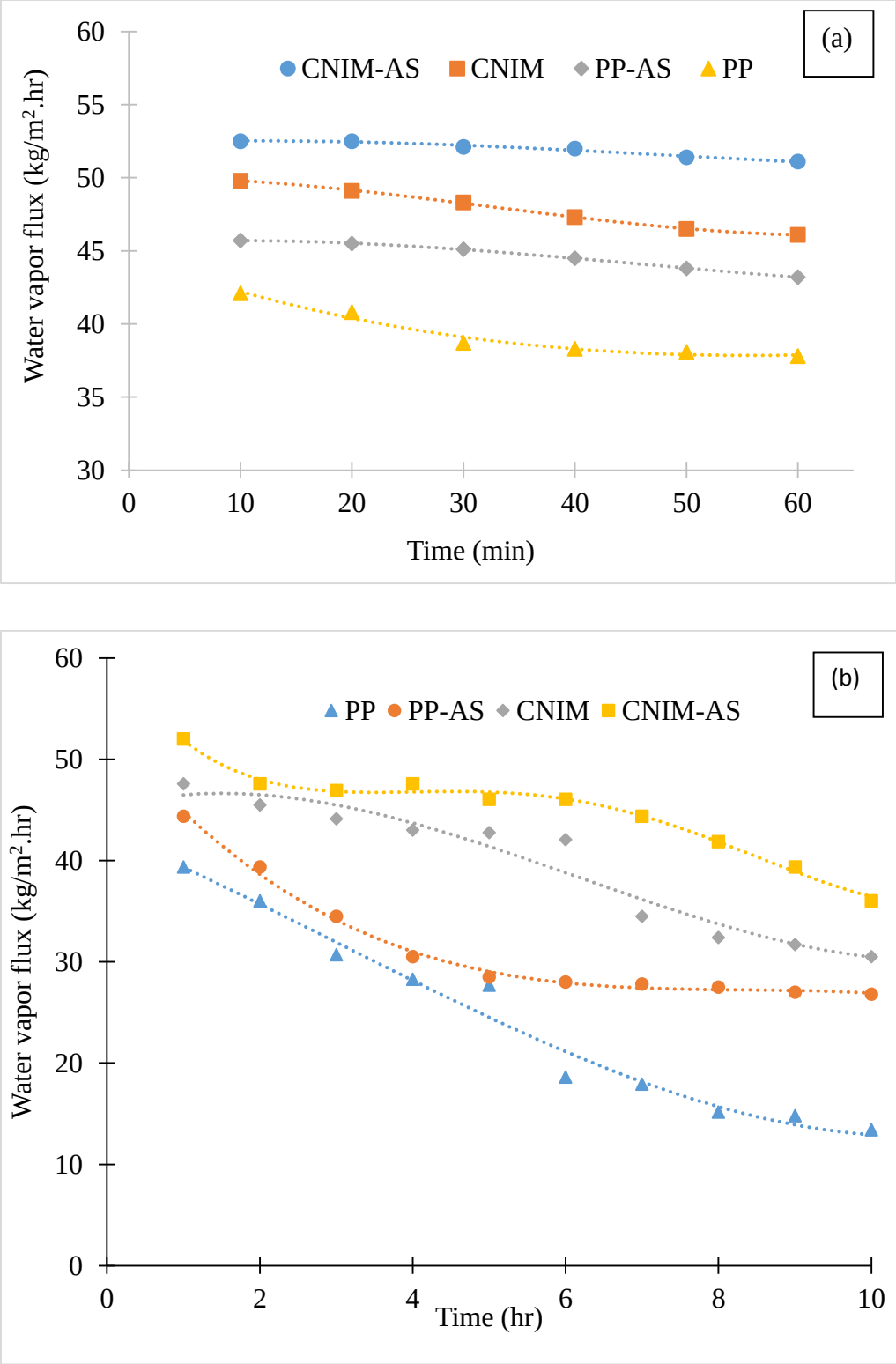

Figure 4.6 Water vapor flux in PP membrane and CNIM at 70°C and 200 mL/min feed flow rate for (a) pure water (run time 1 hr); (b) $CaSO_4$ solution (2.95g/L) (c) $CaCO_3$ solution (3.5g/L); and (d) $BaSO_4$ solution (2.5g/L) (b-d run time 10 hr).(continued).

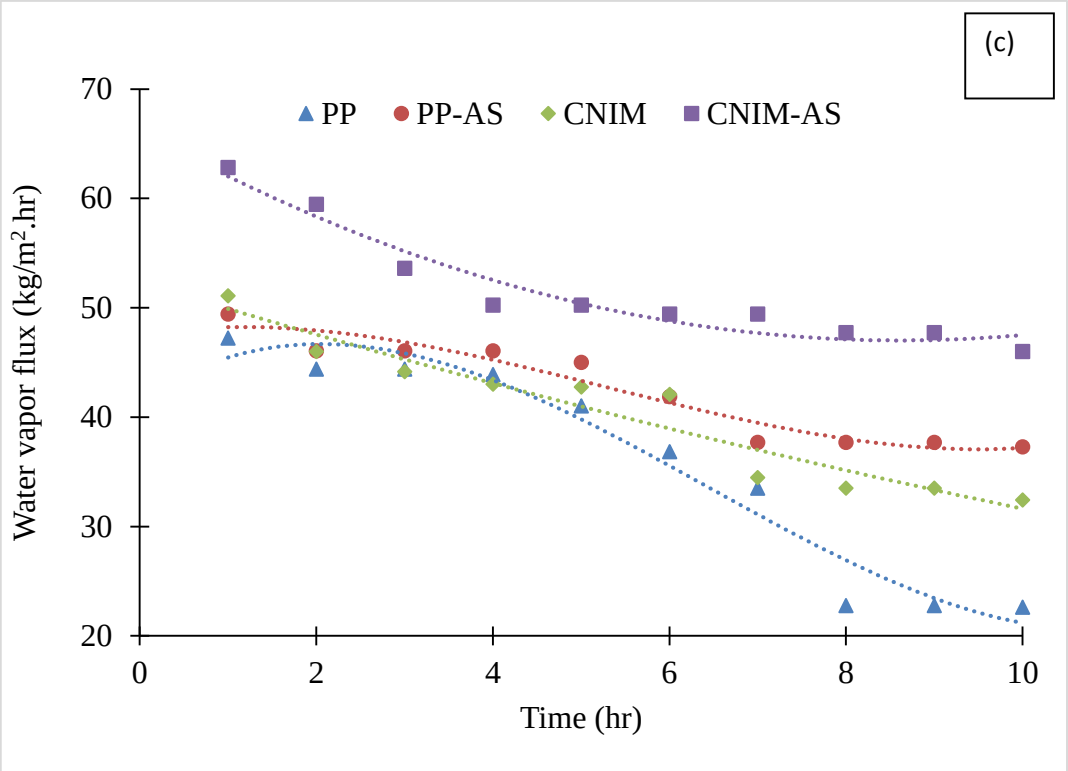

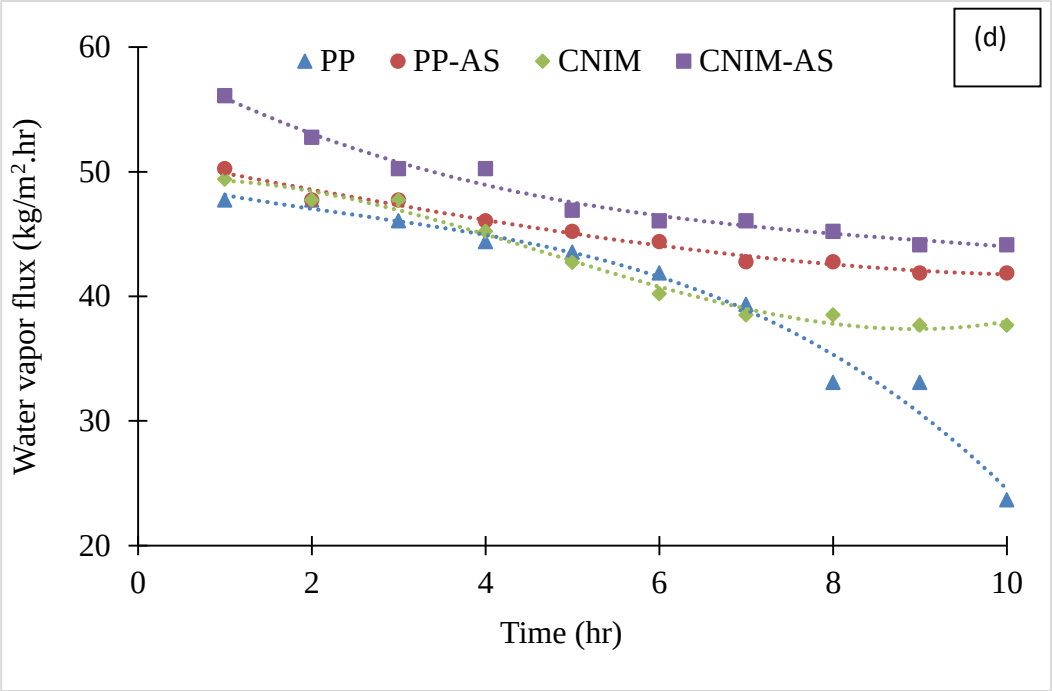

Figure 4.6 (continued) Water vapor flux in PP membrane and CNIM at 70°C and 200 mL/min feed flow rate for (a) pure water (run time 1 hr); (b) $CaSO_4$ solution (2.95g/L) (c) $CaCO_3$ solution (3.5g/L); and (d) $BaSO_4$ solution (2.5g/L) (b-d run time 10 hr).

Figure 4.6 depicts the decline in water vapor fluxes with time for both the membranes as an outcome of scaling. It is clear from the figures that the CNIM exhibited higher antifouling properties in comparison with PP membrane. This may be due to additional screening effect of CNTs which reduced pore blocking from salt deposition (as shown in Figure 4.1). Figure 4.6a shows the short term scaling behavior of $CaSO_4$ salt solutions with PP membrane and CNIM with and without antiscalant. The water vapor flux declined with time as expected. However, the use of antiscalant lowered the fouling tendency, hence generated higher water vapor flux.

It can be seen from Figure 4.6b that for $CaSO_4$ solution, the flux declined to 13.4 from 39.4 $kg/m^2.hr$ for PP, and to 30.5 from 47.6 $kg/m^2.hr$ for the CNIM after 10 hr of operation. The results show that by using CNIM the water vapor flux after 10 hr was still 126.7% higher than the PP membrane. The less fouling tendency of CNIM can be explained via its 'screening effect', where the net-like presence of CNTs prevent the salt clusters to deposit on the membrane surface or pores. Furthermore, the experiments were carried out using antiscalant (PAA) to study its effect on CNIM. It was observed that the use of AS in the feed solution improved the antifouling behavior of the membranes and the water vapor flux after 10 hr of operation was 26.8 $kg/m^2.hr$ and 36 $kg/m^2.hr$ for PP membrane and CNIM, respectively, which is 100% and 18 % higher compared to the system without AS. This may be due to the fact that the antiscalant delays the clustering process and prevents the precipitation of salt on the membrane surface [7, 233-235]. The presence of AS was found to be more effective with the PP membrane than the CNIM.

Similar trends were observed with the other two salts and are shown in Figure 4.6c and 4.6d. As can be seen from the Figure 6c that the water vapor flux of $CaCO_3$ solution

(3.5g/L) declined to 22.6 from 47.2 kg/m^2.hr and 32.4 from 51.1 kg/m^2.hr for PP membrane and CNIM, respectively. These represented 52.1 and 36.6% reduction in flux respectively. The use of AS further subside the flux reduction for both membranes. For $BaSO_4$ salt solution (2.5g/L concentration, shown in Figure 4.6d), the flux declined to 23.7 from 47.7 kg/m^2.hr for PP membrane, and to 37.7 from 49.4 kg/m^2.hr with CNIM. The results exhibited higher membrane antifouling performance using CNIM and the water vapor flux was found to be 59% higher for CNIM compared to PP membrane after 10 hr of operation. However, by using the antiscalant materials with CNIM the membrane fouling reduced further and the flux increased by ~18%. Among all three salts, $CaSO_4$ fouled the membrane most drastically and the use of AS in the feed solution also was found to be more effective for $CaSO_4$. In general, by using CNIM the fouling reduced on the membrane surface and enhanced the MD performance. The addition of AS further increased the antifouling properties of the system.

Table 4.1 Normalized Flux Decline (FD_n) for Various Salt Solutions

Salt	FDn (%) of various salt solutions			
	PP	CNIM	PP- AS	CNIM-AS
$CaSO_4$	66	36	40	30.8
$CaCO_3$	53	37	25	27
$BaSO_4$	51	24	17	22

The normalized flux declination (FD_n) for different membrane systems with various salt solutions are shown in Table 4.1. It is clear from the table that the CNIM exhibited lower flux decline for all salts compared to PP, indicating a clear lowering the fouling tendency. The use of AS further improved the antifouling property of both membranes. For $CaSO_4$, the flux decline for CNIM-AS and CNIM were found to be 30.8 and 36%, respectively, which were 23% and 45% lower than that of the PP membrane.

4.3.4 Deposition of Salts on the Membranes

The deposition of the salt crystals on the membrane surface was measured by weighting the amount of salt on the membrane before and after 6 hours run and then drying the membrane overnight in an oven at 70^{o}C. The weight measurements were done very carefully to avoid any loss of deposited salt from the surface. The results are shown in Table 4.2.

Table 4.2. Deposition of Salts on the Membrane Surface after 6 hr of Operation at 70^{o}C

Salt	Amount of salt deposited on the membrane surface (mg)		% weight decrease
	PP	PP-AS	
$CaSO_4$	12.4	8.9	28.2
$CaCO_3$	22.6	16.8	25.7
$BaSO_4$	6.8	5.3	22.1
	CNIM	CNIM-AS	
$CaSO_4$	8.6	6.4	25.6
$CaCO_3$	10.5	7.9	24.8
$BaSO_4$	5.2	4.1	21.2

From Table 4.2 it is clear that the amount of salts deposited on the membrane surface was lesser for CNIM than the PP membrane for all cases. The lower salt deposition on CNIM may be attributable to the screening effect of CNTs [236]. The table also demonstrates the advantage of using antiscalant in reducing the salt deposition on the membrane surface [237, 238]. The AS influenced the PP membrane based desalination slightly more than the CNIM, where the salt deposition reduced by 25.6% and 28.2% respectively for CNIM and PP for $CaSO_4$.

SEM images of the deposition of various salt crystals on different membrane surfaces with and without using antiscalant is shown in Figure 4.7. The SEM images clearly show the difference in crystal configuration of different salt clusters. It is also revealed from the images that the use of AS significantly reduced the fouling layer on the membrane

surface [95, 119, 239]. The foulants interact with each other and with the membrane surface to form deposits [240-244], The antiscalant interact with the foulants and with the membrane surface to breakdown the salt crystals (foulants) and reduce the fouling as it shows in Figure 4.7 a, b and c for all salts.

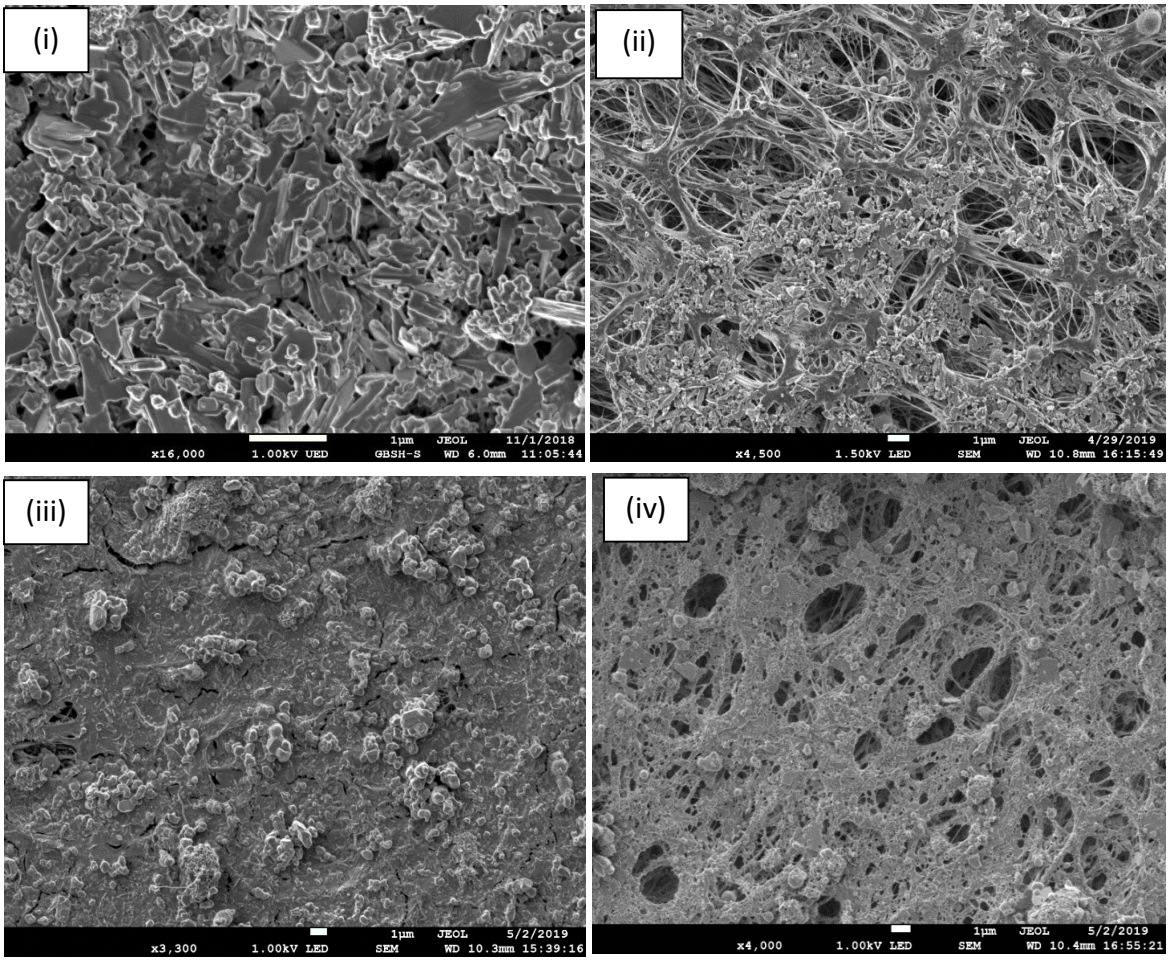

Figure 4.7 (a) SEM image of $CaSO_4$ deposition on (i) PP; (ii) PP-AS; (iii) CNIM and (iv) CNIM-AS after running the experiment given in Figure 4.6b.

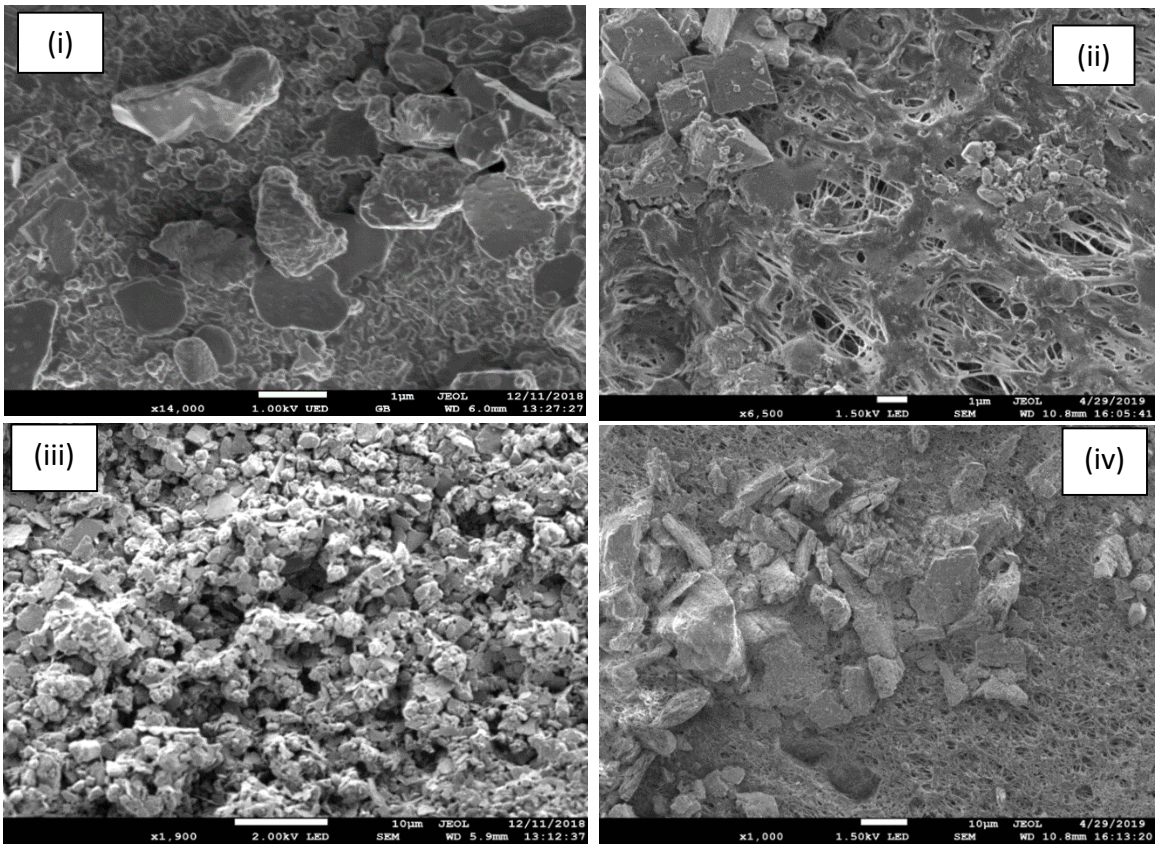

Figure 4.7 (b) SEM image of $CaCO_3$ deposition on (i) PP; (ii) PP-AS; (iii) CNIM and (iv) CNIM-AS after running the experiment given in Figure 4.6c.

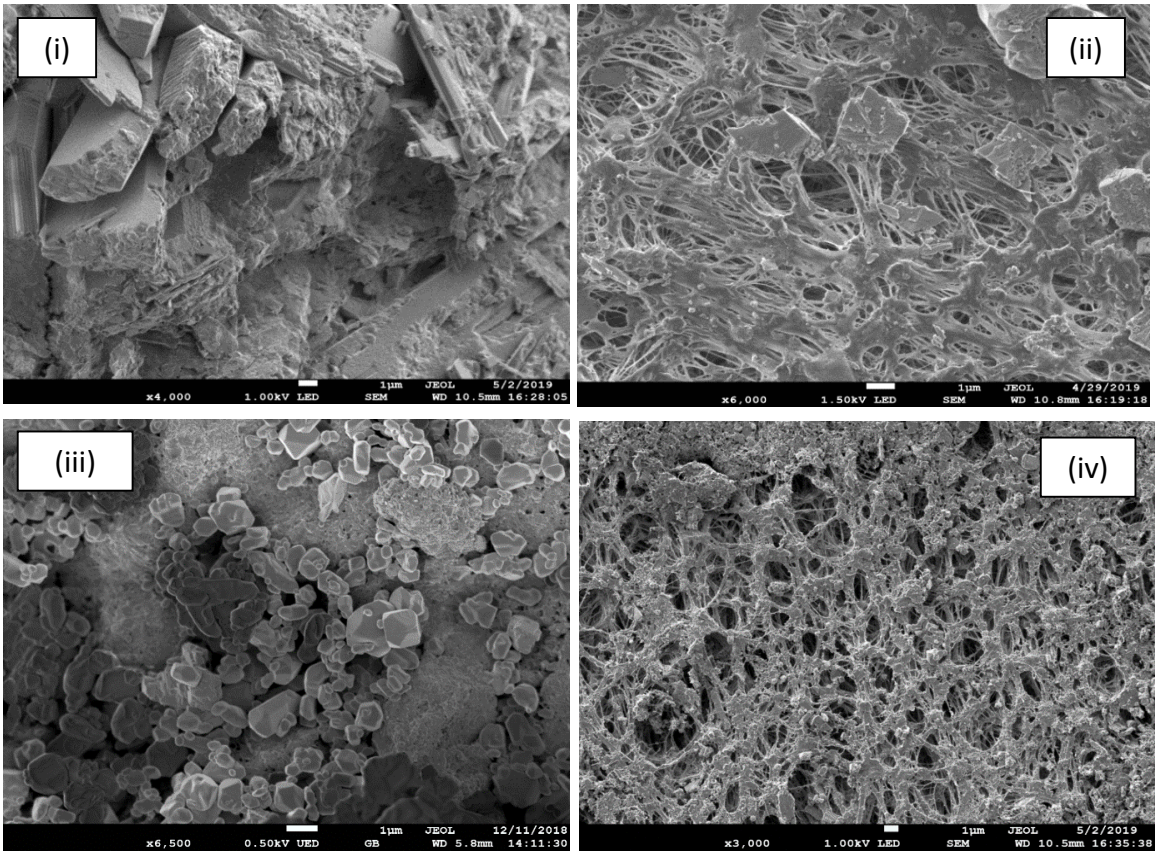

Figure 4.7 (c) SEM image of $BaSO_4$ deposition on (i) PP; (ii) PP-AS; (iii) CNIM and (iv) CNIM-AS after running the experiment given in Figure 4.6d.

4.3.5 Membrane Regeneration and Stability

The regenerability of the fouled membranes using $CaSO_4$ as feed were studied with or without AS in the system. The MD experimentations were continued for 6 hours followed by washing the fouled membrane by circulating DI water at 70^oC for 30 min and then continue the MD experiments again for another 6 hours. The water vapor flux after washing was compared with the initial flux.

Table 4.3 Membrane Regeneration Data

Membrane	1st Day Flux ($kg/m^2.hr$)	2nd Day Flux ($kg/m^2.hr$)	Flux regenerated (%)
PP	39.4	33.5	85.0
PP-AS	44.4	39.4	88.7
CNIM	47.6	45.2	95.0
CNIM-AS	52.0	50.2	96.5

Table 4.3 shows the regenerability of the membranes with $CaSO_4$ with and without AS. It is clear from the Table that the CNIM was able to remove the deposited salts and attained around 97% of its initial water vapor flux. In contrast, the PP membrane only reached up to 85% of its original value, which clearly demonstrated the superiority of CNIM in terms of membrane regeneration.

The outcomes were further confirmed by using SEM and measuring the weight of the salts remained on the membrane surface after washing. Figures 8 a, b, c and d show the surface SEM images of the $CaSO_4$ fouled PP membrane and CNIM with and without AS after washing. The salt precipitation was found to be less on the CNIM surface after washing, which further demonstrated the washability and regenerability of the CNIM.

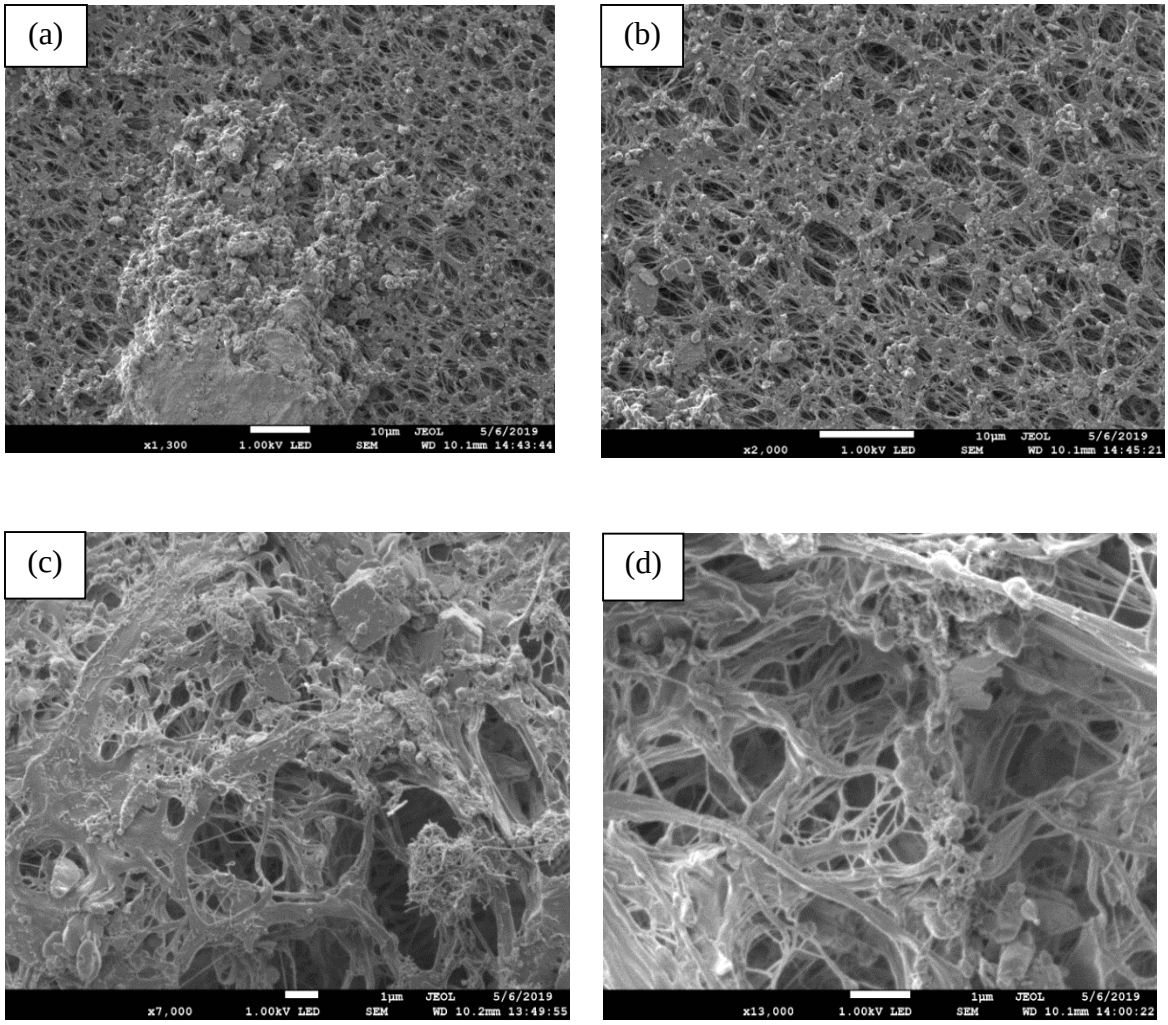

Figure 4.8 SEM image of the fouled membrane after washing (a) PP; (b) PP-AS; (c) CNIM and (d) CNIM-AS

Table 4.4 shows the amount of salt remained on the membrane surface after washing the fouled membranes. The result showed the amount of salt remained on the membrane surface was significantly lower than that of the fouled membrane. Among PP and CNIM, the CNIM showed higher washability of the deposited salts.

Table 4.4 Amount of Salt Deposition on the Membrane Surface after Washing

Salt	Amount of salt remained on the membrane surface after washing (mg)			
$CaSO_4$	PP	PP-AS	CNIM	CNIM-AS
	5.5	4.2	2.3	1.9
Removal (%)	55.6	52.8	73.3	70.3

While running the experiment with CNIM, no CNTs have been detected in the feed solutions that have been recycled. The CNIM was also run with aqueous solutions for 30 days (6hr per day) at 70^{o}C and then inspected to see is there was any loss of CNTs. However, any appreciable loss of CNTs was not observed, which demonstrates the ability of CNTs to retain on the membrane surface[171].

4.4 Conclusion

This paper successfully demonstrates the enhanced antifouling behavior of CNIM over pristine PP membrane. The addition of antiscalant to the feed solution resulted in a reduction in fouling on the surface of the membrane. The desalination performance of PP and CNIM were compared. The CNIM exhibited lower flux decline for all the salts. The washability and regenerability of the CNIM was observed to be superior than the pristine PP membrane. The addition of antiscalant materials and using CNIM in MD was found highly effective in enhancing the membrane performance and membrane regenerability when treating the high concentration fouling salts.

CHAPTER 5

ENHANCED PEREFORMANCE OF CARBON NANOTUBE IMMOBOLIZED MEMBRANE FOR TREATMENT OF HIGH SALINITY PRODUCED WATER VIA DIRECT CONTACT MEMBRANE DISTILATION

5.1 Introduction

Hydraulic fracturing or fracking employs horizontal drilling technique to release oil and hydrocarbon by injecting high pressure water containing particulates and chemical additives. A major problem with fracking is the large volume of wastewater it generates, both initially, as "frac" flow back, and over time as produced water. The U.S. alone generates approximately 70 million barrels of produced water per day or 25 billion barrels per year from oil and gas activities [245]. This volume is increasing as fracking activities expand. At the same time options for waste water disposal are narrowing, putting oil and gas operations in jeopardy. Water pollutants in frack and produced water include total dissolved solids (TDS), oil and grease, suspended solids, volatile organics, heavy metals, dissolved gases, chemical additives such as scale and corrosion inhibitors, guar gum and emulsion/reverse-emulsion breakers. After the recovery of some of the additives, the desalination and TDS removal remains the major challenge, which can be as high as 350,000 or ten times average sea water concentration [246].

The two major approaches to desalination (or desalting) are thermal distillation and membrane separations**.** In the former, the saline water is boiled using thermal energy and recondensed. Commercial thermal distillation methods such as multistage flash, multi-effect distillation and mechanical vapor compression have relatively large footprints and require larger investments. On the other hand, membrane process have lower capital and

operating costs and the most common desalination technique is Reverse osmosis (RO). Some of the limitations of RO come from the increase in osmotic pressure at high salt concentrations, which often makes it ineffective for treating highly saline water (concentrations above 70000 ppm). Moreover, dense hydrophilic membranes used in RO tend to foul easily leading to low water production and reduced membrane life. Therefore, RO often requires extensive pretreatment such as water softening which increases both capital and operational expenses. Subsequently, there is an urgent need to develop new membrane based techniques for treating oil and gas industry produced water [247, 248]. At his point, the two viable techniques for treating high salinity water appear to be are forward osmosis (FO) [249, 250] and membrane distillation (MD) [232, 251]. MD is a thermally driven desalination technology that has seen steady improvements in the design of membranes and technical performance [252, 253]. Previous studies have shown that MD has the potential to achieve up to 99.9% of salt rejection [254, 255] and 99.5% of organic materials removal [256]. Moreover, the low operating temperature (60 to 90^{o}C) of MD also makes it ideally suited for integration with renewable energy sources such as solar or low grade industrial waste heat sources [208, 257] such as flare gas at oil fields [247].

Recently, our group has fabricated carbon nanotube based membranes and used in a variety of separation applications that range from pervaporation, extraction to Nano filtration [171]. The physicochemical interaction between the water vapor and the membrane can be dramatically altered by immobilizing CNTs on the membrane surface [173, 201]. First, CNTs are excellent sorbents that have surface areas between 100 and 1000m2/g [201, 258]. Many factors, such as the presence of defects, capillary forces in nanotubes, polarizability of graphene structure lead to strong H_2O vapor/CNT interactions,

the absence of a porous structure lead to high specific capacity while facilitating fast desorption of large molecules. It is anticipated that the CNIM will provide higher flux in the treatment of produced water [229, 259].

A major obstacle in the widespread use of the membrane technologies in the treatment of high salinity water is the problem of membrane fouling [217, 260, 261] due to the deposition of suspended or dissolved substances on the membrane surface and/or within its pores [262, 263]. This is particularly true for produced water that contains high levels of salts, ions and metals. With concentration of $CaCO_3$ and different ions and cations at near saturation level, any membrane process including MD is expected to foul rapidly. Recently we have reported the development carbon nanotube immobilized membranes (CNIM) that have shown relatively lower fouling as the CNTs immobilized on the surface act as nano-brushes that prevent the salt crystals from depositing on the surface [93]. The CNIM has shown high salt tolerance compared to pure polymeric membranes and has been used to treat water with TDS as high as 230,000 mg/L.

The use of antiscalant has also been reported to be beneficial in RO and other process by reducing scaling of different salts [264, 265]. Various types of antiscalants including acids, bases, enzymes, surfactants, disinfectants and combined cleaning materials has been employed in membrane separation processes[266, 267]. The choice of antiscalants depends on the nature of treated water. Produced water contains iron-based components that deposits on the membrane surface even with relatively low concentrations of iron in the feed side. (1-hydroxy Ethylidene-1, 1- Diphosphonic acid) (HEDP) is threshold inhibitor based on phosphonic acids (or their salts) which have the added advantage of sequestering iron in a stoichiometric reaction [268-270]. This is important in

membrane applications, as any soluble iron will cause rapid fouling as it oxidizes and becomes insoluble. HEDP has the potential to dissolve the oxidized materials on these metal's surfaces [271]. Therefore, there is growing interest in possible options for treatment or reuse of produced waters. The objective of this paper was to investigate the enhancement in water vapor flux and antifouling characteristics of CNIM with addition of HEDP antiscalant in treating produced water via DCMD mode.

5.2 Materials and Methods

5.2.1 Chemicals and Materials

Produced water used in this experiment was collected from Chemtraet Company USA. Deionized water (Barnstead 5023, Dubuque, Iowa) was used in all experiments. Filter papers (Whatman- 1441-150 size 41 with Diameter of 150mm) from Cole-Parmer, 625 East Bunker Ct Vernon Hills, IL 60061 United States. MWCNTs were purchased from Cheap Tubes Inc., Brattleboro, VT. The average diameters of the CNTs were ~ 30 nm and a length range of 15 μm. 1-Hydroxy Ethylidene-1,1-Diphosphonic Acid (HEDP) antiscalant purchased from (Fisher Scientific Company, Hanover Park,60133 IL).

5.2.2 Water Sample Composition

Produced water samples used for experiments were collected from Chemtraet in Pennsylvania. The sample contains sand and different types of chemicals that provided in Table1.

Table 5.1 Analysis of Produced Water before Filtration (A) in Figure (5.1)

Analysis	Produced Water
pH	2.19
Conductivity, μmho	239651
Calcium Hardness, as $CaCO_3$, mg/L	119500
Magnesium Hardness, as CaCO3, mg/L	12590
Iron, as Fe, mg/L	90
Copper, as Cu, mg/L	<1.0
Zinc, as Zn, mg/L	2.4
Sodium, as Na, mg/L	71820
Potassium, as K, mg/L	1780
Chloride, as Cl, mg/L	118
Sulfate, as SO4, mg/L	130
Nitrate, as NO3, mg/L	<100
Ortho−Phosphate, as PO4, mg/L	<500
Silica, as SiO2, mg/L	41

5.2.3 Water Sample and Pretreatment Methods

The water sample was first filtered with Whatman-41 filter paper to remove the large solid particles from the produced water. The antiscalant HEDP was added to the filtered water prior to the DCMD experiment. Figure1 showed the produced water sample before, after filtration, and with HEDP antiscalant. Also, Table 2 shows the ICP-MS results for the filtered produced water with and without using HEDP.

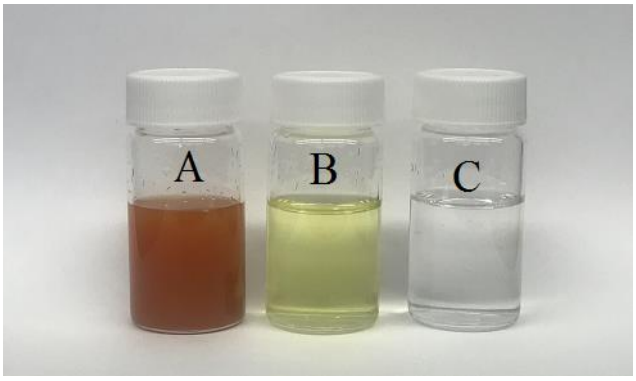

Figure 5.1 (A) Produced water sample before filtration; (B) Produced water sample after filtration; and (C) Produced water sample with HEDP

Table 5.2 Analysis of Produced Water after Filtration (b) and with HEDP (c).

Element	Conc. PPM [B]	Conc. PPM [c]
Li	12.85105519	1.627538997
Be	<0.0017	<0.0017
Na	153.9527754	28.95956318
Al	0.0136204867	0.01304088831
K	12.50826194	1.257055475
Ca	1455.058891	52.68469769
Sc	0.000066141186	<0.0
Ti	<0.0004	<0.0004
V	0.000173930282	0.000020687219
Cr	0.000140303226	<0.0
Mn	1.274097669	0.01115449473
Fe	1.390113521	0.008039872058
Co	0.000066371033	0.000011111706
Ni	0.000636449023	0.000108444154
Cu	0.01369814176	0.006227625894
Zn	0.02490735413	0.001189185756
Ge	<0.0	<0.0
As	0.001758593414	0.00049789394
Se	<0.0018	<0.0018
Rb	0.3650287873	0.02602917761
Sr	597.9545132	10.85984992
Mo	0.000017699723	<0.0
Ag	0.000038914761	0.000008988294
Cd	<0.0	<0.0
In	<0.0	<0.0
Sn	0.000089764015	0.00002671536
Sb	0.000186120956	0.000041128582
Cs	0.1027199687	0.008031620967
Ba	288.5929217	11.43338683
TI	0.000238425152	0.000008223622
Pb	0.001336379863	0.001715917264
Bi	0.000010316481	<0.0

5.2.4 CNIM Fabrication

Effective dispersal of CNTs and immobilization on the membrane surface was an essential step in CNIM fabrication. The CNT membrane was prepared using a polytetra-fluoroethylene (PTFE) laminate sup-ported on polypropylene composite membrane (Advantec, 0.2 μm poresize, 74% porosity). The CNTs dispersion was carried out as follows: 1.5 mg of CNTs were dispersed in a solution containing 8 g of acetone and sonicated for four hours. 0.2 mg of polyvinylidene di fluoride (PVDF), which acted as a binder during immobilization of the CNTs was dissolved in 2 g of acetone and mixed with CNTs dispersion as it mentioned in our previous papers [201]. The PVDF-nanotube dispersion was thereafter applied uniformly with a dropper over the membrane held on a flat surface to form the CNIM. The wet CNIM was kept under the hood for overnight drying. The CNIM was characterized using scanning electron microscopy (SEM) Leo 1530 VP, Carl Zeiss SMT AG Company, Oberkochen, Germany.

5.2.5 Experimental Procedure

MD experiments were conducted in the direct contact MD (DCMD) configuration. Figure 2 shows the schematic diagram of the MD system used in the laboratory. The membrane module used for DCMD was a cylindrical module utilizing a flat membrane with a gasket diameter of 3.9 cm and an effective membrane area of 11.94 cm^2. The membrane used was flat composite PTFE membrane supported with polypropylene nonwoven fabric (Advantec MFS, Dublin, CA, USA; 129 μm thick, 0.2 μm pore size and 70% porosity). The preheated hot produced water was passed through a heat exchanger, which was used to maintain the desired temperature throughout the experiment. The hot feed was recycled to the feed tank and permeate was collected in the distillate tank. DI water was used as cold distillate. Both

hot and cold sides were circulated through the module using peristaltic pumps (Cole Parmer, model 7518-60). Inlet and outlet temperatures of the feed and distillate were monitored continuously throughout the experiment. Viton and PFA tubings and connectors (Cole Parmer) were used to make connections in the experimental set up. The ionic strength of the original feed solution and permeate were measured using an Electrode Conductivity Meter (Jenway4310).

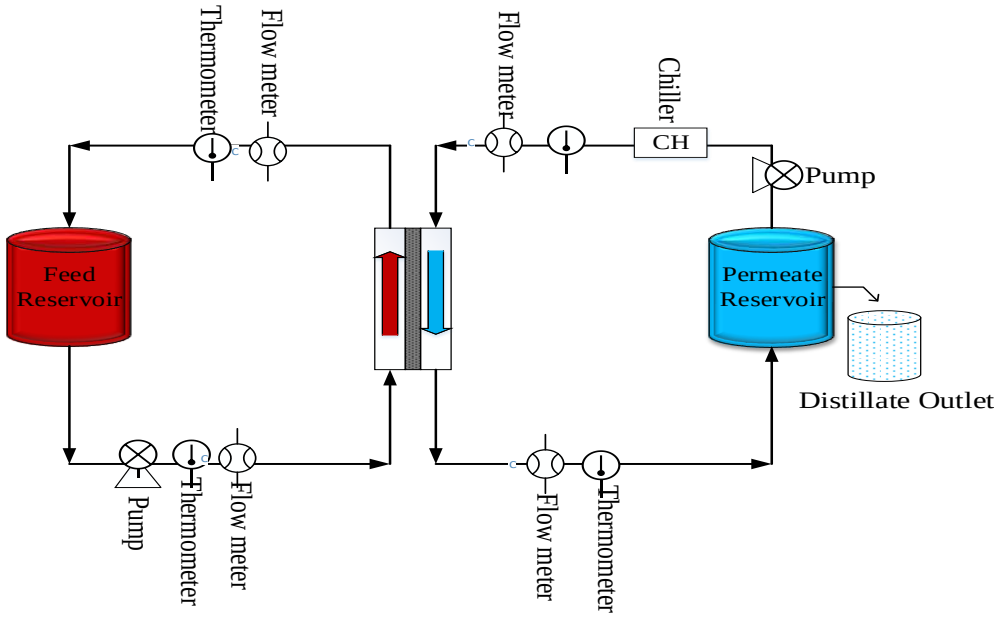

Figure 5. 2 Schematic representation of the experimental setup.

5.2.6 DCMD Performance using CNIM and PTFE Membrane

The MD performances of PTFE and CNIM was studied as a function of time, temperature, and feed flow rate. The water vapor flux, Jw, measured as:

$$Jw = wp/t.A \qquad (5.1)$$

Where wp is the mass of permeated water in time t through surface area A. To compare the fouling on both membranes, the flux measured over time and the normalized flux decline, FDn, measured as:

$$FD_n(\%) = \left(1 - {J_f}/{J_0}\right) \times 100 \quad (5.2)$$

Where, J_f and J_0 are the final permeate flux and initial flux, respectively. Table 5.2 shows the normalized flux decline FD_n (%) of produced water with and without using HEDP.

5.3 Results and Discussion

5.3.1 Membrane Characterization

The SEM images of the CNIM and the PTFE membrane shown in Figure 5.3 a; and b. SEM images shows porous structure of the pristine PTFE membrane and presence of CNTs on the CNIM surface. The distribution of CNTs was relatively uniform over the entire membrane surface. The TGA curves of PTFE and CNIM membranes shown in Figure 5.3c. It is clear from the figure that the membranes are quite stable within the experimental temperature ranges.

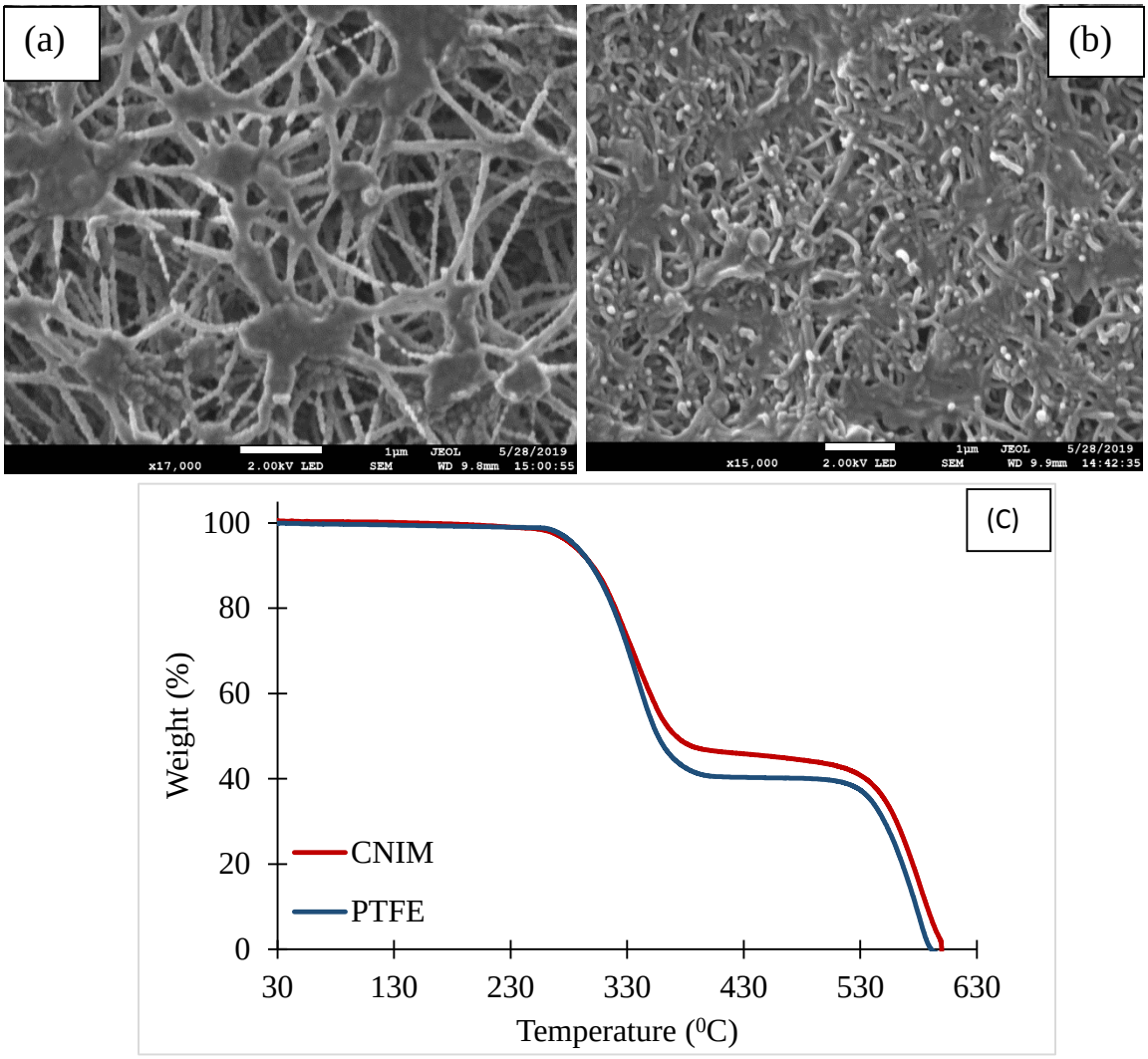

Figure 5.3 (a) SEM image of PTFE membrane; (b) CNIM; and c) The TGA curves of PTFE membrane and CNIM.

5.3.2 Effect of Temperature and Feed Flow Rate on Water Vapor Flux

The effect of temperature on permeate flux for both membranes is illustrated in Figure 5.4a at feed flow rate 200 mL/min and distillate flowrate of 200 mL/min1. It is clear from the figure that the water vapor flux increased with increase in temperature as higher feed temperature generates high vapor pressure gradient. The CNIM demonstrates higher flux compared to the PTFE membrane at all temperatures. The flux enhancement in CNIM is in line with our previously reported data [149, 171, 175]. Further, the addition of HEDP

(antiscalant) on the feed side led to enhanced performance of MD for both membranes. At a temperature of 70^{o}C, the water vapor flux increased from 30.9 to 35.2 kg/m^2.h for PTFE and 46.1 to 51.6 kg/m^2.h with CNIM with the incorporation of HEDP at the same experimental conditions.

In addition, the influence of increasing feed flow rate at a constant temperature of 70 ^{o}C and 200 mL/min permeate flow rate is displayed in Figure 5.4b. It was observed that the permeate flux increased with an increase in feed flow rate for all membranes and the CNIM offered higher water vapor flux when compared to PTFE. The increased feed flow rate reduces the fouling by increasing the turbulence, which in turn reduces the boundary layer effect at the membrane-feed solution interface [272]. As can be seen from Figure 5.4b, at a feed flowrate of 150 mL/min, the water vapor flux increased from 25.1 to 29.3 kg/m^2.h for PTFE and from 30.9 to 41.9 kg/m^2.h with CNIM using antiscalant, which was 17% and 36% higher, respectively.

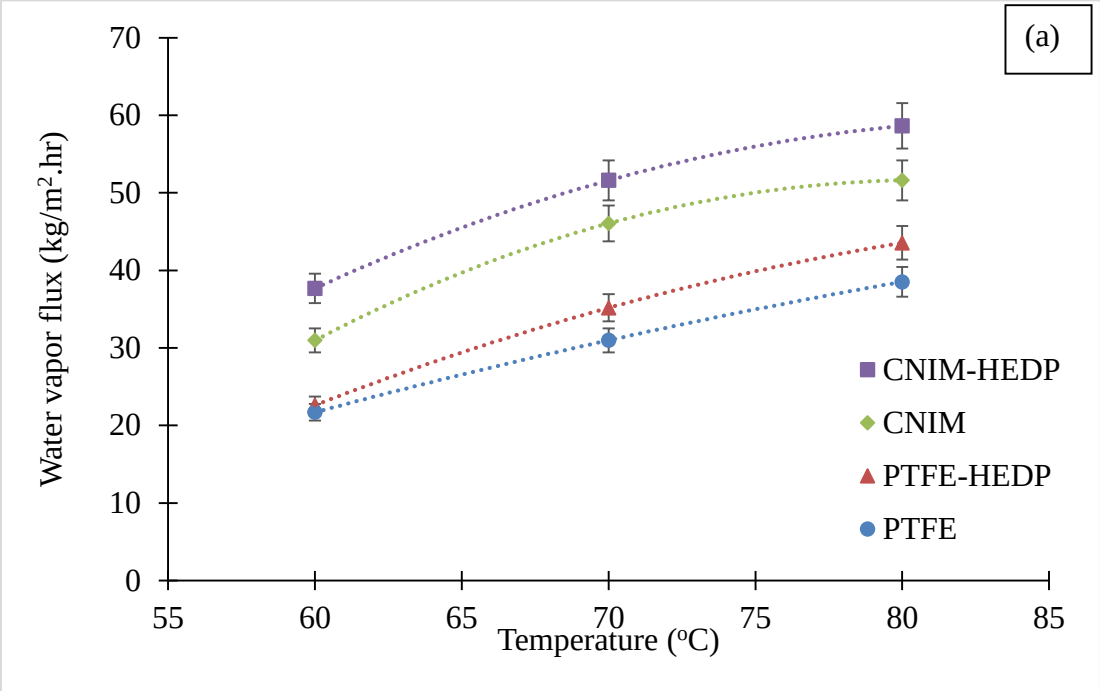

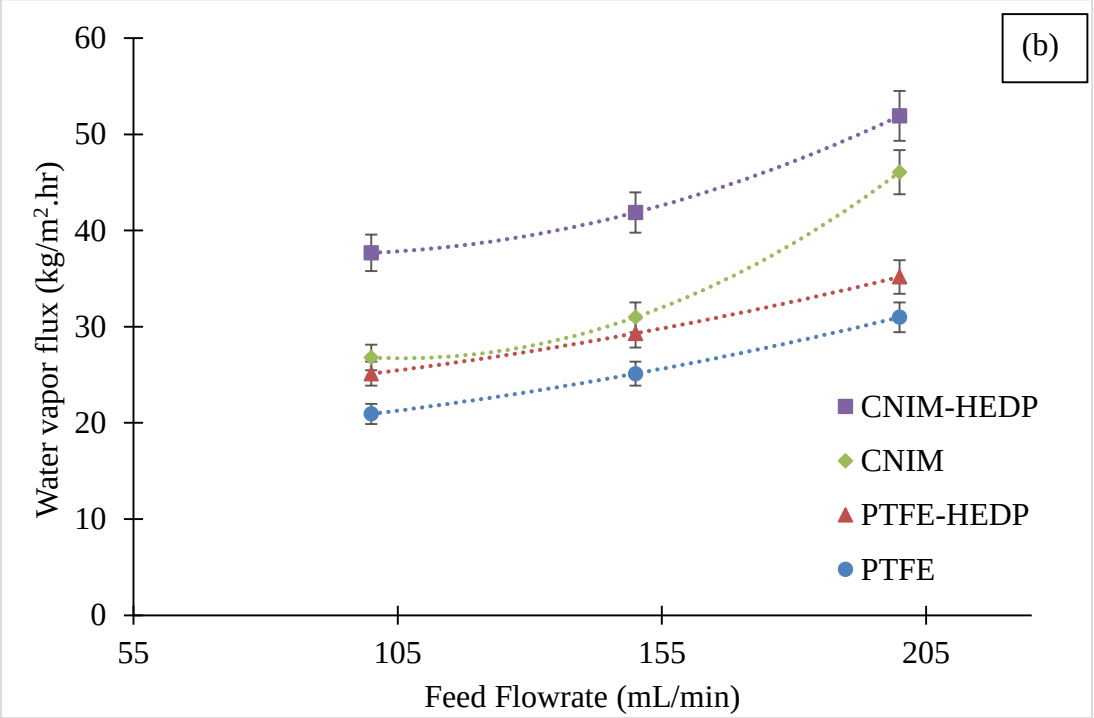

Figure 5.4 (a) Effect of temperature on permeate flux of produced water solution at 200mL/min flowrate; (b) Effect of flowrate on permeate flux of produced water solution at 70^{o}C temperature and 200 mL/min flow rate.

5.3.3 Fouling Behavior of Produced water

The fouling behavior of filtered produced water was studied on pristine PTFE membrane and CNIM using HEDP antiscalant and was characterized by the reduction of permeated water flux as a function of time. Figure 5.5 showed that the water vapor flux reduced significantly with time for all membranes as an outcome of scaling. It is clear from the figure that the CNIM exhibited higher antifouling properties in comparison with PTFE membrane. This may be due to additional screening effect of CNTs which reduced pore blocking from salt deposition on membrane pores. For produced water solution, the flux declined to 10.9 from 30.9 kg/m^2.hr for PTFE and to 19.3 from 46.1 kg /m2.hr for the CNIM after 7 hr of operation. The results show that by using CNIM the water vapor flux after 7 hr was still 77% higher than that of the PTFE membrane. The use of HEDP in the feed solution further improved the antifouling behavior of both membranes and the water vapor flux after 7 hr of operation was 35.2 kg/m^2.hr and 51.6 kg/m^2.hr for PTFE membrane and CNIM, respectively, which is 32.4% and 74% higher compared to the system without HEDP. This may be due to the fact that the antiscalant delays the clustering process and prevents the precipitation of salt on the membrane surface [7].

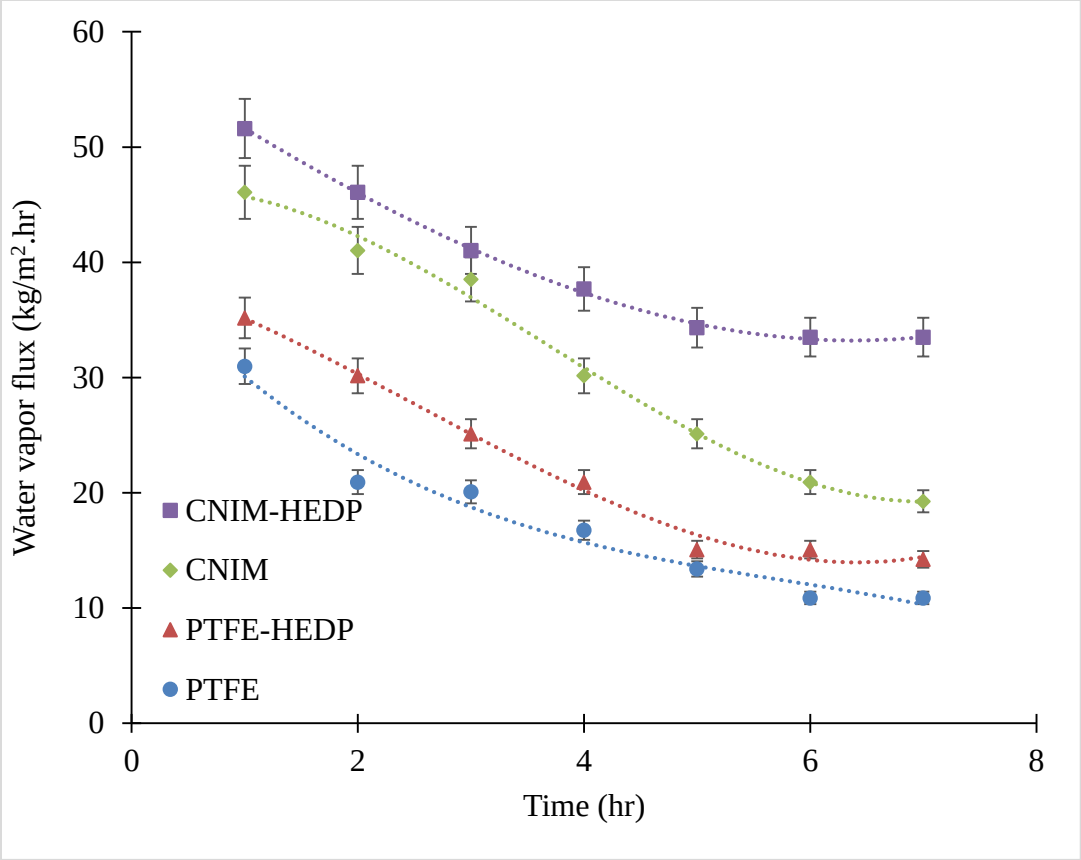

Figure 5.5 Water vapor flux in PTFE and CNIM membranes for produced water solution with and without using HEDP (antiscalant).

Table 5.3 Normalized Flux Decline (FD_n) for Produced Water Solution

Solution	FDn (%) of produced water solution			
	PTFE	CNIM	PTFE-HEDP	CNIM-HEDP
Produced water	64.8	58.2	59.5	35.1

The normalize flux declination (FD_n) for all membranes after 7 hr of operation with produced water are shown in Table 5.2. It is clear from the table that the reduction in flux was lower in CNIM compared to the PTFE membrane, indicating lower fouling tendency. The use of HEDP further improved the antifouling property of both membranes. Under

similar conditions, the CNIM with HEDP exhibited an improvement of 41% in FD_n compared to the pristine PTFE membrane.

5.3.4 Deposition of Foulants on the Membrane Surface

The deposition of the foulants on the membrane surface was evaluated by measuring the membrane weight before and after the experiment. The weight measurements were done with precision by drying the membrane overnight in the oven at 70^{o}C to avoid any loss of deposited foulants from the surface.

Table 5.4 Deposition of Foulants on the Membrane Surface after 7 hr of Operation at 70^{o}C

Solution	Amount of salt deposited on the membrane surface (mg)		% weight decrease
	PTFE	PTFE-HEDP	
Produced water	15.76	4.68	70.3
	CNIM	CNIM-HEDP	
	1.02	0.79	22.5

From Table 5.3 it is clear that the amount of salts deposited on the membrane surface was lesser for CNIM than the pristine PTFE membrane for all cases. The lower salt deposition on CNIM may be attributable to the screening effect of CNTs. The table also demonstrates the advantage of using antiscalant in reducing the salt deposition on the membrane surface. The CNIM along with HEDP in feed successfully lowered the salt deposition on membrane surface, which is a major concern in treating the feed containing higher amount of foulants, such as produced water.

SEM images of the deposition of various salt crystals on different membrane surfaces with and without using HEDP antiscalant is shown in Figure 5.6. The SEM images clearly show the variation of foulants' morphology and amounts deposited on the membrane surfaces with and without using HEDP for both membranes. It is also revealed

from the images that the use of HEDP significantly reduced the fouling layer on the membrane surface. The antiscalant interact with the foulants and with the membrane surface to breakdown the crystals (foulants) and reduce the fouling as it shows in Figure 5.6 b and d.

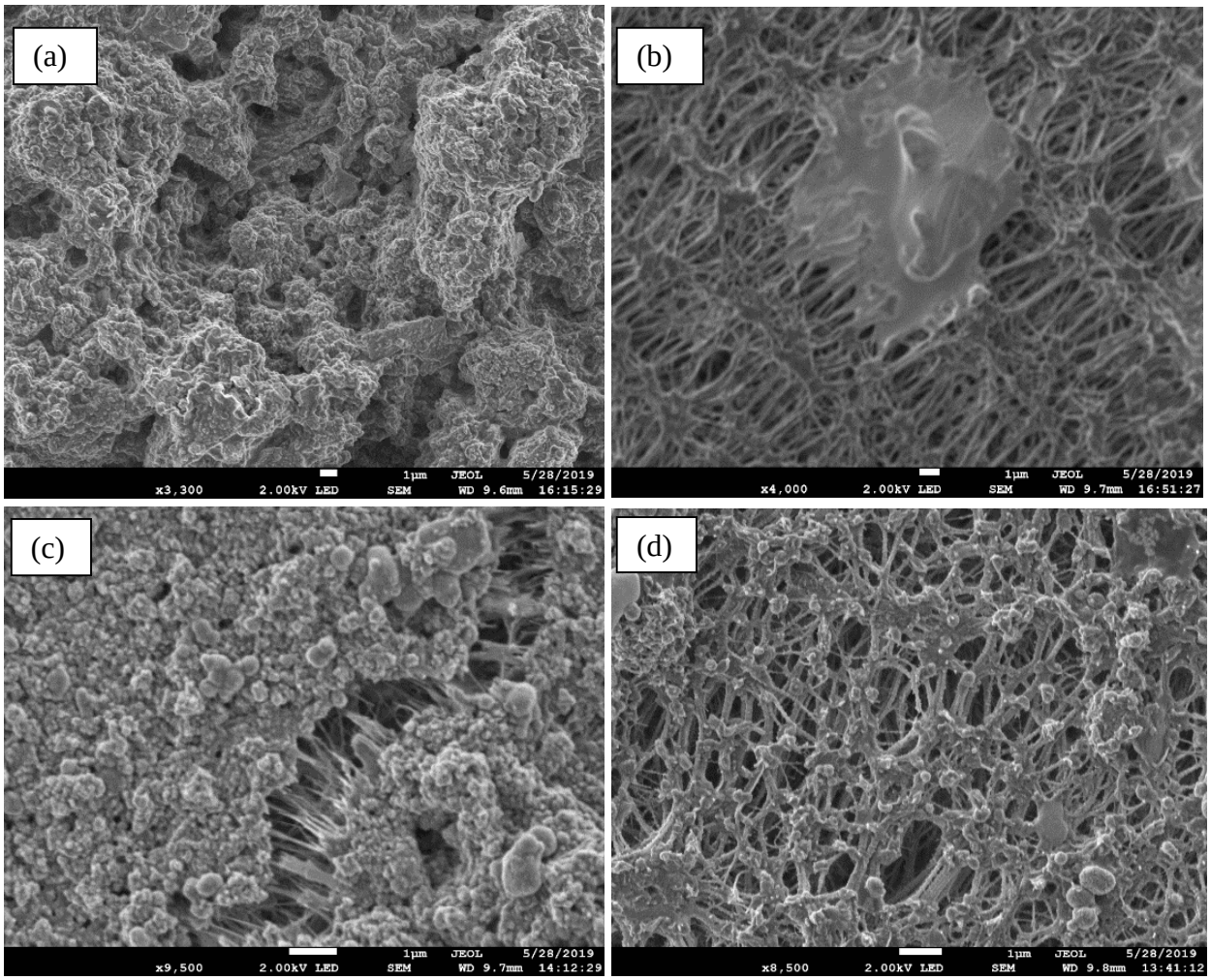

Figure 5.6 SEM image of foulants deposition on (a) PTFE; (b) PTFE-HEDP; (c) CNIM and (d) CNIM-HEDP.

5.3.5 Membrane Regeneration

The regenerability of the fouled PTFE membrane and CNIM, treating the produced water were studied with and without HEDP (antiscalant). Here, the MD experiments were running for 6 hours continuously (1st day) followed by washing the fouled membrane for 30 minutes with DI water at 70^{o}C and then continue the MD experiments again for another 6 hours continually on the next day for 5 days by taking the first data after washing at 70^{o}C as it shown in Table 5.4.

Table 5.5 Membrane Regeneration Data

Membrane	1st Day Flux (kg/m^2.hr)	2nd Day Flux (kg/m^2.hr)	Flux regenerated (%)
PTFE	30.9	25.1	81.1
PTFE-HEDP	35.2	33.5	95.2
CNIM	46.1	41.9	90.9
CNIM-HEDP	51.9	49.4	95.2

Table 5.4 shows the regenerability of the membranes with produced water with and without HEDP. It is clear from the Table that the CNIM was able to attain around 91% of its initial water vapor flux, which clearly indicated significant removal the deposited salts from the membrane surface and pores. In contrast, the PTFE membrane only reached up to 81% of its original value, which clearly demonstrated the superiority of CNIM in terms of membrane regeneration. The use of HEDF further helped regeneration of both membranes, which showed around 95% recovery of initial flux.

5.3.6 Mass transfer Coefficient

The overall, mass transfer coefficient can be described as:

$$Jw = k\,(P_f - P_p) \quad (5.3)$$

$$\text{Or} \qquad k = Jw\,/\,(P_f - P_p) \quad (5.4)$$

Where, J_w is the water vapor flux, k is mass transfer coefficient, and P_f and P_p are partial vapor pressure of average feed and permeate temperatures. The mass transfer coefficients were found to be higher for CNIM membrane as compared to the PTFE membrane.

Table 5.5a summarizes the change in mass transfer coefficients of PTFE membrane and CNIM with varying feed flow rate at 70 ^{o}C. Both membranes exhibited increased mass transfer coefficient with increase in feed flow rate. The diffusion of the water vapor through the boundary layers mainly controls the overall mass transfer rate of the process. At higher feed flow rate, the turbulence increased that led to the reduction in the boundary layer resistance and significantly increased the mass transfer coefficients. Between these two membranes, CNIM exhibited higher mass transfer coefficient in comparison with the PTFE membrane.

Table 5.5b shows the mass transfer coefficients at different temperatures. It is evident from the table that the CNIM showed higher mass transfer coefficients compared to pristine PTFE membrane in all cases. Rapid sorption/desorption on CNTs surfaces along with activated diffusion led to increase the overall water vapor transport. The mass transfer coefficients was found to decrease with increase in temperature for both membranes.

Table 5.6a. Effect of varying feed flow rate on mass transfer coefficient at 70 ºC.

Mass transfer coefficient ($kg/m^2\ sec^{-1}\ Pa$) × 10^{-7}		
Feed Flowrate(ml/min)	PTFE	CNIM
100	1.9	2.6
150	2.4	3.0
200	3.7	4.4

Table 5.6b. Mass Transfer Coefficient of Various Membranes as a Function of Temperature.

Mass transfer coefficient ($kg/m^2\ sec^{-1}\ Pa$) × 10^{-7}		
Temperature (°C)	PTFE	CNIM
60	3.4	4.9
70	3.0	4.4
80	2.4	3.1

5.4 Membrane Stability

The quality of permeate side water was carefully investigated to monitor the stability of modified membrane and salt breakthrough. The stability of CNIM was tested for 60 days. The permeated water was monitored throughout the experiment to ensure the quality of water by measuring the conductivity of the permeate side water and using Raman spectroscopy [7]. The permeated water sample did not show any presence of salts or CNTs after long period of operation.

5.5 Proposed Mechanism

The proposed mechanism for enhanced antifouling behavior of CNIM in presence of HEDP antiscalant is shown in Figure 5.7. The HEDP is known to be the most effective threshold inhibitors based on phosphonic acids (or their salts) that prevents the precipitation of the foulants on the membrane surface by delaying the clustering process of charged ions protonuclei [7]. This is important in membrane applications especially with produced water as it contains large quantity of inorganic salts that deposits on the membrane surface, causing significant reduction in membrane performances and wetting. Our previous studies with CNTs have demonstrated that CNTs are excellent sorbents that enhance partition coefficient of the solutes leading to higher flux in membranes [7]. Further, the presence of CNTs could act as an additional screen that also prevents the salt deposition on the membrane pores.

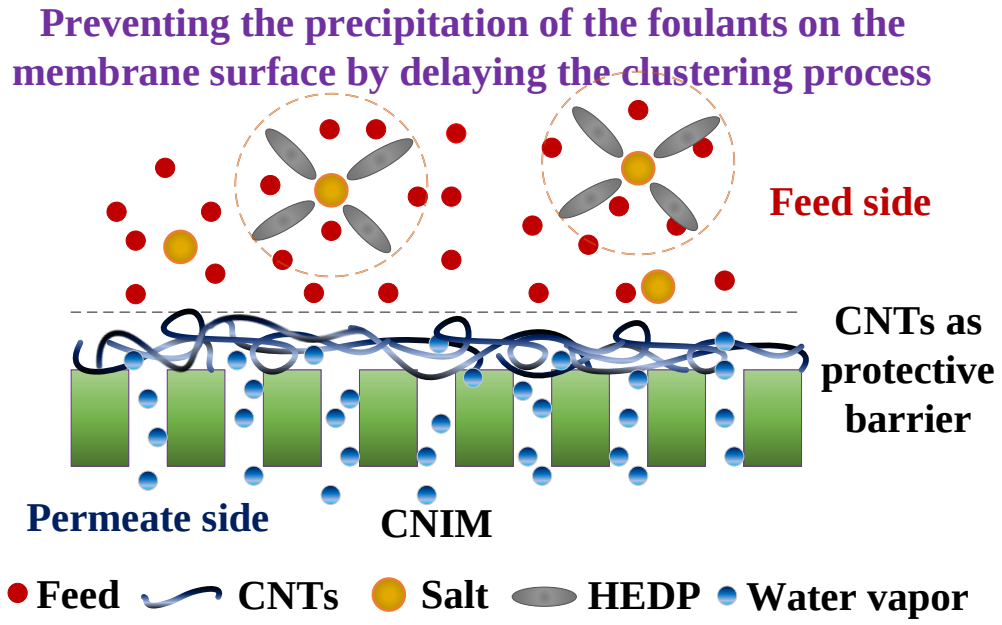

Figure 5.7 Proposed Mechanism.

5.6 Conclusion

The CNIM was successfully employed in treating the produced water. The MD performance was compared with pristine PTFE membrane. The addition of HEDP antiscalant in the produced water feed solution, further helped to reduce fouling and prevented the deposition of foulants on the membrane surface. The CNIM exhibited lower flux decline and the regenerability of the CNIM was also found superior than the pristine PTFE membrane. In summary, treating the produced water solution using HEDP antiscalant on CNIM in MD was found to be highly effective in reducing the fouling behavior, which in turn led to an enhancement in water vapor permeation through the membrane.

CHAPTER 6

SUMMARY

In summary, this research successfully demonstrates the enhanced antifouling behavior. First, by using the CNIM membrane over pristine membrane with microwave irradiation as a heat source in the DCMD system. Besides the enhancement of water vapor flux, the MIMD (microwave heating) exhibited significantly less fouling and the normalized flux decline was lower than conventional MD. The salt deposition on the membrane surface was observed to be between 50-79% less during MIMD and the morphology of the deposits from MIMD was quite different from those of conventional MD. It appears that non-thermal effect, such as, localized super heating, the breakdown of hydrogen bonding, alternation of surface tension, the increase in ionic mobility altered colloidal behavior and particle formation in MIMD. Apart from the less energy requirement and higher flux in MIMD, the lower flux decline at very high salt concentrations could lead to dramatic improvements to the MD technology in the future. Also, the addition of PAA antiscalant to the feed solution resulted in a reduction in fouling on the surface of the membrane. The desalination performance of pristine and CNIM membranes were compared. The CNIM exhibited lower flux decline for all the salts. The washability and regenerability of the CNIM was observed to be superior to the pristine membrane. The addition of antiscalant materials and using CNIM in MD was found highly effective in enhancing the membrane performance and membrane regenerability when treating the high concentration fouling salts. Finally, the addition of HEDP antiscalant in the produced water feed solution, further helped to reduce fouling and prevented the deposition of foulants on the membrane surface. The CNIM exhibited lower flux decline and the regenerability of the CNIM was also found

superior than the pristine PTFE membrane. In summary, treating the produced water solution using HEDP antiscalant on CNIM in MD was found to be highly effective in reducing the fouling behavior, which in turn led to an enhancement in water vapor permeation through the membrane.

REFERENCES

[1] E. Viala, Water for food, water for life a comprehensive assessment of water management in agriculture, Springer, 2008.

[2] J.E. Miller, Review of water resources and desalination technologies, Sandia national labs unlimited release report SAND-2003-0800, DOI (2003).

[3] H. Cooley, P.H. Gleick, G.H. Wolff, Desalination, with a grain of salt: a California perspective, Pacific Institute for Studies in Development, Environment, and Security …, 2006.

[4] A.D. Khawaji, I.K. Kutubkhanah, J.-M. Wie, Advances in seawater desalination technologies, Desalination, 221 (2008) 47-69.

[5] M. Elimelech, W.A. Phillip, The future of seawater desalination: energy, technology, and the environment, science, 333 (2011) 712-717.

[6] L.K. Wang, N.K. Shammas, M. Cheryan, Y.-M. Zheng, S.-W. Zou, Treatment of food industry foods and wastes by membrane filtration, Membrane and Desalination Technologies, Springer2011, pp. 237-269.

[7] A. Antony, J.H. Low, S. Gray, A.E. Childress, P. Le-Clech, G. Leslie, Scale formation and control in high pressure membrane water treatment systems: a review, Journal of membrane science, 383 (2011) 1-16.

[8] G.P. Narayan, M.H. Sharqawy, E.K. Summers, J.H. Lienhard, S.M. Zubair, M.A. Antar, The potential of solar-driven humidification–dehumidification desalination for small-scale decentralized water production, Renewable and sustainable energy reviews, 14 (2010) 1187-1201.

[9] A. Alkhudhiri, N. Darwish, N. Hilal, Membrane distillation: A comprehensive review, Desalination, 287 (2012) 2-18.

[10] O.A. Hamed, H.A. Al-Otaibi, Prospects of operation of MSF desalination plants at high TBT and low antiscalant dosing rate, Desalination, 256 (2010) 181-189.

[11] J. Oldfield, B. Todd, The use of stainless steels and related alloys in reverse osmosis desalination plants, Desalination, 55 (1985) 261-280.

[12] K.W. Lawson, D.R. Lloyd, Membrane distillation, Journal of membrane Science, 124 (1997) 1-25.

[13] N. Dow, S. Gray, J. Zhang, E. Ostarcevic, A. Liubinas, P. Atherton, G. Roeszler, A. Gibbs, M. Duke, Pilot trial of membrane distillation driven by low grade waste heat: Membrane fouling and energy assessment, Desalination, 391 (2016) 30-42.

[14] W.G. Shim, K. He, S. Gray, I.S. Moon, Solar energy assisted direct contact membrane distillation (DCMD) process for seawater desalination, Separation and Purification Technology, 143 (2015) 94-104.

[15] L.D. Nghiem, T. Cath, A scaling mitigation approach during direct contact membrane distillation, Separation and Purification Technology, 80 (2011) 315-322.

[16] M. Gryta, Fouling in direct contact membrane distillation process, Journal of membrane science, 325 (2008) 383-394.

[17] P. Wang, T.-S. Chung, Recent advances in membrane distillation processes: Membrane development, configuration design and application exploring, Journal of membrane science, 474 (2015) 39-56.

[18] E. Drioli, A. Ali, F. Macedonio, Membrane distillation: Recent developments and perspectives, Desalination, 356 (2015) 56-84.

[19] J. Zhang, M. Duke, Z. Xie, S. Gray, Performance of asymmetric hollow fibre membranes in membrane distillation under various configurations and vacuum enhancement, Journal of Membrane Science, 362 (2010) 517-528.

[20] T.Y. Cath, V.D. Adams, A.E. Childress, Experimental study of desalination using direct contact membrane distillation: a new approach to flux enhancement, Journal of Membrane Science, 228 (2004) 5-16.

[21] S. Al-Obaidani, E. Curcio, F. Macedonio, G. Di Profio, H. Al-Hinai, E. Drioli, Potential of membrane distillation in seawater desalination: thermal efficiency, sensitivity study and cost estimation, Journal of Membrane Science, 323 (2008) 85-98.

[22] E.K. Summers, H.A. Arafat, Energy efficiency comparison of single-stage membrane distillation (MD) desalination cycles in different configurations, Desalination, 290 (2012) 54-66.

[23] S. Cerneaux, I. Strużyńska, W.M. Kujawski, M. Persin, A. Larbot, Comparison of various membrane distillation methods for desalination using hydrophobic ceramic membranes, Journal of membrane science, 337 (2009) 55-60.

[24] T.D. Dao, S. Laborie, C. Cabassud, Direct As (III) removal from brackish groundwater by vacuum membrane distillation: Effect of organic matter and salts on membrane fouling, Separation and Purification Technology, 157 (2016) 35-44.

[25] C. Cabassud, D. Wirth, Membrane distillation for water desalination: how to chose an appropriate membrane?, Desalination, 157 (2003) 307-314.

[26] D.M. Warsinger, Thermodynamic design and fouling of membrane distillation systems, arXiv preprint arXiv:1711.07348, DOI (2017).

[27] G. Guan, X. Yang, R. Wang, R. Field, A.G. Fane, Evaluation of hollow fiber-based direct contact and vacuum membrane distillation systems using aspen process simulation, Journal of Membrane Science, 464 (2014) 127-139.

[28] W.J. LI BY, J. WANG, Modeling and optimization of hollow fiber air gap membrane distillation for seawater desalination, CIESC Journal, 66 (2015) 597-604.

[29] P. Zhang, P. Knötig, S. Gray, M. Duke, Scale reduction and cleaning techniques during direct contact membrane distillation of seawater reverse osmosis brine, Desalination, 374 (2015) 20-30.

[30] J. Ge, Y. Peng, Z. Li, P. Chen, S. Wang, Membrane fouling and wetting in a DCMD process for RO brine concentration, Desalination, 344 (2014) 97-107.

[31] J.-P. Mericq, S. Laborie, C. Cabassud, Vacuum membrane distillation of seawater reverse osmosis brines, Water Research, 44 (2010) 5260-5273.

[32] C.R. Martinetti, A.E. Childress, T.Y. Cath, High recovery of concentrated RO brines using forward osmosis and membrane distillation, Journal of membrane science, 331 (2009) 31-39.

[33] X.-M. Li, B. Zhao, Z. Wang, M. Xie, J. Song, L.D. Nghiem, T. He, C. Yang, C. Li, G. Chen, Water reclamation from shale gas drilling flow-back fluid using a novel forward osmosis–vacuum membrane distillation hybrid system, Water Science and Technology, 69 (2014) 1036-1044.

[34] M. Xie, L.D. Nghiem, W.E. Price, M. Elimelech, A forward osmosis–membrane distillation hybrid process for direct sewer mining: system performance and limitations, Environmental science & technology, 47 (2013) 13486-13493.

[35] P. Termpiyakul, R. Jiraratananon, S. Srisurichan, Heat and mass transfer characteristics of a direct contact membrane distillation process for desalination, Desalination, 177 (2005) 133-141.

[36] J. Phattaranawik, R. Jiraratananon, A.G. Fane, Heat transport and membrane distillation coefficients in direct contact membrane distillation, Journal of membrane science, 212 (2003) 177-193.

[37] J. Phattaranawik, R. Jiraratananon, Direct contact membrane distillation: effect of mass transfer on heat transfer, Journal of Membrane Science, 188 (2001) 137-143.

[38] J. Phattaranawik, R. Jiraratananon, A. Fane, Effects of net-type spacers on heat and mass transfer in direct contact membrane distillation and comparison with ultrafiltration studies, Journal of membrane science, 217 (2003) 193-206.

[39] J. Phattaranawik, R. Jiraratananon, A. Fane, C. Halim, Mass flux enhancement using spacer filled channels in direct contact membrane distillation, Journal of membrane science, 187 (2001) 193-201.

[40] S. Meng, Y.-C. Hsu, Y. Ye, V. Chen, Submerged membrane distillation for inland desalination applications, Desalination, 361 (2015) 72-80.

[41] H.C. Duong, Membrane distillation for strategic desalination applications, DOI (2017).

[42] K.W. Lawson, D.R. Lloyd, Membrane distillation. II. Direct contact MD, Journal of Membrane Science, 120 (1996) 123-133.

[43] K.W. Lawson, M.S. Hall, D.R. Lloyd, Compaction of microporous membranes used in membrane distillation. I. Effect on gas permeability, Journal of membrane science, 101 (1995) 99-108.

[44] G. Rao, S.R. Hiibel, A.E. Childress, Simplified flux prediction in direct-contact membrane distillation using a membrane structural parameter, Desalination, 351 (2014) 151-162.

[45] E. Curcio, E. Drioli, Membrane distillation and related operations—a review, Separation and Purification Reviews, 34 (2005) 35-86.

[46] G. Rao, S.R. Hiibel, A. Achilli, A.E. Childress, Factors contributing to flux improvement in vacuum-enhanced direct contact membrane distillation, Desalination, 367 (2015) 197-205.

[47] M. Khayet, Solar desalination by membrane distillation: Dispersion in energy consumption analysis and water production costs (a review), Desalination, 308 (2013) 89-101.

[48] A.G. Fane, R. Schofield, C.J.D. Fell, The efficient use of energy in membrane distillation, Desalination, 64 (1987) 231-243.

[49] S. Lin, N.Y. Yip, T.Y. Cath, C.O. Osuji, M. Elimelech, Hybrid pressure retarded osmosis–membrane distillation system for power generation from low-grade heat: Thermodynamic analysis and energy efficiency, Environmental science & technology, 48 (2014) 5306-5313.

[50] M. Asim, M. Imran, M.K. Leung, N.U. Kumar, A.R. Martin, F. Kashif, Experimental analysis of solar thermal integrated MD system for cogeneration of drinking water and hot water for single family villa in Dubai using flat plate and evacuated tube solar collectors, Desalination and Water Treatment, 92 (2017) 46-59.

[51] M.R. Qtaishat, F. Banat, Desalination by solar powered membrane distillation systems, Desalination, 308 (2013) 186-197.

[52] S.A. Galema, Microwave chemistry, Chemical Society Reviews, 26 (1997) 233-238.

[53] A. de la Hoz, A. Diaz-Ortiz, A. Moreno, Microwaves in organic synthesis. Thermal and non-thermal microwave effects, Chemical Society Reviews, 34 (2005) 164-178.

[54] R.N. Gedye, W. Rank, K.C. Westaway, The rapid synthesis of organic compounds in microwave ovens. II, Canadian journal of chemistry, 69 (1991) 706-711.

[55] F. Langa, P. de la Cruz, A. de la Hoz, A. Díaz-Ortiz, E. Díez-Barra, Microwave irradiation: more than just a method for accelerating reactions, Contemporary organic synthesis, 4 (1997) 373-386.

[56] Y. Mansourpanah, S. Madaeni, A. Rahimpour, Preparation and investigation of separation properties of polyethersulfone supported poly (piperazineamide) nanofiltration membrane using microwave-assisted polymerization, Separation and Purification Technology, 69 (2009) 234-242.

[57] A. Huang, W. Yang, Hydrothermal synthesis of NaA zeolite membrane together with microwave heating and conventional heating, Materials Letters, 61 (2007) 5129-5132.

[58] H. Zhou, Y. Li, G. Zhu, J. Liu, W. Yang, Preparation of zeolite T membranes by microwave-assisted in situ nucleation and secondary growth, Materials Letters, 63 (2009) 255-257.

[59] C. Gibson, I. Matthews, A. Samuel, Microwave enhanced diffusion in polymeric materials, Journal of microwave power and electromagnetic energy, 23 (1988) 17-28.

[60] Y. Nakai, H. Yoshimizu, Y. Tsujita, Enhanced gas permeability of cellulose acetate membranes under microwave irradiation, Journal of membrane science, 256 (2005) 72-77.

[61] Y. Hua, C. Cai, Y. Cui, Microwave-enhanced roasting of copper sulfide concentrate in the presence of CaCO3, Separation and purification technology, 50 (2006) 22-29.

[62] J. Gujar, S. Wagh, V. Gaikar, Experimental and modeling studies on microwave-assisted extraction of thymol from seeds of Trachyspermum ammi (TA), Separation and Purification Technology, 70 (2010) 257-264.

[63] X. Li, X. Zhang, L. Lei, Preparation of CuNaY zeolites with microwave irradiation and their application for removing thiophene from model fuel, Separation and purification technology, 64 (2009) 326-331.

[64] L. Lei, X. Li, X. Zhang, Ammonium removal from aqueous solutions using microwave-treated natural Chinese zeolite, Separation and purification Technology, 58 (2008) 359-366.

[65] L. Lin, S. Yuan, J. Chen, Z. Xu, X. Lu, Removal of ammonia nitrogen in wastewater by microwave radiation, Journal of hazardous materials, 161 (2009) 1063-1068.

[66] D.E. Clark, D.C. Folz, J.K. West, Processing materials with microwave energy, Materials Science and Engineering: A, 287 (2000) 153-158.

[67] Z. Ji, J. Wang, D. Hou, Z. Yin, Z. Luan, Effect of microwave irradiation on vacuum membrane distillation, Journal of membrane science, 429 (2013) 473-479.

[68] Z. Ji, J. Wang, Z. Yin, D. Hou, Z. Luan, Effect of microwave irradiation on typical inorganic salts crystallization in membrane distillation process, Journal of membrane science, 455 (2014) 24-30.

[69] H. Zhu, H. Wang, F. Wang, Y. Guo, H. Zhang, J. Chen, Preparation and properties of PTFE hollow fiber membranes for desalination through vacuum membrane distillation, Journal of membrane science, 446 (2013) 145-153.

[70] S. Khemakhem, R.B. Amar, Grafting of fluoroalkylsilanes on microfiltration Tunisian clay membrane, Ceramics International, 37 (2011) 3323-3328.

[71] A. Franken, J. Nolten, M. Mulder, D. Bargeman, C. Smolders, Wetting criteria for the applicability of membrane distillation, Journal of Membrane Science, 33 (1987) 315-328.

[72] E. Alhseinat, R. Sheikholeslami, A completely theoretical approach for assessing fouling propensity along a full-scale reverse osmosis process, Desalination, 301 (2012) 1-9.

[73] K.L. Tu, A.R. Chivas, L.D. Nghiem, Effects of membrane fouling and scaling on boron rejection by nanofiltration and reverse osmosis membranes, Desalination, 279 (2011) 269-277.

[74] L.D. Tijing, Y.C. Woo, J.-S. Choi, S. Lee, S.-H. Kim, H.K. Shon, Fouling and its control in membrane distillation—A review, Journal of Membrane Science, 475 (2015) 215-244.

[75] D. Warsinger, J. Swaminathan, E. Guillen-Burrieza, H. Arafat, V. Lienhard, Scaling and fouling in membrane distillation for desalination applications: a review. Desalination 356, 294e313, 2014.

[76] C. Park, H. Kim, S. Hong, S. Lee, S.-I. Choi, Evaluation of organic matter fouling potential by membrane fouling index, Water Science and Technology: Water Supply, 7 (2007) 27-33.

[77] L.D. Nghiem, N. Oschmann, A.I. Schäfer, Fouling in greywater recycling by direct ultrafiltration, Desalination, 187 (2006) 283-290.

[78] G. Zuo, R. Wang, Novel membrane surface modification to enhance anti-oil fouling property for membrane distillation application, Journal of membrane science, 447 (2013) 26-35.

[79] L.D. Nghiem, F. Hildinger, F.I. Hai, T. Cath, Treatment of saline aqueous solutions using direct contact membrane distillation, Desalination and Water Treatment, 32 (2011) 234-241.

[80] F. He, K.K. Sirkar, J. Gilron, Studies on scaling of membranes in desalination by direct contact membrane distillation: CaCO3 and mixed CaCO3/CaSO4 systems, Chemical Engineering Science, 64 (2009) 1844-1859.

[81] J. Gilron, Y. Ladizansky, E. Korin, Silica fouling in direct contact membrane distillation, Industrial & Engineering Chemistry Research, 52 (2013) 10521-10529.

[82] F. He, J. Gilron, H. Lee, L. Song, K.K. Sirkar, Potential for scaling by sparingly soluble salts in crossflow DCMD, Journal of Membrane Science, 311 (2008) 68-80.

[83] M. Gryta, Alkaline scaling in the membrane distillation process, Desalination, 228 (2008) 128-134.

[84] L. Wang, B. Li, X. Gao, Q. Wang, J. Lu, Y. Wang, S. Wang, Study of membrane fouling in cross-flow vacuum membrane distillation, Separation and Purification Technology, 122 (2014) 133-143.

[85] S. Meng, Y. Ye, J. Mansouri, V. Chen, Crystallization behavior of salts during membrane distillation with hydrophobic and superhydrophobic capillary membranes, Journal of membrane science, 473 (2015) 165-176.

[86] L.D. Tijing, Y.C. Woo, J.-S. Choi, S. Lee, S.-H. Kim, H.K. Shon, Fouling and its control in membrane distillation—A review, Journal of Membrane Science, 2015, pp. 215-244.

[87] K.L. Hickenbottom, T.Y. Cath, Sustainable operation of membrane distillation for enhancement of mineral recovery from hypersaline solutions, Journal of Membrane Science, 454 (2014) 426-435.

[88] S. Adham, A. Hussain, J.M. Matar, R. Dores, A. Janson, Application of membrane distillation for desalting brines from thermal desalination plants, Desalination, 314 (2013) 101-108.

[89] G. Chen, X. Yang, R. Wang, A.G. Fane, Performance enhancement and scaling control with gas bubbling in direct contact membrane distillation, Desalination, 308 (2013) 47-55.

[90] D. Hou, Z. Wang, G. Li, H. Fan, J. Wang, H. Huang, Ultrasonic assisted direct contact membrane distillation hybrid process for membrane scaling mitigation, Desalination, 375 (2015) 33-39.

[91] Y. Peng, J. Ge, Z. Li, S. Wang, Effects of anti-scaling and cleaning chemicals on membrane scale in direct contact membrane distillation process for RO brine concentrate, Separation and Purification Technology, 154 (2015) 22-26.

[92] D. Hou, G. Dai, H. Fan, H. Huang, J. Wang, An ultrasonic assisted direct contact membrane distillation hybrid process for desalination, Journal of membrane science, 476 (2015) 59-67.

[93] M.S. Humoud, W. Intrchom, S. Roy, S. Mitra, Reduction of scaling in microwave induced membrane distillation on a carbon nanotube immobilized membrane, Environmental Science: Water Research & Technology, 5 (2019) 1012-1021.

[94] S. Roy, M.S. Humoud, W. Intrchom, S. Mitra, Microwave-Induced Desalination via Direct Contact Membrane Distillation, ACS Sustainable Chemistry & Engineering, 6 (2017) 626-632.

[95] F. He, K.K. Sirkar, J. Gilron, Effects of antiscalants to mitigate membrane scaling by direct contact membrane distillation, Journal of Membrane Science, 345 (2009) 53-58.

[96] A. Al-Karaghouli, L.L. Kazmerski, Energy consumption and water production cost of conventional and renewable-energy-powered desalination processes, Renewable and Sustainable Energy Reviews, 24 (2013) 343-356.

[97] G. Zaragoza, A. Ruiz-Aguirre, E. Guillén-Burrieza, Efficiency in the use of solar thermal energy of small membrane desalination systems for decentralized water production, Applied Energy, 130 (2014) 491-499.

[98] L. Carlsson, The new generation in sea water desalination SU membrane distillation system, Desalination, 45 (1983) 221-222.

[99] M. Taulis, M. Milke, Coal seam gas water from Maramarua, New Zealand: characterisation and comparison to United States analogues, Journal of Hydrology (New Zealand), DOI (2007) 1-17.

[100] F. Banat, N. Jwaied, M. Rommel, J. Koschikowski, M. Wieghaus, Performance evaluation of the “large SMADES” autonomous desalination solar-driven membrane distillation plant in Aqaba, Jordan, Desalination, 217 (2007) 17-28.

[101] A. Criscuoli, M.C. Carnevale, E. Drioli, Evaluation of energy requirements in membrane distillation, Chemical Engineering and Processing: Process Intensification, 47 (2008) 1098-1105.

[102] S. Lin, N.Y. Yip, M. Elimelech, Direct contact membrane distillation with heat recovery: Thermodynamic insights from module scale modeling, Journal of membrane science, 453 (2014) 498-515.

[103] R.B. Saffarini, E.K. Summers, H.A. Arafat, Technical evaluation of stand-alone solar powered membrane distillation systems, Desalination, 286 (2012) 332-341.

[104] R.D. Vidic, S.L. Brantley, J.M. Vandenbossche, D. Yoxtheimer, J.D. Abad, Impact of shale gas development on regional water quality, science, 340 (2013) 1235009.

[105] J. Baffes, M.A. Kose, F. Ohnsorge, M. Stocker, The great plunge in oil prices: Causes, consequences, and policy responses, Consequences, and Policy Responses (June 2015), DOI (2015).

[106] A. Kondash, A. Vengosh, Water footprint of hydraulic fracturing, Environmental Science & Technology Letters, 2 (2015) 276-280.

[107] N. Shrestha, G. Chilkoor, J. Wilder, V. Gadhamshetty, J.J. Stone, Potential water resource impacts of hydraulic fracturing from unconventional oil production in the Bakken shale, Water Research, 108 (2017) 1-24.

[108] A. Vengosh, R.B. Jackson, N. Warner, T.H. Darrah, A. Kondash, A critical review of the risks to water resources from unconventional shale gas development and hydraulic fracturing in the United States, Environmental science & technology, 48 (2014) 8334-8348.

[109] W.Y. Kim, Induced seismicity associated with fluid injection into a deep well in Youngstown, Ohio, Journal of Geophysical Research: Solid Earth, 118 (2013) 3506-3518.

[110] W.L. Ellsworth, Injection-induced earthquakes, Science, 341 (2013) 1225942.

[111] Y. He, C. Sun, Y. Zhang, E.J. Folkerts, J.W. Martin, G.G. Goss, Developmental toxicity of the organic fraction from hydraulic fracturing flowback and produced waters to early life stages of Zebrafish (Danio rerio), Environmental science & technology, 52 (2018) 3820-3830.

[112] A. Butkovskyi, H. Bruning, S.A. Kools, H.H. Rijnaarts, A.P. Van Wezel, Organic pollutants in shale gas flowback and produced waters: identification, potential ecological impact, and implications for treatment strategies, Environmental science & technology, 51 (2017) 4740-4754.

[113] S. Kim, P. Omur-Ozbek, A. Dhanasekar, A. Prior, K. Carlson, Temporal analysis of flowback and produced water composition from shale oil and gas operations: Impact of frac fluid characteristics, Journal of Petroleum Science and Engineering, 147 (2016) 202-210.

[114] J. Rosenblum, E.M. Thurman, I. Ferrer, G. Aiken, K.G. Linden, Organic chemical characterization and mass balance of a hydraulically fractured well: From fracturing fluid to produced water over 405 days, Environmental science & technology, 51 (2017) 14006-14015.

[115] D.L. Shaffer, L.H. Arias Chavez, M. Ben-Sasson, S. Romero-Vargas Castrillón, N.Y. Yip, M. Elimelech, Desalination and reuse of high-salinity shale gas produced water: drivers, technologies, and future directions, Environmental science & technology, 47 (2013) 9569-9583.

[116] A.M. Alklaibi, N. Lior, Membrane-distillation desalination: status and potential, Desalination, 171 (2005) 111-131.

[117] T. Tong, M. Elimelech, The global rise of zero liquid discharge for wastewater management: drivers, technologies, and future directions, Environmental science & technology, 50 (2016) 6846-6855.

[118] A. Deshmukh, C. Boo, V. Karanikola, S. Lin, A.P. Straub, T. Tong, D.M. Warsinger, M. Elimelech, Membrane distillation at the water-energy nexus: limits, opportunities, and challenges, Energy & Environmental Science, 11 (2018) 1177-1196.

[119] D.M. Warsinger, J. Swaminathan, E. Guillen-Burrieza, H.A. Arafat, Scaling and fouling in membrane distillation for desalination applications: a review, Desalination, 356 (2015) 294-313.

[120] D. Lloyd, K. Lawson, Review membrane distillation, Membrane Science, 124 (1996) 1-25.

[121] S. Lin, S. Nejati, C. Boo, Y. Hu, C.O. Osuji, M. Elimelech, Omniphobic membrane for robust membrane distillation, Environmental Science & Technology Letters, 1 (2014) 443-447.

[122] C. Boo, J. Lee, M. Elimelech, Omniphobic polyvinylidene fluoride (PVDF) membrane for desalination of shale gas produced water by membrane distillation, Environmental science & technology, 50 (2016) 12275-12282.

[123] C. Boo, J. Lee, M. Elimelech, Engineering surface energy and nanostructure of microporous films for expanded membrane distillation applications, Environmental science & technology, 50 (2016) 8112-8119.

[124] A. Razmjou, E. Arifin, G. Dong, J. Mansouri, V. Chen, Superhydrophobic modification of TiO2 nanocomposite PVDF membranes for applications in membrane distillation, Journal of membrane science, 415 (2012) 850-863.

[125] Z. Wang, J. Jin, D. Hou, S. Lin, Tailoring surface charge and wetting property for robust oil-fouling mitigation in membrane distillation, Journal of Membrane Science, 516 (2016) 113-122.

[126] Z. Wang, D. Hou, S. Lin, Composite membrane with underwater-oleophobic surface for anti-oil-fouling membrane distillation, Environmental science & technology, 50 (2016) 3866-3874.

[127] Z. Wang, S. Lin, Membrane fouling and wetting in membrane distillation and their mitigation by novel membranes with special wettability, Water research, 112 (2017) 38-47.

[128] Y.C. Woo, Y. Kim, M. Yao, L.D. Tijing, J.-S. Choi, S. Lee, S.-H. Kim, H.K. Shon, Hierarchical composite membranes with robust omniphobic surface using layer-by-layer assembly technique, Environmental science & technology, 52 (2018) 2186-2196.

[129] E.-J. Lee, B.J. Deka, J. Guo, Y.C. Woo, H.K. Shon, A.K. An, Engineering the re-entrant hierarchy and surface energy of PDMS-PVDF membrane for membrane distillation using a facile and benign microsphere coating, Environmental science & technology, 51 (2017) 10117-10126.

[130] Y.-X. Huang, Z. Wang, J. Jin, S. Lin, Novel Janus membrane for membrane distillation with simultaneous fouling and wetting resistance, Environmental science & technology, 51 (2017) 13304-13310.

[131] R.W. Baker, Membrane technology, Wiley Online Library2000.

[132] S. Loeb, S. Sourirajan, Sea water demineralization by means of an osmotic membrane, ACS Publications1962.

[133] D.S. Sholl, J.K. Johnson, Making high-flux membranes with carbon nanotubes, Science, 312 (2006) 1003-1004.

[134] B.J. Hinds, N. Chopra, T. Rantell, R. Andrews, V. Gavalas, L.G. Bachas, Aligned multiwalled carbon nanotube membranes, Science, 303 (2004) 62-65.

[135] K. Gethard, O. Sae-Khow, S. Mitra, Water desalination using carbon-nanotube-enhanced membrane distillation, ACS Applied Materials and Interfaces, 3 (2011) 110-114.

[136] G. Arora, S.I. Sandler, Molecular sieving using single wall carbon nanotubes, Nano Letters, 7 (2007) 565-569.

[137] D. Huang, C. Fu, Z. Li, C. Deng, Development of magnetic multiwalled carbon nanotubes as solid-phase extraction technique for the determination of p-hydroxybenzoates in beverage, Journal of Separation Science, 35 (2012) 1667-1674.

[138] G.-Z. Fang, J.-X. He, S. Wang, Multiwalled carbon nanotubes as sorbent for on-line coupling of solid-phase extraction to high-performance liquid chromatography for simultaneous determination of 10 sulfonamides in eggs and pork, Journal of Chromatography A, 1127 (2006) 12-17.

[139] C.M. Hussain, C. Saridara, S. Mitra, Microtrapping characteristics of single and multi-walled carbon nanotubes, Journal of Chromatography A, 1185 (2008) 161-166.

[140] C. Saridara, S. Ragunath, Y. Pu, S. Mitra, Methane preconcentration in a microtrap using multiwalled carbon nanotubes as sorbents, Analytica Chimica Acta, 677 (2010) 50-54.

[141] M.D. Ellison, A.P. Good, C.S. Kinnaman, N.E. Padgett, Interaction of water with single-walled carbon nanotubes: Reaction and adsorption, Journal of Physical Chemistry B, 109 (2005) 10640-10646.

[142] A. Fujiwara, K. Ishii, H. Suematsu, H. Kataura, Y. Maniwa, S. Suzuki, Y. Achiba, Gas adsorption in the inside and outside of single-walled carbon nanotubes, Chemical Physics Letters, 336 (2001) 205-211.

[143] M. Bhadra, O. Sae-Khow, S. Mitra, Effect of carbon nanotube functionalization in micro-solid-phase extraction (μ-SPE) integrated into the needle of a syringe, Analytical and Bioanalytical Chemistry, 402 (2012) 1029-1039.

[144] C.M. Hussain, S. Mitra, Micropreconcentration units based on carbon nanotubes (CNT), Analytical and Bioanalytical Chemistry, 399 (2011) 75-89.

[145] O. Sae-Khow, S. Mitra, Fabrication and characterization of carbon nanotubes immobilized in porous polymeric membranes, Journal of Materials Chemistry, 19 (2009) 3713-3718.

[146] O. Sae-Khow, S. Mitra, Simultaneous extraction and concentration in carbon nanotube immobilized hollow fiber membranes, Analytical chemistry, 82 (2010) 5561-5567.

[147] O. Sae-Khow, S. Mitra, Carbon nanotube immobilized composite hollow fiber membranes for pervaporative removal of volatile organics from water, Journal of Physical Chemistry C, 114 (2010) 16351-16356.

[148] K. Gethard, S. Mitra, Membrane distillation as an online concentration technique: Application to the determination of pharmaceutical residues in natural waters, Analytical and Bioanalytical Chemistry, 400 (2011) 571-575.

[149] K. Gethard, S. Mitra, Carbon nanotube enhanced membrane distillation for online preconcentration of trace pharmaceuticals in polar solvents, Analyst, 136 (2011) 2643-2648.

[150] F. Peng, F. Pan, H. Sun, L. Lu, Z. Jiang, Novel nanocomposite pervaporation membranes composed of poly(vinyl alcohol) and chitosan-wrapped carbon nanotube, Journal of Membrane Science, 300 (2007) 13-19.

[151] M. Bhadra, S. Mitra, Nanostructured membranes in analytical chemistry, TrAC Trends in Analytical Chemistry, 45 (2013) 248-263.

[152] J.H. Choi, J. Jegal, W.N. Kim, Modification of performances of various membranes using MWNTs as a modifier, Macromolecular Symposia, 249-250 (2007) 610-617.

[153] F. Peng, C. Hu, Z. Jiang, Novel ploy(vinyl alcohol)/carbon nanotube hybrid membranes for pervaporation separation of benzene/cyclohexane mixtures, Journal of Membrane Science, 297 (2007) 236-242.

[154] S. Mondal, J.L. Hu, Microstructure and water vapor transport properties of functionalized carbon nanotube-reinforced dense-segmented polyurethane composite membranes, Polymer Engineering & Science, 48 (2008) 1718-1724.

[155] Z. Es'haghi, M.A. Golsefidi, A. Saify, A.A. Tanha, Z. Rezaeifar, Z. Alian-Nezhadi, Carbon nanotube reinforced hollow fiber solid/liquid phase microextraction: A novel extraction technique for the measurement of caffeic acid in Echinacea purpurea herbal extracts combined with high-performance liquid chromatography, Journal of Chromatography A, 1217 (2010) 2768-2775.

[156] K. Hylton, Y. Chen, S. Mitra, Carbon nanotube mediated microscale membrane extraction, Journal of Chromatography A, 1211 (2008) 43-48.

[157] M. Bhadra, S. Mitra, Carbon nanotube immobilized polar membranes for enhanced extraction of polar analytes, Analyst, 137 (2012) 4464-4468.

[158] J.-H. Tsai, F. Macedonio, E. Drioli, L. Giorno, C.-Y. Chou, F.-C. Hu, C.-L. Li, C.-J. Chuang, K.-L. Tung, Membrane-based zero liquid discharge: Myth or reality?, Journal of the Taiwan Institute of Chemical Engineers, 80 (2017) 192-202.

[159] K. Nakoa, K. Rahaoui, A. Date, A. Akbarzadeh, Sustainable zero liquid discharge desalination (SZLDD), Solar Energy, 135 (2016) 337-347.

[160] G. Chen, Y. Lu, W.B. Krantz, R. Wang, A.G. Fane, Optimization of operating conditions for a continuous membrane distillation crystallization process with zero salty water discharge, Journal of Membrane Science, 450 (2014) 1-11.

[161] F. Farahbod, D. Mowla, M.J. Nasr, M. Soltanieh, Experimental study of forced circulation evaporator in zero discharge desalination process, Desalination, 285 (2012) 352-358.

[162] M.K. Souhaimi, T. Matsuura, Membrane distillation: principles and applications, Elsevier2011.

[163] J. Walton, H. Lu, C. Turner, S. Solis, H. Hein, Solar and waste heat desalination by membrane distillation, Desalination and water purification research and development program report, DOI (2004) 20.

[164] R. Schwantes, A. Cipollina, F. Gross, J. Koschikowski, D. Pfeifle, M. Rolletschek, V. Subiela, Membrane distillation: Solar and waste heat driven demonstration plants for desalination, Desalination, 323 (2013) 93-106.

[165] R. Sarbatly, C.-K. Chiam, Evaluation of geothermal energy in desalination by vacuum membrane distillation, Applied Energy, 112 (2013) 737-746.

[166] V.G. Gude, Exergy Evaluation of Desalination Processes, ChemEngineering, 2 (2018) 28.

[167] E. Ali, J. Orfi, A. Najib, J. Saleh, Enhancement of brackish water desalination using hybrid membrane distillation and reverse osmosis systems, PloS one, 13 (2018) e0205012.

[168] D.M. Warsinger, J. Swaminathan, E. Guillen-Burrieza, H.A. Arafat, J.H. Lienhard V, Scaling and fouling in membrane distillation for desalination applications: A review, Desalination, 356 (2015) 294-313.

[169] P. Biniaz, N. Torabi Ardekani, M.A. Makarem, M.R. Rahimpour, Water and Wastewater Treatment Systems by Novel Integrated Membrane Distillation (MD), ChemEngineering, 3 (2019) 8.

[170] P. Onsekizoglu, Membrane distillation: principle, advances, limitations and future prospects in food industry, Distillation-Advances from Modeling to Applications, InTech2012.

[171] S. Roy, M. Bhadra, S. Mitra, Enhanced desalination via functionalized carbon nanotube immobilized membrane in direct contact membrane distillation, Separation and Purification Technology, 136 (2014) 58-65.

[172] M. Bhadra, S. Roy, S. Mitra, Desalination across a graphene oxide membrane via direct contact membrane distillation, Desalination, 378 (2016) 37-43.

[173] M. Bhadra, S. Roy, S. Mitra, Enhanced desalination using carboxylated carbon nanotube immobilized membranes, Separation and Purification Technology, 120 (2013) 373-377.

[174] M. Bhadra, S. Roy, S. Mitra, Nanodiamond immobilized membranes for enhanced desalination via membrane distillation, Desalination, 341 (2014) 115-119.

[175] M. Bhadra, S. Roy, S. Mitra, Flux enhancement in direct contact membrane distillation by implementing carbon nanotube immobilized PTFE membrane, Separation and Purification Technology, 161 (2016) 136-143.

[176] M. Bhadra, S. Roy, S. Mitra, A bilayered structure comprised of functionalized carbon nanotubes for desalination by membrane distillation, ACS applied materials & interfaces, 8 (2016) 19507-19513.

[177] H.C. Duong, A.R. Chivas, B. Nelemans, M. Duke, S. Gray, T.Y. Cath, L.D. Nghiem, Treatment of RO brine from CSG produced water by spiral-wound air gap membrane distillation—a pilot study, Desalination, 366 (2015) 121-129.

[178] X. Yu, H. Yang, H. Lei, A. Shapiro, Experimental evaluation on concentrating cooling tower blowdown water by direct contact membrane distillation, Desalination, 323 (2013) 134-141.

[179] S. Roy, S. Ragunath, Emerging Membrane Technologies for Water and Energy Sustainability: Future Prospects, Constraints and Challenges, Energies, 11 (2018) 2997.

[180] D.M. Warsinger, E.W. Tow, J. Swaminathan, Theoretical framework for predicting inorganic fouling in membrane distillation and experimental validation with calcium sulfate, Journal of Membrane Science, 528 (2017) 381-390.

[181] J. Wang, D. Qu, M. Tie, H. Ren, X. Peng, Z. Luan, Effect of coagulation pretreatment on membrane distillation process for desalination of recirculating cooling water, Separation and Purification Technology, 64 (2008) 108-115.

[182] Z. Ding, L. Liu, Z. Liu, R. Ma, The use of intermittent gas bubbling to control membrane fouling in concentrating TCM extract by membrane distillation, Journal of Membrane Science, 372 (2011) 172-181.

[183] A.a. Metaxas, R.J. Meredith, Industrial microwave heating, IET1983.
[184] E. Grant, B.J. Halstead, Dielectric parameters relevant to microwave dielectric heating, Chemical society reviews, 27 (1998) 213-224.

[185] A.A. Barba, M. d'Amore, Relevance of dielectric properties in microwave assisted processes, Microwave materials characterization, InTech2012.

[186] M. D MP, D. Baghurst, Applictions of mi-crowave dielectricheatingeffects to synthetic problems in chemistry, Chem, Soc. Rev., voL2e, no, 1 3-19.

[187] G. Baffou, J. Polleux, H. Rigneault, S. Monneret, Super-heating and micro-bubble generation around plasmonic nanoparticles under cw illumination, The Journal of Physical Chemistry C, 118 (2014) 4890-4898.

[188] L. Wang, X. Miao, G. Pan, Microwave-induced interfacial nanobubbles, Langmuir, 32 (2016) 11147-11154.

[189] Y. Asakuma, R. Nakata, M. Asada, Y. Kanazawa, C. Phan, Bubble formation and interface phenomena of aqueous solution under microwave irradiation, International Journal of Heat and Mass Transfer, 103 (2016) 411-416.

[190] R. Cai, H. Yang, J. He, W. Zhu, The effects of magnetic fields on water molecular hydrogen bonds, Journal of Molecular Structure, 938 (2009) 15-19.

[191] L. Zhao, K. Ma, Z. Yang, Changes of water hydrogen bond network with different externalities, International journal of molecular sciences, 16 (2015) 8454-8489.

[192] J. Sun, W. Wang, Q. Yue, Review on microwave-matter interaction fundamentals and efficient microwave-associated heating strategies, Materials, 9 (2016) 231.

[193] R.A. Abramovitch, Applications of microwave energy in organic chemistry. A review, Organic preparations and procedures international, 23 (1991) 683-711.

[194] P. Puligundla, S. Abdullah, W. Choi, S. Jun, S. Oh, S. Ko, Potentials of microwave heating technology for select food processing applications: a brief overview and update, Journal of Food Processing & Technology, 4 (2013).

[195] M. Fortuny, C.B. Oliveira, R.L. Melo, M. Nele, R.C. Coutinho, A.F. Santos, Effect of salinity, temperature, water content, and pH on the microwave demulsification of crude oil emulsions, Energy & Fuels, 21 (2007) 1358-1364.

[196] H. Parmar, M. Asada, Y. Kanazawa, Y. Asakuma, C.M. Phan, V. Pareek, G.M. Evans, Influence of microwaves on the water surface tension, Langmuir, 30 (2014) 9875-9879.

[197] M.L. Rao, S.R. Sedlmayr, R. Roy, J. Kanzius, Polarized microwave and RF radiation effects on the structure and stability of liquid water, Current Science, 98 (2010) 1500-1504.

[198] J. Wojnarowicz, T. Chudoba, S. Gierlotka, W. Lojkowski, Effect of Microwave Radiation Power on the Size of Aggregates of ZnO NPs Prepared Using Microwave Solvothermal Synthesis, Nanomaterials, 8 (2018) 343.

[199] X.-q. Yang, L.-j. Yang, K.-m. Huang, Influence of Microwave Radiation on Growth of Calcium Sulphate Crystal by Monte Carlo Method, Asian Journal of Chemistry, 22 (2010) 781.

[200] V. Pavlenko, S. Lapteva, V. Barbanyagre, Influence of Microwave Irradiation of Tempering Water on the Process of Crystallization of Calcium Sulfate Dihydrate, Russian Physics Journal, 60 (2017).

[201] O. Gupta, S. Roy, S. Mitra, Enhanced membrane distillation of organic solvents from their aqueous mixtures using a carbon nanotube immobilized membrane, Journal of membrane science, 568 (2018) 134-140.

[202] T. Humplik, J. Lee, S. O'hern, B. Fellman, M. Baig, S. Hassan, M. Atieh, F. Rahman, T. Laoui, R. Karnik, Nanostructured materials for water desalination, Nanotechnology, 22 (2011) 292001.

[203] E. Guillén-Burrieza, J. Blanco, G. Zaragoza, D.-C. Alarcón, P. Palenzuela, M. Ibarra, W. Gernjak, Experimental analysis of an air gap membrane distillation solar desalination pilot system, Journal of Membrane Science, 379 (2011) 386-396.

[204] S. Burn, M. Hoang, D. Zarzo, F. Olewniak, E. Campos, B. Bolto, O. Barron, Desalination techniques—A review of the opportunities for desalination in agriculture, Desalination, 364 (2015) 2-16.

[205] T.-x. He, L.-j. Yan, Application of alternative energy integration technology in seawater desalination, Desalination, 249 (2009) 104-108.

[206] C. Charcosset, A review of membrane processes and renewable energies for desalination, Desalination, 245 (2009) 214-231.

[207] N. Ghaffour, T.M. Missimer, G.L. Amy, Technical review and evaluation of the economics of water desalination: current and future challenges for better water supply sustainability, Desalination, 309 (2013) 197-207.

[208] V.G. Gude, N. Nirmalakhandan, S. Deng, Renewable and sustainable approaches for desalination, Renewable and sustainable energy reviews, 14 (2010) 2641-2654.
[209] N.N. Li, A.G. Fane, W.W. Ho, T. Matsuura, Advanced membrane technology and applications, John Wiley & Sons2011.

[210] W.L. Ang, A.W. Mohammad, N. Hilal, C.P. Leo, A review on the applicability of integrated/hybrid membrane processes in water treatment and desalination plants, Desalination, 363 (2015) 2-18.

[211] K. Scott, Handbook of industrial membranes, Elsevier1995.

[212] K. Soldenhoff, J. McCulloch, A. Manis, P. Macintosh, Nanofiltration in metal and acid recovery, Elsevier Advanced Technology: Oxford, UK, 2005, pp. 459-477.

[213] M. Al-Shammiri, M. Safar, M. Al-Dawas, Evaluation of two different antiscalants in real operation at the Doha research plant, Desalination, 128 (2000) 1-16.

[214] F. Meng, S.-R. Chae, A. Drews, M. Kraume, H.-S. Shin, F. Yang, Recent advances in membrane bioreactors (MBRs): membrane fouling and membrane material, Water research, 43 (2009) 1489-1512.

[215] R. Bian, K. Yamamoto, Y. Watanabe, The effect of shear rate on controlling the concentration polarization and membrane fouling, Desalination, 131 (2000) 225-236.

[216] M. Goosen, S. Sablani, H. Al-Hinai, S. Al-Obeidani, R. Al-Belushi, a. Jackson, Fouling of reverse osmosis and ultrafiltration membranes: a critical review, Separation science and technology, 39 (2005) 2261-2297.

[217] W. Guo, H.-H. Ngo, J. Li, A mini-review on membrane fouling, Bioresource technology, 122 (2012) 27-34.

[218] E. Curcio, X. Ji, G. Di Profio, E. Fontananova, E. Drioli, Membrane distillation operated at high seawater concentration factors: Role of the membrane on CaCO3 scaling in presence of humic acid, Journal of Membrane Science, 346 (2010) 263-269.

[219] B. Peñate, L. García-Rodríguez, Current trends and future prospects in the design of seawater reverse osmosis desalination technology, Desalination, 284 (2012) 1-8.

[220] M. Yorgun, I.A. Balcioglu, O. Saygin, Performance comparison of ultrafiltration, nanofiltration and reverse osmosis on whey treatment, Desalination, 229 (2008) 204-216.

[221] B. Van der Bruggen, C. Vandecasteele, Distillation vs. membrane filtration: overview of process evolutions in seawater desalination, Desalination, 143 (2002) 207-218.

[222] A. Ghadimkhani, W. Zhang, T. Marhaba, Ceramic membrane defouling (cleaning) by air Nano Bubbles, Chemosphere, 146 (2016) 379-384.

[223] S. Muthukumaran, S.E. Kentish, G.W. Stevens, M. Ashokkumar, Application of ultrasound in membrane separation processes: a review, Reviews in chemical engineering, 22 (2006) 155-194.

[224] B.D. Coday, P. Xu, E.G. Beaudry, J. Herron, K. Lampi, N.T. Hancock, T.Y. Cath, The sweet spot of forward osmosis: Treatment of produced water, drilling wastewater, and other complex and difficult liquid streams, Desalination, 333 (2014) 23-35.

[225] M. Rezaei, D.M. Warsinger, M.C. Duke, T. Matsuura, W.M. Samhaber, Wetting phenomena in membrane distillation: mechanisms, reversal, and prevention, Water research, 139 (2018) 329-352.

[226] T. Istirokhatun, M. Dewi, H. Ilma, H. Susanto, Separation of antiscalants from reverse osmosis concentrates using nanofiltration, Desalination, 429 (2018) 105-110.

[227] M. Gryta, Polyphosphates used for membrane scaling inhibition during water desalination by membrane distillation, Desalination, 285 (2012) 170-176.

[228] S. Mitra, S. Roy, M. Bhadra, Nanocarbon immobilized membranes, Google Patents, 2015.

[229] K. Gethard, O. Sae-Khow, S. Mitra, Water desalination using carbon-nanotube-enhanced membrane distillation, ACS applied materials & interfaces, 3 (2010) 110-114.

[230] W. Intrchom, S. Roy, S. Mitra, Functionalized Carbon Nanotube Immobilized Membrane for Low Temperature Ammonia Removal via Membrane Distillation, Separation and Purification Technology, DOI (2019) 116188.

[231] C. Han, E. Sahle-Demessie, E. Varughese, H. Shi, Polypropylene–MWCNT composite degradation, and release, detection and toxicity of MWCNTs during accelerated environmental aging, Environmental Science: Nano, DOI (2019).

[232] L.M. Camacho, L. Dumée, J. Zhang, J.-d. Li, M. Duke, J. Gomez, S. Gray, Advances in membrane distillation for water desalination and purification applications, Water, 5 (2013) 94-196.

[233] C. Tzotzi, T. Pahiadaki, S. Yiantsios, A. Karabelas, N. Andritsos, A study of CaCO3 scale formation and inhibition in RO and NF membrane processes, Journal of membrane science, 296 (2007) 171-184.

[234] A. Drak, K. Glucina, M. Busch, D. Hasson, J.-M. Laîne, R. Semiat, Laboratory technique for predicting the scaling propensity of RO feed waters, Desalination, 132 (2000) 233-242.

[235] R. Eriksson, J. Merta, J.B. Rosenholm, The calcite/water interface: I. Surface charge in indifferent electrolyte media and the influence of low-molecular-weight polyelectrolyte, Journal of colloid and interface science, 313 (2007) 184-193.

[236] Y. Takizawa, S. Inukai, T. Araki, R. Cruz-Silva, J. Ortiz-Medina, A. Morelos-Gomez, S. Tejima, A. Yamanaka, M. Obata, A. Nakaruk, Effective Antiscaling Performance of Reverse-Osmosis Membranes Made of Carbon Nanotubes and Polyamide Nanocomposites, ACS Omega, 3 (2018) 6047-6055.

[237] M. Gloede, T. Melin, Physical aspects of membrane scaling, Desalination, 224 (2008) 71-75.

[238] S. Ghani, N.S. Al-Deffeeri, Impacts of different antiscalant dosing rates and their thermal performance in Multi Stage Flash (MSF) distiller in Kuwait, Desalination, 250 (2010) 463-472.

[239] Q. Yang, Y. Liu, Y. Li, Control of protein (BSA) fouling in RO system by antiscalants, Journal of Membrane Science, 364 (2010) 372-379.

[240] S. Shirazi, C.-J. Lin, D. Chen, Inorganic fouling of pressure-driven membrane processes—A critical review, Desalination, 250 (2010) 236-248.

[241] J.A. Brant, A.E. Childress, Assessing short-range membrane–colloid interactions using surface energetics, Journal of Membrane Science, 203 (2002) 257-273.

[242] A. Hausmann, P. Sanciolo, T. Vasiljevic, M. Weeks, K. Schroën, S. Gray, M. Duke, Fouling of dairy components on hydrophobic polytetrafluoroethylene (PTFE) membranes for membrane distillation, Journal of membrane science, 442 (2013) 149-159.

[243] N. D'souza, A. Mawson, Membrane cleaning in the dairy industry: a review, Critical reviews in food science and nutrition, 45 (2005) 125-134.

[244] P. Shakkthivel, T. Vasudevan, Acrylic acid-diphenylamine sulphonic acid copolymer threshold inhibitor for sulphate and carbonate scales in cooling water systems, Desalination, 197 (2006) 179-189.

[245] D. O'Rourke, S. Connolly, Just oil? The distribution of environmental and social impacts of oil production and consumption, Annual Review of Environment and Resources, 28 (2003) 587-617.

[246] Y.C. Choi, G.D. Kim, Z. Hendren, Low-Energy Water Recovery from Subsurface Brines, RTI International, Research Triangle Park, NC (United States), 2018.

[247] S. Tavakkoli, O.R. Lokare, R.D. Vidic, V. Khanna, A techno-economic assessment of membrane distillation for treatment of Marcellus shale produced water, Desalination, 416 (2017) 24-34.

[248] N.A. Ahmad, P.S. Goh, Z. Abdul Karim, A.F. Ismail, Thin film composite membrane for oily waste water treatment: Recent advances and challenges, Membranes, 8 (2018) 86.

[249] R.L. McGinnis, N.T. Hancock, M.S. Nowosielski-Slepowron, G.D. McGurgan, Pilot demonstration of the NH3/CO2 forward osmosis desalination process on high salinity brines, Desalination, 312 (2013) 67-74.

[250] T.Y. Cath, A.E. Childress, M. Elimelech, Forward osmosis: principles, applications, and recent developments, Journal of membrane science, 281 (2006) 70-87.

[251] M. El-Bourawi, Z. Ding, R. Ma, M. Khayet, A framework for better understanding membrane distillation separation process, Journal of membrane science, 285 (2006) 4-29.

[252] J. Koschikowski, M. Wieghaus, M. Rommel, Solar thermal-driven desalination plants based on membrane distillation, Desalination, 156 (2003) 295-304.

[253] H.E. Fath, S.M. Elsherbiny, A.A. Hassan, M. Rommel, M. Wieghaus, J. Koschikowski, M. Vatansever, PV and thermally driven small-scale, stand-alone solar desalination systems with very low maintenance needs, Desalination, 225 (2008) 58-69.

[254] S. Zhang, P. Wang, X. Fu, T.-S. Chung, Sustainable water recovery from oily wastewater via forward osmosis-membrane distillation (FO-MD), water research, 52 (2014) 112-121.

[255] C.H. Cho, K.Y. Oh, S.K. Kim, J.G. Yeo, P. Sharma, Pervaporative seawater desalination using NaA zeolite membrane: mechanisms of high water flux and high salt rejection, Journal of Membrane Science, 371 (2011) 226-238.

[256] M.S.I. Mozumder, C. Picioreanu, M.C. van Loosdrecht, E.I. Volcke, Effect of heterotrophic growth on autotrophic nitrogen removal in a granular sludge reactor, Environmental technology, 35 (2014) 1027-1037.

[257] V.G. Gude, Energy storage for desalination processes powered by renewable energy and waste heat sources, Applied Energy, 137 (2015) 877-898.

[258] W. Schwieger, T. Selvam, M. Klumpp, M. Hartmann, Porous Inorganic Materials as Potential Supports for Ionic Liquids, Supported Ionic Liquids: Fundamentals and Applications, DOI (2014).

[259] M. Bhadra, S. Mitra, Advances in nanostructured membranes for water desalination, Nanotechnology Applications for Clean Water, Elsevier2014, pp. 109-122.

[260] G.-d. Kang, Y.-m. Cao, Development of antifouling reverse osmosis membranes for water treatment: a review, Water research, 46 (2012) 584-600.

[261] B.L. Pangarkar, M.G. Sane, M. Guddad, Reverse osmosis and membrane distillation for desalination of groundwater: a review, ISRN Materials Science, 2011 (2011).

[262] H. Lin, W. Peng, M. Zhang, J. Chen, H. Hong, Y. Zhang, A review on anaerobic membrane bioreactors: applications, membrane fouling and future perspectives, Desalination, 314 (2013) 169-188.

[263] X. Zhang, Z. Wang, Z. Wu, T. Wei, F. Lu, J. Tong, S. Mai, Membrane fouling in an anaerobic dynamic membrane bioreactor (AnDMBR) for municipal wastewater treatment: characteristics of membrane foulants and bulk sludge, Process Biochemistry, 46 (2011) 1538-1544.

[264] F. Rahman, Calcium sulfate precipitation studies with scale inhibitors for reverse osmosis desalination, Desalination, 319 (2013) 79-84.

[265] A. Zach-Maor, R. Semiat, A. Rahardianto, Y. Cohen, S. Wilson, S. Gray, Diagnostic analysis of RO desalting treated wastewater, Desalination, 230 (2008) 239-247.

[266] N. Hilal, O.O. Ogunbiyi, N.J. Miles, R. Nigmatullin, Methods employed for control of fouling in MF and UF membranes: a comprehensive review, Separation Science and Technology, 40 (2005) 1957-2005.

[267] B.P. Ho, M.W. Wu, E.K. Zeiher, M. Chattoraj, Method of monitoring biofouling in membrane separation systems, Google Patents, 2004.

[268] W.H. Dickinson, Use of cerium salts to inhibit manganese deposition in water systems, Google Patents, 2007.

[269] N.S. Sherwood, M.A. Yorke, Method for controlling calcium carbonate scaling in high pH aqueous systems, Google Patents, 1992.

[270] X. Kowalski, Methods of scale inhibition using substoichiometric amounts of amino alcohol and phosphonic acids, Google Patents, 1972.

[271] G. Ritter, Method of dissolving, and solvents for, difficult to dissolve carbonates, Google Patents, 1988.

[272] T. Gullinkala, B. Digman, C. Gorey, R. Hausman, I.C. Escobar, Desalination: reverse osmosis and membrane distillation, Sustainability Science and Engineering, 2 (2010) 65-93.